A STUDY ON MULTI-EXPOSURE LASER SPECKLE CONTRAST IMAGING USING A VIDEO-RATE MULTI-TAP CHARGE MODULATION CMOS IMAGE SENSOR

THESIS

A STUDY ON MULTI-EXPOSURE LASER SPECKLE CONTRAST IMAGING USING A VIDEO-RATE MULTI-TAP CHARGE MODULATION CMOS IMAGE SENSOR

Panneer Selvam SIVAKUMAR

Graduate School of

Science and Technology, Educational Division

Department of Nanovision Technology

Shizuoka University

December 2019

THESIS

A STUDY ON MULTI-EXPOSURE LASER SPECKLE CONTRAST IMAGING USING A VIDEO-RATE MULTI-TAP CHARGE MODULATION CMOS IMAGE SENSOR

ビデオレートマルチタップ電荷変調CMOSイメージセンサによる
多重露光レーザースペックルコントラストイメージングに関する研究

Panneer Selvam SIVAKUMAR

静 岡 大 学

大学院自然科学系教育部

ナノビジョン工学専攻

２０１９年１２月

A STUDY ON MULTI-EXPOSURE LASER SPECKLE CONTRAST IMAGING USING A VIDEO-RATE MULTI-TAP CHARGE MODULATION CMOS IMAGE SENSOR

by

Panneer Selvam SIVAKUMAR

Submitted for the degree of Doctor of Engineering

January 2020

Abstract

Multi-Exposure Laser Speckle Contrast Imaging (MELSCI) is a wide-field and non-invasive optical technique to monitor the blood flow movement and produce the two-dimensional (2D) blood flow maps with high spatial and temporal resolution in real-time. It has been widely used for several blood flow studies in clinical and research level. In recent years, MELSCI has developed with the advancement of high-speed CMOS image sensors. Recent studies suggest that, the MELSCI system utilize the high-speed camera with a frame rate of about 1kfps to monitor the blood flow changes. Nevertheless, the high-frame rate sensors have the capability to produce real-time blood flow maps, it has some limitation. Because of the high-frame rate the camera requires high power consumption, which is not an energy efficient system. Furthermore, the system requires huge memory to store the raw images and high-efficient processing capability is necessary to process the speckle signals and reconstruct the blood flow map. This limitation may lead to the need of adequately large and expensive hardware. In general, the usage of high-frame camera is not power and cost-efficient.

In this study, a power-efficient MELSCI system which can monitor the blood flow movement at about the video rate (30 frames per second (fps)) is proposed. A laboratory-developed multi-tap charge modulation CMOS image sensor originally designed for time-of-flight (TOF) range imaging is utilized to build a video-rate MELSCI system. In general,

the rate of blood flow change happens at each cardiac cycle. Generally, a cardiac cycle lasts for about 0.8 second which is of 1Hz. Therefore, to monitor the blood flow changes during each cardiac cycle, the video rate of 30 fps is sufficient. But, the speckle pattern observing by the CMOS image sensor tends to fluctuates in the fast manner due to flow of red blood cells (RBCs), during the exposure time of the image sensor. So, a fast-frame rate higher than 1kfps is essential to record the movement of fast changing of the speckle pattern. The utilization of multi-tap charge modulator developed at laboratory helps to sample the charges efficiently at the high modulation frequency than the video rate to detect rapid fluctuation of the speckles and readout the images of shorter and longer exposure times simultaneously at the near video rate. This time-multiplexed approach provides the advantage of eliminating a dead time during the charge modulation and accumulation operation, and the problem of inter-frame delay also be removed. It believes, this sensor can be applicable to MELSCI system with low power consumption and cost efficient. This multi-tap image sensor operates in the global shutter mode and each pixel is equipped with multiple charge-storage nodes and the exposure patterns of the taps are programmable.

The exposure pattern of equal and exponential exposure case was designed to implement with multi-tap sensor. The ratio of equal and exponential exposure case is 1:4 and 1:8, respectively. The exposure time in each tap is same for equal case. To cover a wide flow speed range, the ratio of the longest exposure and the shortest exposure should be large. The designed exposure patterns were verified by simulation of reference high-speed camera data. The high-speed camera operated at 40kfps to capture the raw speckle images. The measurement was carried for 2 seconds to capture 80,000 frames. The solid and fluid phantoms of Ground glass plate and Intralipose were used for measurement. A CW wavelength-stabilized laser (ONDAX, RO-USB-785-PLR-100-1, λ of 785nm, output power of 100 mW) with linear polarization was used as a light source. The phantoms were illuminated with the laser power of 8 mW and diameter of 10mm. A high-speed CMOS global shutter camera (Mikrotron, MC1362), visible and near-infrared C-mount lens (Edmund Optics, #67-715, focal length of 25mm) were used for imaging.

The captured raw speckle images of high-speed camera were simulated with coded, equal and exposure patterns. The simulation was carried out with different unit exposure

times (T_0). The mean flow speed-to-noise-ratio (FNR) was estimated for various T_0's. As expected, the simulation results confirmed that the equal exposure pattern provides the better mean FNR than exponential exposure case. Because the equal exposure pattern utilizes all the taps efficiently for averaging and the standard deviation of the calculated contrast will be improved by a factor of 2 by averaging. On the other hand, the exponential exposure pattern is more suitable for monitoring wide range of flow speeds. For Ground glass plate, mean FNR of equal and exponential exposure pattern is 14.29 and 5.99, respectively. In case of Intralipose, mean FNR of equal and exponential exposure pattern is 11.89 and 6.11, respectively. The feasibility of 4-tap sensor was evaluated by relative error. From the analysis, it is clear that 4-tap sensor has the capability to measure flow speed with acceptable errors.

The multi-exposure laser speckle experiment was carried out with the laboratory-developed multi-tap CMOS charge modulator. The phantom of Ground glass plate and Intralipose was used. The phantom was controlled at the flow-speed of 1-5 mm/s with the incremental step size of 1mm/s. The experiment was carried out with equal and exponential exposure patterns. The experiment results with 4-tap CMOS image sensor also confirms that equal exposure pattern has better FNR than exponential exposure pattern. The movie acquisition was carried out with equal exposure pattern and it confirms that the 4-tap CMOS image sensor can monitor the flow speed changes with the frame rate of 45 fps for a flowing intralipose.

Declaration

The work in this thesis is based on research carried out at the Imaging Devices Laboratory, Research Institute of Electronics, Shizuoka University. No part of this thesis has been submitted elsewhere for any other degree or qualification and it is all my own work unless referenced to the contrary in the text.

List of Figures

List of Table

Table of Contents

Chapter1

Introduction

1.1 Background

In the human body, individual cells together build into whole system. The human cells are not self-capable to supply the essential immune substances to them. Cardio Vascular Systems (CVS) that consists of heart and blood vessels will help to transport the immune substances to the organs. The heart and blood vessels work together to supply adequate blood to all parts of the body. The blood vessels play a major role in transporting oxygen (O_2) and essential nutrients to individual cells and taking out the carbon dioxide (CO_2) and waste products from the cells.

Microcirculation is the process of flowing blood in the vessels smaller than 100µm which present within the organ tissues. The heart pumps the blood which flows through the vessels that consists of arteries, capillaries, and veins. Blood vessels control the amount of blood flow to specific parts of body. Arteries carry blood away from the heart which is divided into large and small arteries. Large arteries receive highest pressure of blood flow and are thicker and elastic. Smaller arteries have more smooth muscle which contracts and relaxes to regulate blood flow. Capillaries consists of single layer of endothelium which allows for exchange of nutrients, gases, waste with tissues and organs. Veins carry the de-oxygenated blood towards the heart. In order to supply the oxygen and nutrition to the human tissues, and to remove the waste products of metabolism, the microcirculation is very much essential.

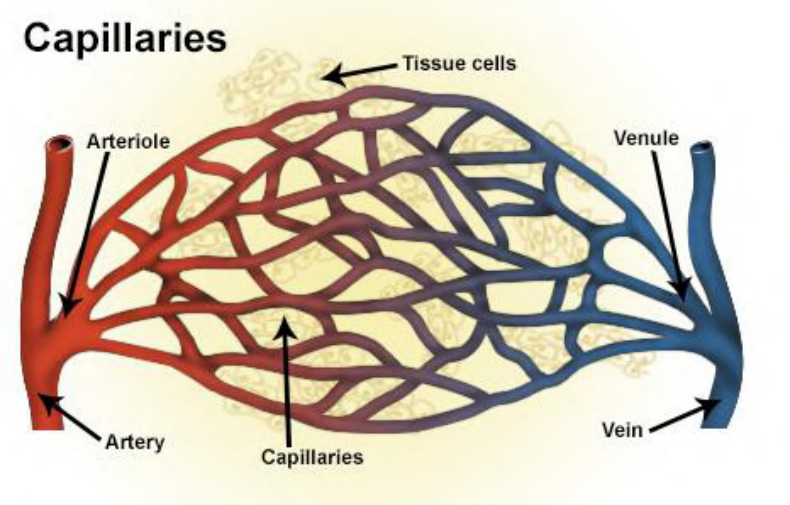

Fig. 1.1 Vascular structure of microcirculation unit. Adopted from: https://training.seer.cancer.gov/anatomy/cardiovascular/blood/classification.html

The CVS consists of systemic and pulmonary circulation. Systemic circulation which provides oxygenated blood and nutrients to reach rest of the body and Pulmonary circulation for oxygenation of blood. Vasculature plays a significant role in the regulation of blood flow throughout the body. Velocity of blood in the vasculature has an inverse relationship with cross sectional area. As cross-sectional area increases, velocity decreases. Arteries, veins have smaller cross-sectional area and highest velocities whereas capillaries have the most cross-sectional area and the lowest velocities. The diameter and its flow speed of each blood vessels are mentioned in table 1.1.

Table. 1.1 Blood vessel types and its flow speed

Type of Blood Vessel	**Diameter of Blood Vessel**	**Flow Speed**
Arteries and aorta	Up to 2.5 cm	400 - 1200 mm/s
Arterioles	20 - 50 µm	Up to 15 mm/s
Veins and venae cavae	Up to 3 cm	80 - 150 mm/s
Venules	20 µm	Up to 5 mm/s
Capillaries	5 - 9 µm	0.3 - 0.4 mm/s

The understanding of structure and physiology of the heart is helpful to pursue a clear knowledge of microcirculation and how fast the microcirculation performs. Heart is a muscular pump that controls the circulation of blood to each tissues in the body. It has four chambers. The upper two chambers are called atria, which receives blood from the veins. The lower two chambers are called ventricles which pump the blood into arteries. As blood leaves each chamber of the heart, it passes through the valve.

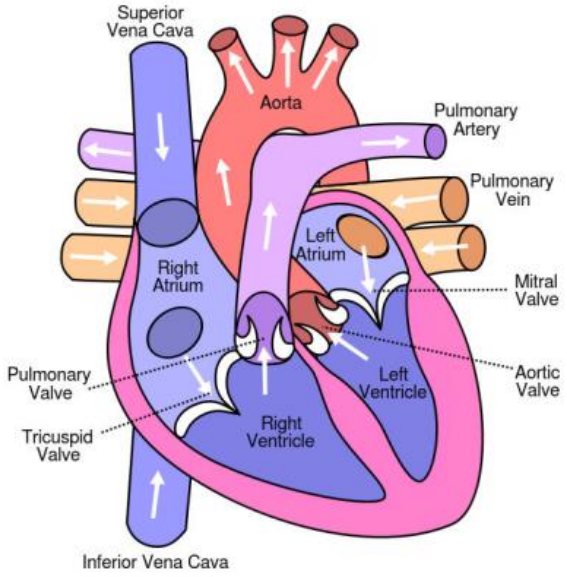

Fig. 1.2 Structure of heart. Adopted from [1]

The cardiac cycle is initiated in the Sino-arterial (SA) node, which is also called as cardiac pacemaker. The SA node rhythmically initiates impulses about 70 to 80 times per minute. From SA node impulses gets transmitted to both right and left atrium, which cause it to contract. From the atria, impulse travels to Atrioventricular (AV) node and then to both ventricles. The contraction of ventricles ejects the blood into arteries. Therefore, at a normal heart rate, one cardiac cycle lasts for about 0.8 second. In other words, the blood flow changes happen at each impulse of 1 Hz.

It is fundamental to visualize the blood vessels and to understand the changes in blood flow to analyze the health condition of human organs. By measuring the blood flow speed, the possibility of differentiating the blood vessels is also feasible. The knowledge of blood flow in the human tissue is vital in many branches of medicine include surgery, ophthalmology, neurology, cardiology.

The microcirculation blood flow has been monitored using several techniques from the past. In the earlier days, the assessment of blood flow has been performed using xenon washout technique. The determination of blood flow measurement through adipose tissue using the radioactive element xenon was proposed. The xenon washout technique uses the clearance rate as a parameter to observe the blood flow in a tissue. The radioactive xenon dissolved in saline injected into the blood. However, the proposed technique measures the blood flow in the single-point but cannot give the information of the blood flow over the region. It also has disadvantage of injecting radioactive element into the blood vessels.

The other technique which monitors the changes in blood flow is thermography. It is based on the changes in temperature of the skin, since there is a correlation between the skin temperature and skin blood flow. The working principle of this technique is to illuminate the infra-red radiation on the skin surface and the thermal imager records the thermal images. The recorded images are processed using the microcomputer for the analysis of skin blood flow based on the temperature.

The above mentioned methods are non-optical and invasive which needs contact with the patient every time during the measurement and that cause inconvenience to patients. By the advancement of many optical and non-invasive techniques the estimation of blood flow reached to the next level. It makes microvascular monitoring technique easily accessible. One of the optical techniques uses the television microscopy to measure the flow of red blood cells (RBCs) in human nail fold capillaries. The flow of RBCs in the capillaries is determined by measuring the displacement of plasma gaps. Photoplethysmography (PPG) is another optical diagnostic tool which uses invisible infra-red light as a source to monitor the blood flow movement. This technique has the advantage of non-invasive because of no physical contact with the patient. The invisible infra-red light is incident on the tissue region and variation in blood volume or blood flow for each pumping of heart can be analyzed by the amount of light backscattered from the tissue.

Optical Doppler Tomography (ODT) is an optical technique also called as Doppler optical coherence tomography, because it uses Doppler principle to image the structure of the tissue and to monitor the flow speed of moving particles. This technique is useful to

provide tissue images at high spatial resolution. High speed imaging is achieved. But it has the disadvantage of high cost.

Nowadays estimation of microcirculation has achieved greater heights due to rapid advancements in laser-based techniques. These developed techniques for microvascular blood flow assessment are becoming portable and easily accessible. Among these laser-based techniques, laser doppler perfusion imaging (LDPI) and laser speckle contrast imaging (LSCI) are well established techniques in clinical and research applications. To perform the blood flow imaging, recent techniques utilize the random interference pattern which is called as speckle pattern. The most established technique which using the speckle pattern are Laser Doppler Flowmetry (LDF) and Laser Speckle Contrast Analysis (LASCA). Doppler is an effective technique to determine the speed of the flow. The general principle of Doppler effect is changes in the frequency content of the monochromatic wave when interact with the moving object. Laser Doppler Flowmetry (LDF) and Laser Speckle Contrast Analysis (LASCA) is an optical technique which is used to monitor the microcirculatory blood flow in tissue. Both methods generate the laser speckle pattern, but the way of analyzing the speckle pattern is different. The technique is non-invasive which can assess the blood flow without physical contact with the patient, so it can avoid unwanted discomfort and eradicate the risk of infection. LDF has been used in wide range of clinical applications such as burn depth assessment, organ transplants, peripheral vascular diseases, dermatology and neurology. The basic idea of the technique is to illuminate the moving red blood cells (RBCs) with coherent light source. When the laser light incident on the moving particle, the photons are scattered, and it broadens the optical power spectrum. Because of the simple optical setup, the LSCI keep on to improve in both clinical and research studies.

LSI started to advance in the 1990s to image the blood flow in the retina and skin, with the development of faster digital acquisition techniques and processing technologies. The first scheme of LSCI was proposed by Briers and Webster to monitor the capillary blood flow [2]. Multiple studies started to use LSCI to monitor the blood flow in the cerebral, measurement of perfusion in tissues, monitoring of perfusion in the burn scar and its healing [3], to observe the vasculature of human retina vein and measure its flow speed

[4]. In general, during the measurement of blood flow speed it is unaffected by the presence of proteins in the blood. But some studies considered the effect of high-protein diet on coronary blood flow [5]. The high-protein diets may precipitate progression of Celiac Artery Infusion (CAI) through increase in lipid deposition and inflammatory of coagulation pathways. In the earlier days, traditional LSCI system monitors the movement of blood with the use single-exposure. Majorly, the single-exposure LSCI is sensitive to the parameters which are exposure time of the camera and the presence of static scatterers. Because of exposure-time dependent, LSCI's sensitivity to monitor flow speed is limited. A single-exposure time is not good enough to monitor the wide range of flow speeds. A major drawback of LSI is that it underestimates the large changes in blood flow velocity. Another drawback is conventional speckle models do not have ability to estimate the accurate blood flow in the presence of static tissue elements such as skull part, especially in cerebral blood flow imaging.

The development of Multi-Exposure Laser Speckle Contrast Imaging techniques (MELSCI) aided to eliminate the limitation face by single-exposure LSCI. MELSCI method uses multiple exposure times. MELSCI technique takes advantage of the speckle contrast dependence on the camera exposure durations. Because of multiple exposure time, the sensitivity range of flow has increased and it estimates the flow velocity with higher accuracy. A few studies using MELSCI method such as chronic imaging of cortical blood flow [6], in vivo imaging of microvascular changes in an angiogenic environment [7] has been proposed.

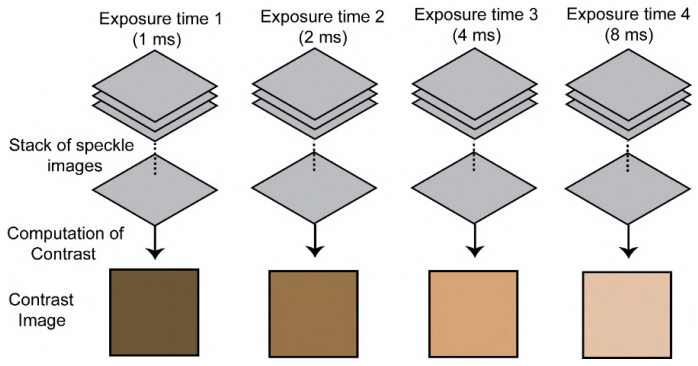

Fig. 1.3 Methodology of conventional multi-exposure laser speckle contrast imaging

The MELSCI methodology is explained, the stack of speckle images was acquired at the exposure time 1 and the contrast value (K) was computed from the stack of images and finally contrast imaging was mapped as shown in Fig. 1.3. These operations are repeated for multiple sets of exposure time. As the exposure time increases, the contrast value reduces. The effective exposure time was controlled by switching the laser with an acoustic optical modulator or electronic shutter function of the image sensor. However, these studies have the potential drawback of additional time required for image acquisition at different exposure times. Therefore, temporal resolution to monitor the rapid changes in the speckle movement was sacrificed.

To overcome these limitations in the conventional MELSCI setup, a high-speed multi-exposure laser speckle imaging with a single-photon counting camera (SPAD) for in-vivo imaging of the mouse brain [8] was proposed. It utilizes the fast frame-rate capability to increase the acquisition speed and single-shot acquisition MESI (sMESI) to acquire thousands of frames (short exposure time) rapidly with negligible inter-frame delay. In the post-processing, these images are accumulated to obtain N different exposure times. MELSCI system using high frame rate CMOS sensor implemented on a field programmable gate array (FPGA) [9] [10], continuously captured speckle images at the frame rate of 15 fps. The synthesization of short exposure time was performed to simulate the longer exposure time as in SPAD chip. The practical frame rate of processed blood perfusion images is 0.225fps with the spatial resolution of 1.31-megapixel. The recent work of MELSCI to visualize the blood perfusion images was developed using an FPGA, connected to 1000fps 1-megapixel camera [11]. A set of multi-exposure contrast images with 256 × 250 pixels was produced at the frame rate of 15.625fps and the effective frame rate on the computer is 1.5fps. These conventional MELSCI systems as discussed here, utilizes the high-speed cameras, to monitors the rapid speckle fluctuations and blood flow changes and it can reproduce wide-field blood flow velocity maps. However, these expensive high-speed cameras, generally operating at a high frame rate of around several thousand frames per second (fps). It needs high processing power and huge processing capability to process the data. These high-speed camera is also cost-inefficient because of large hardware setup.

1.2 Motivation and Research Objective

The multi-exposure laser speckle contrast imaging system (MELSCI) with a high-speed camera (frame rate of around 1000 fps) can produce the high spatial and temporal resolution blood flow maps. Nevertheless, such high-speed operation consumes high-power and need the huge capability to process the speckle images. It leads to use the expensive hardware, which is not efficient in terms of cost.

In general, blood flow changes caused by pulsation and the rate of change is about 1 Hz. To observe the blood flow changes during each pulsation, the moderate video rate of 30 fps is adequate. However, the fast frame rate is required to record the fast changing of the speckle pattern. In an optical phenomenon, the requirement of the high-speed camera is essential to monitor the rapid speckle fluctuation changes. But, in a biomedical phenomenon, that is to observe the blood flow changes with the frame rate of 20kHz is inconsequential. It leads to an inefficient sampling of the same blood flow signal redundantly. The aim of this study is to build the MELSCI system, which can sample the charges efficiently to monitor the speckle movement and to readout the different exposure time images at the frame rate of about the video rate. With this kind of approach, the blood flow change can monitor at a moderate frame rate of around the video rate (typically 30fps), which contributes to low power consumption and requires less processing capability.

1.3 Organization of thesis

The thesis explains the multi-exposure laser speckle contrast imaging method and its study with laboratory-developed multi-tap charge modulation CMOS image sensor. It composed of six chapters.

Chapter 1 gives the introduction about the structure of the heart and microcirculation process and its importance. It discusses the background studies of micro-vascular blood flow, motivation and research objective of this study.

In Chapter 2, the theoretical study of laser speckle contrast imaging (LSCI) was discussed. The basic principle of speckle formation and its statistical properties of speckles are explained. The properties of time-varying speckle and expressions to calculate the speckle contrast are discussed. The mathematical expression is derived to extract flow speed of moving scatterers from the speckle contrast value. The general measuremernt setup of LSCI is explained and the essential parameters to define the speckle such as F/#, camera exposure time are discussed. The signal processing of speckle and its essential parameters are discussed.

In Chapter 3, multi-exposure laser speckle contrast imaging system with the multi-tap charge modulation CMOS image sensor originally developed in the laboratory for Time-of-flight (TOF) range imaging is discussed. The simple layout and the operation and timing chart of multi-tap charge modulation pixels are explained. The coded exposure pattern, equal exposure pattern and exponential exposure pattern are designed to implement with multi-tap charge modulator.

In Chapter 4, the verification of multi-tap charge modulation pixels was performed by simulating the reference high-speed camera data. The measurement setup and acquisition of raw speckle data with high-speed camera were explained. The simulation of exposure patterns with reference data and the comparison of its performance are discussed.

Chapter 5 explains the implementation of multi-exposure laser speckle contrast imaging with multi-tap charge modulation pixels. The flow speed measurement result with equal and exponential exposure pattern is discussed. The demonstration of flow map acquisition at a video-rate with a multi-tap pixel is discussed.

Chapter 6 gives the summary of this study and the main findings.

Bibliography

[1] G. N. Balaji, T. S. Subashini, and A. Suresh, “An efficient view classification of echocardiogram using morphological operations,” *J. Theor. Appl. Inf. Technol.*, vol. 67, no. 3, pp. 732–735, 2014.

[2] J. D. Briers, “Laser speckle contrast analysis (LASCA): a nonscanning, full-field technique for monitoring capillary blood flow,” *J. Biomed. Opt.*, vol. 1, no. 2, p. 174, 2006.

[3] C. J. Stewart, R. Frank, K. R. Forrester, J. Tulip, R. Lindsay, and R. C. Bray, “A comparison of two laser-based methods for determination of burn scar perfusion: Laser Doppler versus laser speckle imaging,” *Burns*, vol. 31, no. 6, pp. 744–752, 2005.

[4] M. Nagahara, Y. Tamaki, M. Araie, and H. Fujii, “Real-Time Blood Velocity Measurements in Human Retinal,” *Jpn. J. Ophthalmol.*, vol. 5155, no. 99, 1998.

[5] M. Richard and L. B. Boyd, “The Effect of High-Protein Diets on Coronary Blood Flow,” *Journal of Vascular Diseases.*, vol. 51, no. 10, pp. 817–826, 2000.

[6] S. M. S. Kazmi, A. B. Parthasarthy, N. E. Song, T. A. Jones, and A. K. Dunn, “Chronic imaging of cortical blood flow using Multi-Exposure Speckle Imaging,” *J. Cereb. Blood Flow Metab.*, vol. 33, no. 6, pp. 798–808, 2013.

[7] A. P. Pathak, A. Seifert, N. V. Thakor, A. Rege, and K. Murari, “Multiexposure laser speckle contrast imaging of the angiogenic microenvironment,” *J. Biomed. Opt.*, vol. 16, no. 5, p. 056006, 2011.

[8] F. Zappa *et al.*, “High-speed multi-exposure laser speckle contrast imaging with a

single-photon counting camera," *Biomed. Opt. Express*, vol. 6, no. 8, p. 2865, 2015.

[9] S. Sun, Y. Zhu, S. P. Morgan, D. He, and B. R. Hayes-Gill, "Multi-exposure laser speckle contrast imaging using a high frame rate CMOS sensor with a field programmable gate array," *Opt. Lett.*, vol. 40, no. 20, p. 4587, 2015.

[10] S. Sun, B. R. Hayes-Gill, D. He, Y. Zhu, N. T. Huynh, and S. P. Morgan, "Comparison of laser Doppler and laser speckle contrast imaging using a concurrent processing system," *Opt. Lasers Eng.*, vol. 83, pp. 1–9, 2016.

[11] M. Hultman, I. Fredriksson, M. Larsson, A. Alvandpour, and T. Strömberg, "A 15.6 frames per second 1-megapixel multiple exposure laser speckle contrast imaging setup," *J. Biophotonics*, vol. 11, no. 2, pp. 1–9, 2018.

Chapter 2

Overview of Laser Speckle Contrast Imaging (LSCI)

2.1 Introduction

The advancement of optical techniques has offered many promising possibilities to investigate the information about tissues [1]. Many optical methods have evolved over the years to study the microvascular blood flow. Most of the techniques uses the principle of random interference pattern also known as speckle pattern to obtain the blood flow speed information. The speckle pattern is usually generated by the backscattered light from the diffusive material and these generated speckle patterns are recorded by the detector. The detector used to observe the speckle patterns are Charge-Coupled Device (CCD) or Complementary Metal Oxide Semiconductor (CMOS). The most popular techniques based on the interference pattern to monitor the blood flow of microvascular structures are Laser Doppler Perfusion Imaging (LDPI) and Laser Speckle Contrast Imaging (LSCI). In this chapter, the general introduction and theoretical background about LSCI, the measurement requirements of LSCI and its transformation over the years to several blood flow studies are discussed.

LSCI is a commercialized optical technique to monitor the blood flow in micro blood vessels. It has an advantage of being a wide-field, non-contact optical technique to visualize the two-dimensional (2D) blood flow from the volume from which we are probing. The LSCI can reproduce the high spatial and temporal resolution images of the micro-vasculatures with simple optical setup.

2.2 Theoretical Background of Laser Speckle Contrast Imaging (LSCI)

The simple principle and easy implementation makes LSCI a useful tool in blood flow imaging. It is essential to understand the principle of laser speckle formation and the analysis of speckles, and most importantly to extract the flow speed of the moving scatterers from the generated speckle. And it is key to consider the experimental parameters which has the direct impact on the speckles. In this chapter, the general theoretical concept of laser speckle contrast imaging method and experimental setup and its essential parameter are discussed.

2.2.1 Speckle and its Statistical Properties

After the invention of laser in 1960's, the speckle generating from laser received the attention of researchers in the field of optics. At the earlier days, because of the speckle nature, it was termed as granularity. Speckles are generated, by the coherent of laser light sources. When a coherent laser light incident on the scattering surface which can be both static and dynamic, the backscattered light from the scattering medium produces the random interference pattern of bright and dark pixels called as speckles [2]. Based on the same principle, bio-speckles are formed, when the coherent laser light travels through the diffusing medium such as biological tissues, which consists of randomly distributed particles. The speckles generated are interfered on the camera's imaging plane by the scattering of light diffracted through the aperture of the camera. The speckle pattern generated are imaged on to the image sensor in the absence of lens are called as objective speckle pattern. In contrary, the use of lens to form the image on the detector are called as subjective speckles. The use of coherent and light with same wavelength is essential to

avoid the removal of speckles by averaging [3]. Fig. 2.1 shows the principle of speckle pattern formation on the detector. If the speckle pattern fluctuates over time due to the interaction with the moving scattering particle, it is called as dynamic speckle pattern. And the pattern does not change over the time, it is described as the static speckle pattern.

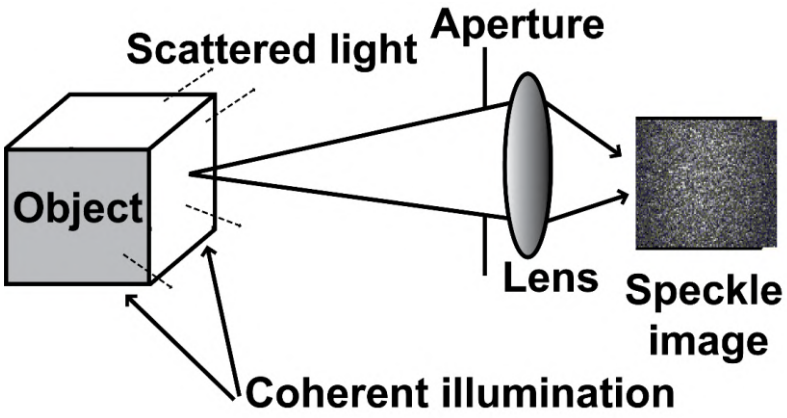

Fig. 2.1 Simplified schematic of laser speckle production

The bright spots of speckle formation are due to the reflected waves formed on the image sensor are in-phase in nature and dark speckles resulted of out-of-phase reflected waves. The conceptual diagram of speckle with bright and dark spots are shown in Fig. 2.2.

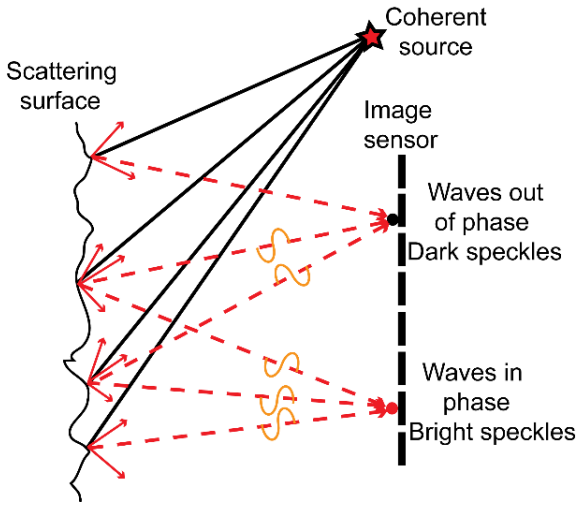

Fig. 2.2 Generation of speckle.

This phenomenon was considered as problematic, because it affects the resolution of the images spatially. Some of the researchers involved in studies to remove the speckles

from the images which obtained from laser illumination [4] [5]. At the same time, other group of researchers focused to analyze the speckle pattern and applied in several applications. One of the significant developments is, the evolution of laser speckle to support biomedical studies [6]. The laser speckles provide the essential information to monitors the blood perfusion level in microvascular structures.

Due to the random phase of the scattered waves interfering on the photodetector, the speckle pattern exhibits a property of spatial intensity in the random manner. Therefore, a proper way to explain the speckle pattern phenomenon is to use the statistics [7]. The first-order statistical analysis gives the amount of contrast the speckle exhibits and the size distribution of the speckles are given by second-order statistical analysis.

2.2.2 Time-varying Speckle

The speckle pattern tends to change, when the scatterers are moving. When the movement of the scatterers is small, the speckles remain correlated. Therefore, by analyzing the speckle changes, the information of the local moving scatterers can be extracted. For the particle with larger motions, the correlation between the speckles are less [8], which means the generated speckles "decorrelate" and the pattern of the speckle changes entirely over the exposure time. The phenomenon of fluctuation of speckles over time is known as "time-varying speckle" [9]. This appearance is frequently detected in laser illuminated living tissues and has been functional in biological studies. When the camera exposure time is in the order of fluctuation period of the moving particle, the reduction in the speckle contrast can be observed because of averaging of the speckle pattern. The most potential application time-varying speckles was first identified by Stern in 1975, when the fluctuations are caused by blood flow.

The concept of time-varying speckle is helpful to determine the speed of the moving scatterers by relating to the temporal fluctuation. If fluctuations are less over the time period, the particle movement is slow and the correlation time is long. The faster movement can be understood from the less correlation time and the fluctuations are more as shown in Fig 2.3.

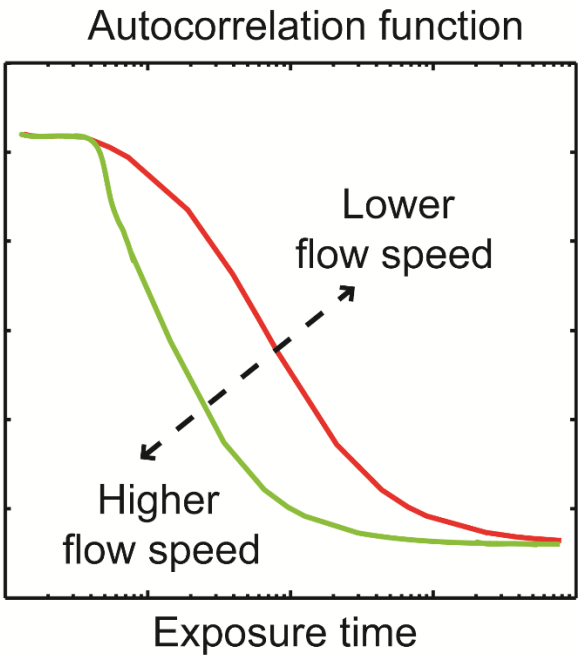

Fig. 2.3 Autocorrelation function of moving particle

2.2.3 Speckle Contrast

The first approach about the speckle contrast has been shown by Goodman. It is useful to interpret the dynamics of the biological signal. The intensity presented in the speckle pattern which is polarized can be described by its moments. Generally, the intensity of the speckle pattern exhibits exponentially distributed intensity probability density function (PDF). The n^{th} moment of the exponential distribution of the intensities is given by:

$$\langle I^n \rangle = n! \left(\frac{2}{\sigma^2} \right)^n , \tag{2.1}$$

The first, second moment and variance is given by:

$$\langle I \rangle = \frac{2}{\sigma^2} ; \quad \langle I^2 \rangle = 2\langle I \rangle ; \quad \sigma_s^2 = 2\langle I \rangle^2 - \langle I \rangle \tag{2.2}$$

The speckle contrast (K) is generally defined as the ratio between the standard deviation (σ_s) and the mean intensity ($\langle I \rangle$) of the pixel [10].

$$K = \frac{\sigma_s}{\langle I \rangle} \tag{2.3}$$

If the speckle pattern is developed fully without any averaging over the camera exposure time, the spatial standard deviation (σ_s) and spatial mean intensity ($\langle I \rangle$) are equal in manner. Therefore, the speckle contrast can achieve the maximum contrast value of 1. But in real conditions, the contrast is always lower than 1 and the speckle contrast value ranges from $0 \leq K \leq 1$ [17]. The properties of the speckle pattern are playing an essential role in the biomedical field for its application [11].

Therefore, by analyzing the relationship of statistical parameters, σ_s and I, for a developed speckle pattern, the amount of speckle contrast can be determined. The computation of speckle contrast is useful to quantify the amount of blurring. During the integration time of the camera, the speckle pattern will blur, if the scatterers are moving. Therefore, the sensitivity of the speckle contrast change depends on the exposure time and with the longer exposure time, the amount of relative changes in speckle contrast increases.

2.2.4 Extraction of Moving Particle Flow Speed

The moving scatter flow speed can be extracted from the measured contrast values (K), provided, the velocity distribution of the moving scatter is assumed. The speckle variance $\sigma_s^2(t)$ of the spatial intensity distribution in a time-averaged speckle pattern with an integration time T is linked to the autocovariance $C_t(\tau)$ of the temporal fluctuations. The relationship of speckle variance to the autocovariance is given by:

$$\sigma_s^2(T) = \frac{2}{T}\int_0^T \left(1 - \frac{\tau}{T}\right) C_t(\tau) d\tau \qquad 2.4$$

The intensity of the speckle tends to fluctuate over the time and it is defined as the autocovariance of the temporal fluctuations as follows:

$$C_t(\tau) = \langle [I(t) - \langle I \rangle_t] [I(t+\tau) - \langle I \rangle_t] \rangle_t \qquad 2.5$$

The intensity temporal autocorrelation function is given by:

$$g_2(\tau) = 1 + \frac{C_t(\tau)}{\langle I \rangle_t^2} \qquad 2.6$$

The second-order autocorrelation related with the first-order autocorrelation or electric field temporal autocorrelation function is given by Siegert relation:

$$g_2(\tau) = 1 + \beta|g_1(\tau)|^2 \quad 2.7$$

where β accounts for speckle averaging parameter. i.e. The loss of speckle contrast value because of the speckle size to pixel size ratio and the effect of polarization. From the above equation, the speckle contrast integrating over the range of exposure time (T) in the spatial area is given by:

$$K^2 = \frac{2\beta}{T}\int_0^T \left(1 - \frac{\tau}{T}\right)|g_1(\tau)|^2 \, d\tau \quad 2.8$$

From the derived equation, the speckle correlation time (τ_c) of the fluctuated intensities can be estimated. By assuming Lorentzian distribution function for the flow speed [12] [13],

$$g_1^{Lorentzian}(\tau) = \exp\left(-\frac{|\tau|}{\tau_c}\right) \quad 2.9$$

$$K^2_{Lorentzian} = \beta\left[\frac{1}{2x} + \frac{1}{2x^2}\,(\exp(-2x) - 1)\right] \quad 2.10$$

where $x = T/\tau_c$.

Alternatively, the electric field temporal autocorrelation function for Gaussian distribution is given by [10],

$$g_1^{Gaussian}(\tau) = \exp\left(\frac{-\tau^2}{\tau_c^2}\right) \quad 2.11$$

$$K^2_{Gaussian} = \frac{\beta\tau_c}{T}\left[\sqrt{2\pi}\,\mathrm{erf}\left(\frac{\sqrt{2}T}{\tau_c}\right) + \frac{\tau_c}{T}\left(exp\left(-\frac{2T^2}{\tau_c^2}\right) - 1\right)\right] \quad 2.12$$

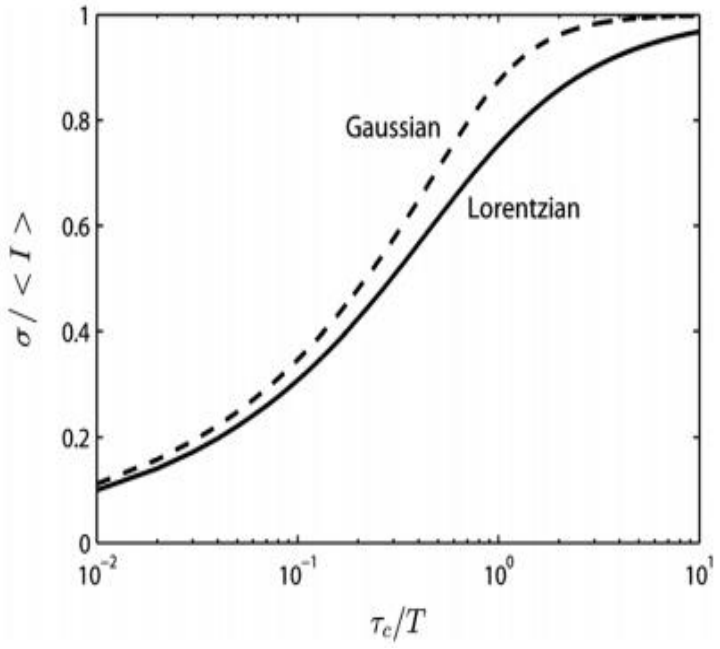

Fig. 2.4 Theoretical relationship between speckle contrast curve and ratio of correlation time to the exposure time for various distribution function. Adapted from [14]

The correlation time τ_c with the moving particles during the microvascular blood circulation is assumed to be inverse in relation. The measured contrast value *K*, which is the function of the exposure time *T*, fitted with derived speckle model can give the estimation of correlation time (τ_c). Then the velocity of the moving particles or the moving blood vessels is given by the following equation [15]:

$$v = \frac{\lambda}{2\pi\tau_c} \tag{2.13}$$

Where λ is the wavelength of the laser source.

2.3 Measurement and Signal Processing Requirements of Laser Speckle Contrast Imaging (LSCI)

The general measurement setup to perform laser speckle contrast imaging (LSCI) is depicted in Fig. 2.5. When a laser light which are coherent are illuminated on the moving sample, the back-scattered light from the sample are recorded by the detector.

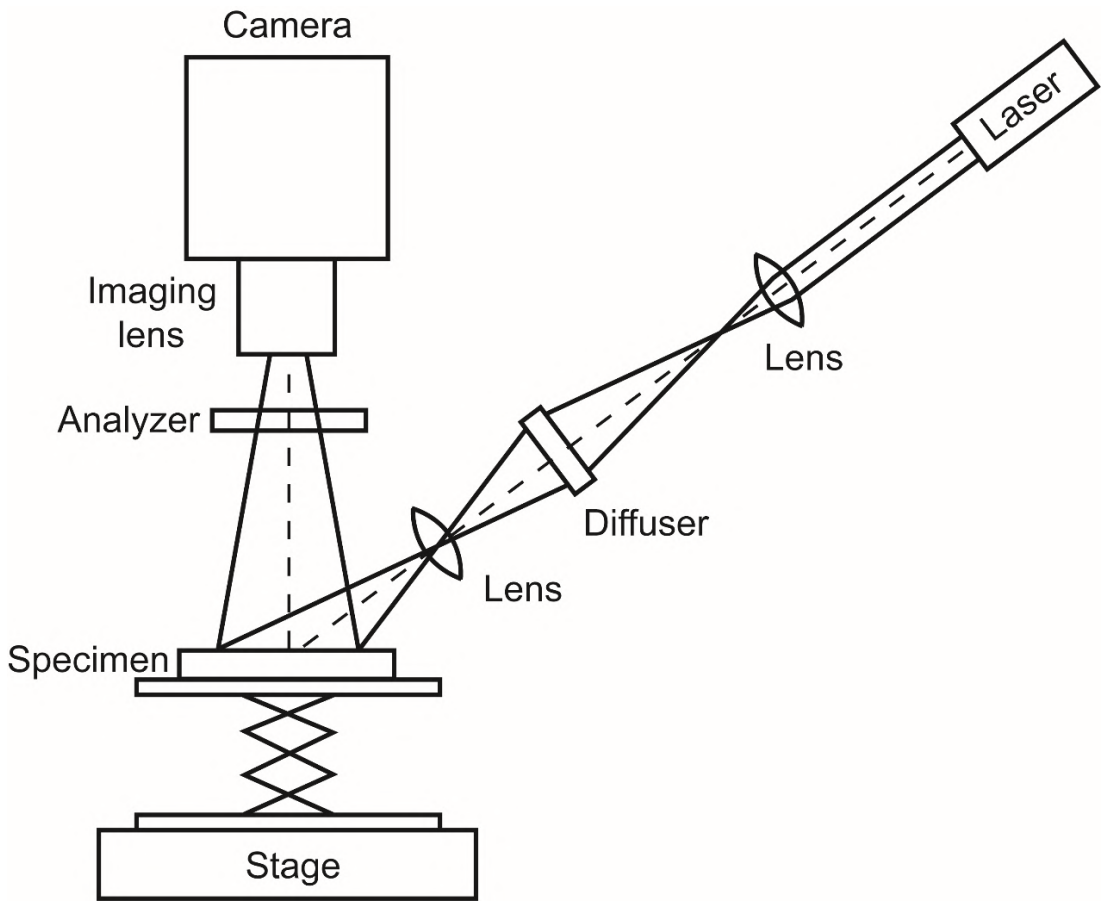

Fig. 2.5 Measurement setup of laser speckle contrast imaging

During the preparation of measurement setup, it is important to consider the parameters such as wavelength of the laser, the optimum F/# to achieve larger speckle size and suitable exposure time (T) in correspondence to the specimen used. The analyzer used to remove the non-scattered surface reflection of the laser illumination [16].

2.3.1 Window Size of Contrast Neighborhood

In the analysis of speckle contrast in the spatial domain, choosing the proper window size to compute is essential. Generally, the compute the speckle contrast K^2, the square window of N_{pixels} is used. The general window size used by the researchers to compute speckle contrast are 3×3, 5×5, or 7×7 pixels [17] [18]. From the square region of N_{pixels}, the variance and the mean pixel intensity values are estimated. There is trade-off always exists between choosing a window size and spatial resolution of the computed

images. The window with too few pixels are good for spatial resolution and the computation time also less. The larger window size will give the better estimation of contrast value, but it results in longer processing time to compute the flow speed distribution map and at the same time the spatial resolution is also sacrificed. The larger window size can be used in computation, when the camera gives the high resolution speckle images and in the case of spatial resolution of flow speed map is not so important. The two-dimensional (2D) contrast images and flow speed maps are obtained by moving the sliding window along the raw speckle images.

2.3.2 Selection of Neighborhood Schemes

The speckle raw images captured by the detector can be statistically analyzed by various neighborhood techniques. The general neighborhood scheme follows by various researchers, to obtain the contrast value as the function of the exposure time are as follows: Spatial Laser Speckle Contrast Analysis simplified as (sLSCI), Temporal Laser Speckle Contrast Analysis (tLSCI) and spatial-temporal domain Laser Speckle Contrast Analysis (stLSCI).

Brier and Webster proposed a method to compute the contrast in small region of pixels ($N \times N$ pixels). Spatial contrast is analyzed from many pixels in a single speckle image. The general equation of spatial contrast computation in raw speckle images is expressed as:

$$\mu^{s}_{(i,j,t)} = \frac{1}{N^2} \sum_{x=i-\frac{N-1}{2}}^{i+\frac{N+1}{2}} \sum_{y=j-\frac{N-1}{2}}^{j+\frac{N+1}{2}} I_{x,y,t} \qquad 2.14$$

$$K^{s}_{i,j,t} = \frac{\sqrt{\frac{1}{N^2} \sum_{x=i-\frac{N-1}{2}}^{i+\frac{N+1}{2}} \sum_{y=j-\frac{N-1}{2}}^{j+\frac{N+1}{2}} \left(I_{x,y,t} - \mu^{s}_{i,j,t}\right)^2}}{\mu^{s}_{i,j,t}} \qquad 2.15$$

where $\mu^{s}_{i,j,t}$ is the mean intensity value in the window with a central pixel in the coordinates (i, j, t), N is the size of the window, and $I_{x,\,y,\,t}$ is the intensity value in the respective coordinates. The window can be sliding or fixed. From these equations the contrast value,

$K^{s}_{i,j,t}$ can be extracted in association with the window centered at (*i*, *j*, *t*). In the case of sliding window, the pixels in the negative coordinates cannot be evaluated. The two possible solutions to evaluate the pixels in the negative coordinates are: 1) For the contrast analysis, the exclusion of the outer borders from the speckle image or 2) padding for the outer borders of the speckle images. The contrast value of the pixels in the boundary computed by the padding techniques and its size is given by (N-1)/2 rows and columns.

Fig. 2.6 (a) illustrates a spatial contrast (s-K), a window with size 3 × 3 pixels (red square) with a center pixel (black square) (*x*, *y*, *t*) = (*i*, *j*,1). Along the rows and columns (x-direction and y-direction), the s-K window is then moved to generate a contrast 2-D image and flow speed map. Although it is good for temporal resolution, it has the disadvantage of lack of spatial resolution.

To overcome this limitation, the another algorithm to produce the flow speed maps was proposed by Cheng *et al*. This algorithm is named as Temporal Laser Speckle Contrast Analysis and simplified as (t-K) and it is useful to improve the spatial resolution of the blood flow speed maps than spatial contrast analysis. The computation of speckle contrast in the temporal domain is based on one pixel in the set of frames (N-frames) captured at different time as shown in Fig. 2.6. (b).

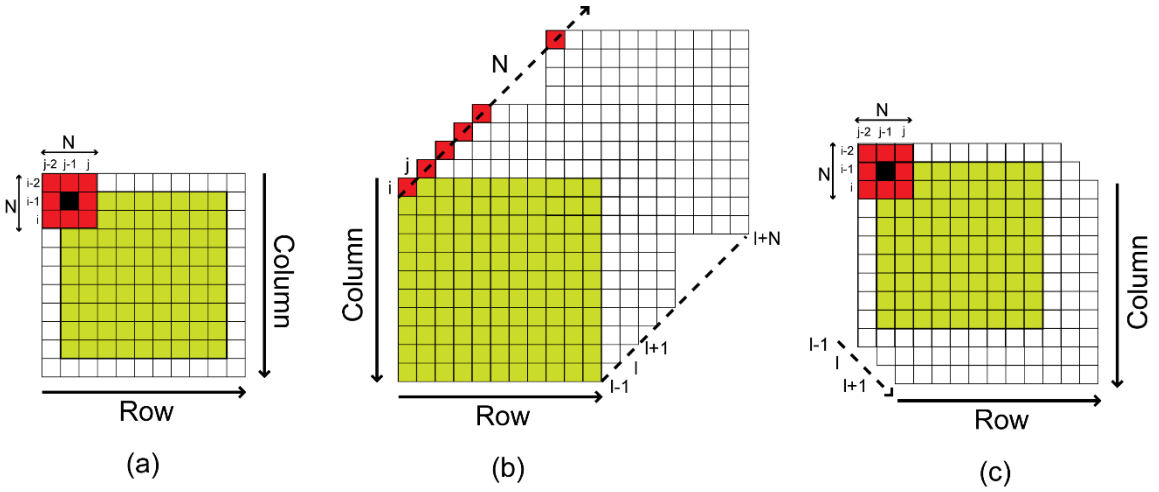

Fig. 2.6 Neighborhood techniques of laser speckle contrast imaging (a) Spatial contrast analysis (b) Temporal contrast analysis (c) Spatial-Temporal contrast analysis

The equation to compute the Temporal-contrast (t-K) is expressed as:

$$\mu^{t}_{(x,y,l)} = \frac{1}{N} \sum_{t=l-\frac{N}{2}}^{l+\frac{N}{2}} I(x,y,t) \qquad 2.16$$

$$K^{t}_{x,y,l} = \frac{\sqrt{\frac{1}{N} \sum_{t=l-\frac{N}{2}}^{l+\frac{N}{2}} \left(I_{x,y,t} - \mu^{t}_{x,y,l}\right)^2}}{\mu^{t}_{x,y,l}} \qquad 2.17$$

where $\mu^{t}_{(x,y,l)}$ is the mean in the temporal domain with central pixel in (x, y, l) and size 1 × 1 × N pixels, $K^{t}_{x,y,l}$ is the temporal contrast within this window. N is the number of frames used in the computation. The window is moves along in the temporal direction to compute the contrast value. Until the last frame, the operation repeats. At the same time, the window moves to the neighboring pixels to compute the contrast value in all pixels. The minimum number of frames (N) used for computation is 15 [19] and the maximum number of frames depends on the temporal resolution of the system, but some studies found it used up to 49 frames [20]. The t-K reduces temporal resolution where s-K reduces spatial resolution. It is important to choose the suitable algorithm. It was verified that t-K is suitable to estimate the estimate the flow speed even in the presence of static scatterers as compared to spatial contrast (s-K) [21]. In conclusion, t-K suitable for monitoring slow hemodynamics patterns which is in the range of seconds. While, t-K is not satisfactory to monitor fast hemodynamics, where temporal resolution may not be sufficient.

Another scheme is spatial-temporal contrast (st-K) the combination of both spatial and temporal algorithms, that can be used to compute the speckle contrast. The window to compute contrast is cubic in nature with size of 3 × 3 × 3 pixels and centered in the pixel (x, y, t) = (i, j, l). The different window can be applied in st-K and Duncan applied a window size of 3 × 3 × 15 (N_x, N_y, N_t) pixels. Temporally averaged spatial contrast (t_{avg}-sK) first calculates the contrast in the spatial domain and then average the calculated contrast value across a temporal domain. These operations are reversed in spatially averaged temporal contrast (s_{avg} -tK). By employing the combination of spatial and temporal algorithm, a tradeoff between the spatial and temporal can be solved.

2.3.3 Speckle Size

The most important thing to consider while modelling the laser speckle contrast imaging system is to consider the size of each speckle. The flow speed measured by laser speckle contrast imaging depends on the size of the speckle. The speckles contain the information of the moving scatterers. The pixel size of the detector (CCD or CMOS) has a finite unit pixel size. The averaging of speckle will occur, when the size of the speckle generated by the image sensor is smaller than the pixel size. It means, the number of speckles sampled by a single pixel in the spatial domain is more than one. It leads to reduction in the speckle contrast because of speckle averaging. Many parameters are contributing to the speckle size and the minimum speckle size is expressed as follows [22]:

$$d = 1.2\,(1 + M)(F/\#)\,\lambda \qquad 2.18$$

where d is the speckle size, M is the optical magnification of the system, λ is the wavelength of the laser source, F/# is the *f*-number of the lens used for imaging. The optical magnification depends on the focal length of the imaging lens. From the above expression, it is very clear that the important parameter which determines the speckle size is F/#. So, choosing the optimized f-number which gives the better speckle contrast value is crucial in LSCI. Fig. 2.7 shows the sampling of speckle in the spatial domain. The two images in the left shows, the pixel and speckle size are equal. The right two images show that a speckle is sampled by 2 or 4 pixels.

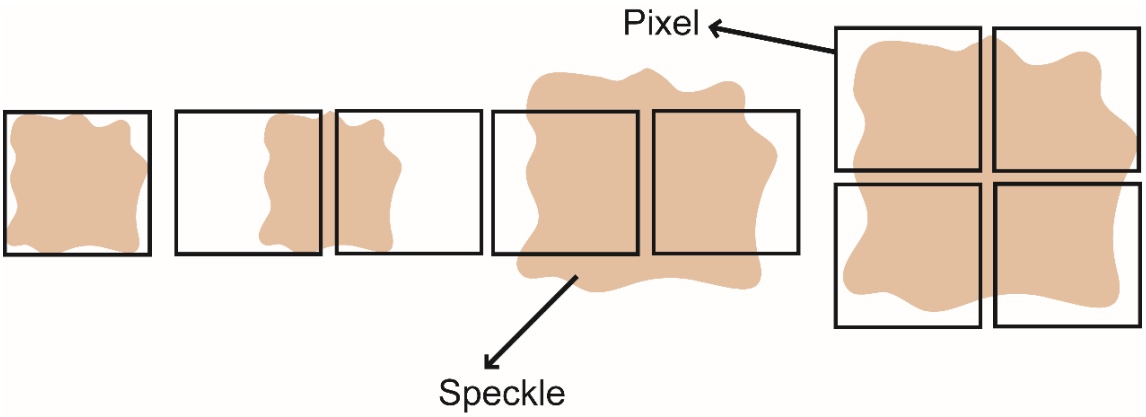

Fig. 2.7 Sampling of speckle in spatial domain

Many researchers have studied the influence of speckle size on the speckle contrast value [23]. Some studies suggest that the speckle size should be equal to the pixel size. Other studies show that the speckle size should be at least twice the pixel size. In other words, it should satisfy the Nyquist sampling criterion, because speckle size under the Nyquist limit can produce the aliasing effect, and leads to reduction in the speckle contrast value by 30%. However, the results suggest that the speckle contrast value keep on increasing for larger speckle size. There is a trade-off existing between the speckle size and spatial resolution. Because the increase in the speckle size means, only fewer speckles are present in the same pixel area. Therefore, increasing the speckle size produces a disadvantage of reducing the spatial resolution of the raw speckle image.

2.3.4 Effect of Static Scattering

The speckle models discussed earlier are based on some assumption and it does not include the presence of static scatterers in the scattering medium it observes. However, static scatterers will produce a speckle contrast component that remains constant when the imaging system exposure time increases. The laser light that is back-scattered by the static scatterers can underestimate the dynamics of the flowing system. That is, the amount of speckle contrast value increases [24]. In the initial researches, the static scatterers has not considered, but recently the researchers started to account of static scatter components. The first instance of inclusion of static scatterers has been given by Parthasarathy *et al.* and Zakharov *et al* [25]. They presented a new speckle model to compute the correlation time (τ_c) with increased accuracy. Therefore, the underestimation of the dynamic value of the flow system has been eliminated. By including the presence static scatter components, the electrical field that detected by the detector can be modified as follows. The electric field is equal to sum of photons scattered by static scatterers and dynamic scatterers.

$$E(t) = E_d(t) + E_s \tag{2.19}$$

where $E_d(t)$ is the electrical field back-scattered by dynamic scatterers and E_s is the electrical field back-scattered by static scatterers, and the static scatterers does not change with time [20], [24]. The updated intensity autocorrelation function can be expressed as:

$$g_2(\tau) = 1 + \beta\,[(1-\rho)^2\,|g_{1d}(\tau)|^2 + 2\rho(1-\rho)|g_{1d}(\tau)| + \rho^2] \tag{2.19}$$

where $g_{1d}(\tau)$ is the electric field autocorrelation function and ρ is the fraction of light that is scattered by static components, and ρ can be expressed as: $\rho = I_s / (I_s + I_d)$. I_s represents static scattered intensity and I_d is dynamic scattered intensity. Inverse notation of ρ also found in some studies. For example, several researchers used to define ρ as the dynamic fraction of scattered light.

The application of the Siegert relation to the intensity autocorrelation function yields to the modified field autocorrelation function.

$$g_{1m}(\tau) = (1-\rho)|g_{1d}(\tau)| + \rho \qquad 2.20$$

The new speckle model that is used to estimate the accurate correlation time (τ_c) by including the effect of static scatterers is expressed as:

$$K^2_{Lorentzian} = \beta\rho^2 \frac{e^{-2x}-1+2x}{2x^2} + 4\beta\rho(1-\rho)\frac{e^{-x}-1+x}{x^2} \qquad 2.21$$

The speckle model which considers the Gaussian velocity distribution function can be expressed as follows:

$$K^2_{Gaussian} = \beta\rho^2 \frac{e^{-2x^2}-1+\sqrt{2\pi}xerf(\sqrt{2x})}{2x^2}\ 2\beta\rho(1-\rho)\frac{e^{-x^2}-1+\sqrt{\pi}xerf(x)}{x^2} \qquad 2.22$$

Nadort *et al.* included an additional term that can quantify the amount of noise present in the speckle system (v_{noise} or C_{noise}). In practice, the v_{noise} is equal to the minimum speckle contrast (K_{min}) that the speckle system can produce. In general, K_{min} can be obtained during speckle experiments by measuring fast moving scatterers. K_{min} is independent of exposure time of the camera and it is constant for different exposure time. It is suggested to add the noise term in the speckle model to estimate the τ_c from the speckle contrast value which contains the flow speed information.

Ramirez *et al.* proposed another speckle model to estimate the τ_c from the speckle contrast value that includes the effect of static scatterers by assuming a Gaussian velocity profile for the moving blood cells. They modelled the speckle equation as:

$$K^2_{Gaussian} = \alpha\left[\sqrt{\frac{1}{M}}\,\mathrm{erf}\left(\sqrt{\pi M}\right) - \left(\frac{1}{\pi M}\right)\left(1 - e^{(-\pi M)}\right)\right] \times \left[\rho^2\,\frac{e^{-2x} - 1 + 2x}{2x^2} + 4\rho(1-\rho)\,\frac{e^{-x} - 1 + x}{x^2} + (1-\rho)^2\right] + v_{noise}$$

2.23

where M = A_D/A_C, A_D is the sensitive area in the detector, A_C is the speckle size on the detector, α is consider as the normalization constant that includes speckle averaging parameter which reduces the estimation in the speckle contrast value due to the polarization effect and spatial sampling of the speckle that forms in the detector.

2.3.5 Choosing Camera Exposure Time

The another important parameter in the laser speckle imaging system, which plays a crucial role in the estimation of flow speed (*v*) is the camera exposure time (*T*). It is essential to choose an optimal exposure time to estimate the relative changes in blood flow [26]. The exposure time that is too short (< 1ms) too long (> 50ms) will introduce noise or signal level make saturated [27]. The single exposure time is not sensitive to wide range of flow speeds. This is the primary reason; the single-exposure laser speckle imaging is not suitable for wide range of flow speed. Because of the flow insensitivity, the single-exposure has been advanced to multi-exposure laser speckle imaging systems (MELSCI). Therefore, always a trade-off exists between choosing an exposure time and estimating the flow speed. For example, shorter exposure time (T) is more suitable for fast-moving scatterers. Because, the speckles get blurred at fast moving particle. In other words, the correlation time (τ_c) is less. So shorter exposure time (*T*) is good enough to extract the moving scatterers information. The use of longer exposure time for fast moving particle means, the generated speckles will average out and it becomes insensitive to the flow speed changes. In contrary, longer exposure time is more suitable for slow flow speed. When the exposure time is short, the slow moving particle does not have sufficient time to observe the speckle movement. So it becomes insensitive to the different flow speeds and estimation becomes flat. In conclusion, longer exposure time is more suitable for slow speed and vice versa. It is obvious that laser speckle contract imaging technique is exposure-time dependent.

In general, the absolute sensitivity (S_a) and relative sensitivity (S_r) are the parameters to choose an optimal exposure time. Sa is defined as the changes in speckle contrast value to unit change in flow speed and it is useful for the system to achieve high signal-to-noise-ratio. The absolute sensitivity can achieve the maximum value, when the camera exposure time (T) is in the order of correlation time (τ_c) of the moving particle ($T \sim \tau_c$). When T > τ_c, the S_a start to reduce as the exposure time (T) increases as shown in Fig. 2.8 (a). S_a can be expressed as follows [28]:

$$S_a = \left|\frac{dK}{dv}\right| \propto -\tau_c x \frac{dK}{d\left(\frac{T}{\tau_c}\right)} = -\tau_c x \frac{dK}{dx} \qquad 2.24$$

$$S_a = \tau_c \frac{r}{2K}\left[\frac{1}{2x^2} - \frac{(2x+1)}{2x^2}e^{-2x}\right] \qquad 2.25$$

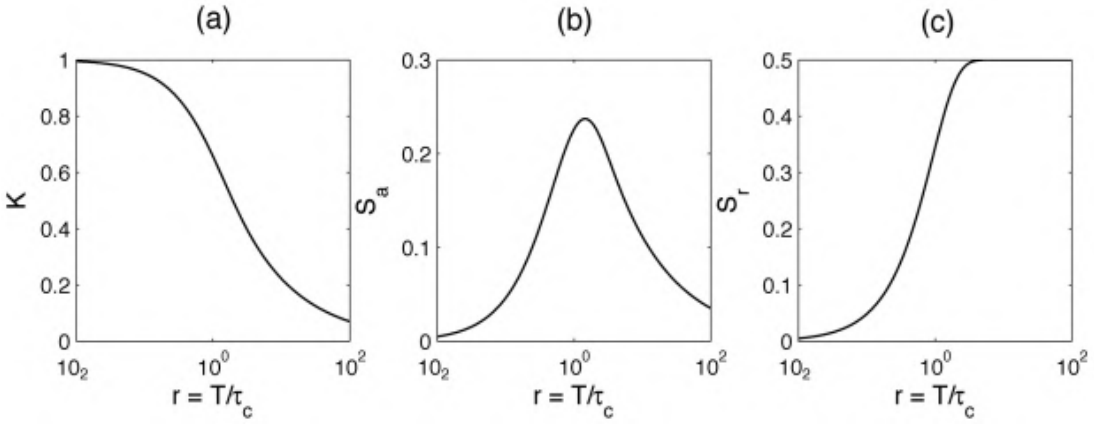

Fig. 2.8 (a) Theoretical speckle contrast curve (b) (c) Absolute and Relative sensitivity plot to the ratio of exposure time to the correlation time. Adapted from [28]

Another parameter which is used to monitor the blood flow changes with higher sensitivity is relative sensitivity (S_r). It is defined as the ratio of relative change in the speckle contrast to the relative change in flow speed and it is expressed as follows:

$$S_r = \left|\frac{\frac{dK}{K}}{\frac{dv}{v}}\right| = -\frac{\frac{dK}{K}}{\frac{dx}{x}} = -\frac{x}{K}\frac{dK}{dx} \quad 2.26$$

$$S_r = \frac{1}{2K^2}\left[\frac{1}{2x} - \frac{(2x+1)}{2x}e^{-2x}\right] \quad 2.27$$

The optimal exposure time (long), will give the better Sr. Therefore, choosing an optimal exposure time is essential to image the blood flow speed of vessels.

Bibliography

[1] J. Rutering *et al.*, “Optical methos for quantitative and lable-free sensing in living human tissues: principles, techniques and applications,” HHS Public Access., vol. 5, no. 6, pp. 1–8, 2016.

[2] L. Allen and D. G. C. Jones, “An analysis of the granularity of scattered optical maser light,” *Phys. Lett.*, vol. 7, no. 5, pp. 321–323, 1963.

[3] J. W. Goodman, “Statistical properties of laser speckle patterns,” Techincal report no. 2303-1., pp. 9–75, 2007.

[4] J. Maycock, B. M. Hennelly, J. B. Mcdonald, A. Castro, and T. J. Naughton, “discrete Fourier filtering,” *America (NY).*, vol. 24, no. 6, pp. 1617–1622, 2007.

[5] C. Y. Chen, W. C. Su, C. H. Lin, M. De Ke, Q. L. Deng, and K. Y. Chiu, “Reduction of speckles and distortion in projection system by using a rotating diffuser,” *Opt. Rev.*, vol. 19, no. 6, pp. 440–443, 2012.

[6] Y. Aizu and T. Asakura, “Bio-speckle application blood flow,” *Opt. Laser Technol.*, vol. 23, no. 4, 1991.

[7] D. D. Duncan, S. J. Kirkpatrick, and R. K. Wang, “Statistics of local speckle contrast,” *J. Opt. Soc. Am. A*, vol. 25, no. 1, p. 9, 2007.

[8] R. Bonner and R. Nossal, “Model for laser Doppler measurements of blood flow in tissue,” vol. 20, no. 12, pp. 2097–2107, 1981.

[9] J. D. Briers, “Laser Doppler, speckle and related techniques for blood perfusion mapping and imaging,” *Physiol. Meas.*, vol. 22, no. 4, 2001.

[10] D. D. Duncan and S. J. Kirkpatrick, “Can laser speckle flowmetry be made a quantitative tool?,” *J. Opt. Soc. Am. A*, vol. 25, no. 8, p. 2088, 2008.

[11] J. D. Briers, “Laser speckle contrast analysis (LASCA): a nonscanning, full-field technique for monitoring capillary blood flow,” *J. Biomed. Opt.*, vol. 1, no. 2, p. 174, 2006.

[12] A. Nadort, R. G. Woolthuis, T. G. van Leeuwen, and D. J. Faber, “Quantitative laser speckle flowmetry of the in vivo microcirculation using sidestream dark field microscopy,” *Biomed. Opt. Express*, vol. 4, no. 11, p. 2347, 2013.

[13] W. J. Tom, X. Zhang, A. Gopal, A. B. Parthasarathy, and A. K. Dunn, “Robust flow measurement with multi-exposure speckle imaging,” *Opt. Express*, vol. 16, no. 3, p. 1975, 2008.

[14] D. Briers *et al.*, “Laser speckle contrast imaging: theoretical and practical limitations,” *J. Biomed. Opt.*, vol. 18, no. 3, 2013.

[15] J. D. Briers, “Laser Speckle Contrast Imaging for measuring Blood Flow,” *Biomed. Appl. Light Scatt.*, vol. XXXVII, no. 1, 2007.

[16] P. G. Vaz, A. Humeau-Heurtier, E. Figueiras, C. Correia, and J. Cardoso, “Laser Speckle Imaging to Monitor Microvascular Blood Flow: A Review,” *IEEE Rev. Biomed. Eng.*, vol. 9, pp. 106–120, 2016.

[17] A. Humeau-Heurtier, P. Abraham, and G. Mahe, “Linguistic analysis of laser speckle contrast images recorded at rest and during biological zero: Comparison with laser doppler flowmetry data,” *IEEE Trans. Med. Imaging*, vol. 32, no. 12, pp. 2311–2321, 2013.

[18] A. K.Dunn, H. Bolay, M. A. Moskowitz, and D. A. Boas, “Dynamic laser speckle imaging of cerebral blood flow.,” *Opt. Express*, vol. 17, no. 16, pp. 13904–17, 2009.

[19] H. Cheng and T. Q. Duong, “Simplified laser-speckle-imaging analysis method and its application to retinal blood flow imaging,” vol. 32, no. 15, pp. 2188–2190, 2007.

[20] M. Draijer, E. Hondebrink, T. Van Leeuwen, and W. Steenbergen, “Review of laser speckle contrast techniques for visualizing tissue perfusion,” *Lasers Med. Sci.*, vol. 24, no. 4, pp. 639–651, 2009.

[21] H. Cheng, Y. Yan, and T. Q. Duong, "Temporal statistical analysis of laser speckle images and its application to retinal blood-flow imaging," vol. 185, no. 2, pp. 974–981, 2013.

[22] A. Fuentes-Garcia, J. C. Ramirez-San-Juan, N. Salazar-Hermenegildo, B. Choi, R. Ramos-Garcia, and E. Mendez-Aguilar, "Effects of speckle/pixel size ratio on temporal and spatial speckle-contrast analysis of dynamic scattering systems: Implications for measurements of blood-flow dynamics," *Biomed. Opt. Express*, vol. 4, no. 10, p. 1883, 2013.

[23] O. Thompson, M. Andrews, and E. Hirst, "Correction for spatial averaging in laser speckle contrast analysis," *Biomed. Opt. Express*, vol. 2, no. 4, p. 1021, 2011.

[24] D. A. Boas and A. K. Dunn, "Laser speckle contrast imaging in biomedical optics," *J. Biomed. Opt.*, vol. 15, no. 1, p. 011109, 2010.

[25] P. Zakharov, A. C. Voelker, A. Buck, B. Weber, and F. Scheffold, "Quantitative modeling of laser speckle imaging," vol. 31, no. 23, pp. 3465–3467, 2006.

[26] J. C. Ramírez-San-Juan, Y. C. Huang, N. Salazar-Hermenegildo, R. Ramos-García, J. Muñoz-Lopez, and B. Choi, "Integration of image exposure time into a modified laser speckle imaging method," *Phys. Med. Biol.*, vol. 55, no. 22, pp. 6857–6866, 2010.

[27] J. Senarathna, A. Rege, N. Li, and N. V. Thakor, "Laser speckle contrast imaging: Theory, instrumentation and applications," *IEEE Rev. Biomed. Eng.*, vol. 6, no. 01, pp. 99–110, 2013.

[28] S. Yuan, A. Devor, D. A. Boas, and A. K. Dunn, "Determination of optimal exposure time for contrast imaging," *Appl. Opt.*, vol. 44, no. 10, pp. 1823–1830, 2005.

Chapter 3

Multi-Exposure Laser Speckle Contrast Imaging with Multi-tap Charge Modulation CMOS Image Sensor

3.1 Introduction

Multi-Exposure Laser Speckle Contrast Imaging (MELSCI) started to advance in clinical and research studies because it offers the advantage of simple optical setup to implement. It has been applicable in the field of retinal imaging, cerebral blood flow imaging, tissue perfusion imaging. In the earlier days, the single exposure images were in practice to reproduce the blood flow imaging. But, Laser Speckle Contrast Imaging (LSCI) has the disadvantage of limited flow sensitivity. Since LSCI is an exposure time-dependent technique, the use of single exposure time does not good enough to provide an accurate estimation of blood flow over the wide range. Later, LSCI started to use multiple-exposure technique which is called as Multi-Exposure LSCI. It utilizes the images acquire at multiple exposure time to extract the blood flow information.

The simplified framework of MELSCI system is depicted in Fig. 3.1. A stack of raw speckle images was captured by a detector when the coherence laser light illuminates the tissue surface. The raw speckle images are processed to generate the

contrast images. The speckle contrast is a function of exposure time (T) and tends to decrease with increase in T. The speckle contrast obained at different exposure is fitted with speckle model to obtain the correlation time (τ_c). Finally, the speckle images are converted to velocity flow maps ($1/\tau_c$) to indicates the relative flow speed.

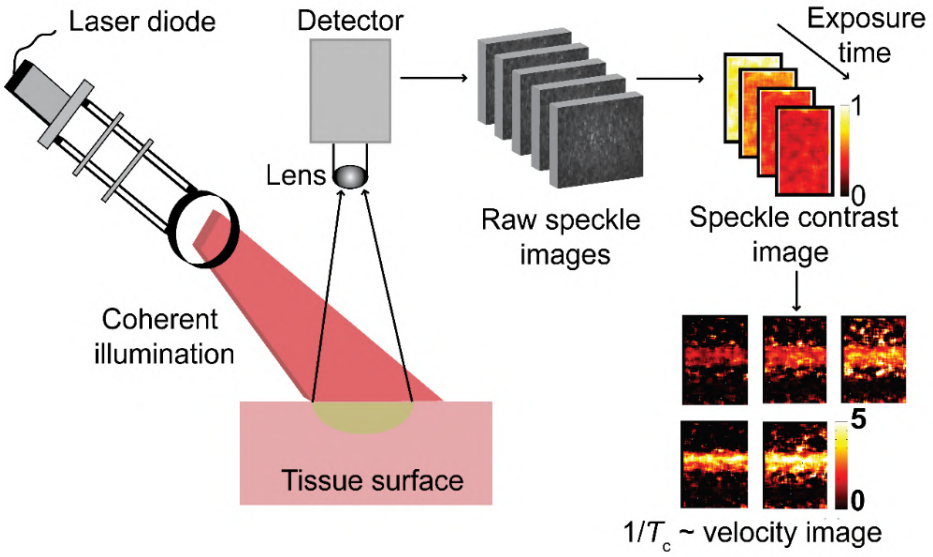

Fig. 3.1. Framework of multi-exposure laser speckle contrast imaging

Table. 3.1 Comparison of proposed MELSCI with a conventional system

Recent Trends in MELSCI	**Proposed MELSCI**
High-speed camera for blood flow studies	Multi-tap charge modulation CMOS image sensor
Frame Rate: 1kfps Detect speckle change and monitor blood flow at high frame-rate	1) Detect speckle movement at a high modulation frequency 2) Readout the images at about the video rate (**~30fps**)
Limitation: 1) Requires huge processing capability 2) Not energy efficient	**Advantages:** 1) Elude the redundant sampling data points to monitor blood flow.

The MELSCI system in the recent days uses the high-speed camera to observe the blood flow changes. But the high-frame rate sensor has the requirement of huge processing power and cost inefficient due to large hardware setup. These limitations are overcome by multi-tap sensor which can monitor flow changes at video rate.

3.2 Multi-tap Charge Modulation CMOS Image Sensor

3.2.1 4-tap Pixel and its Operation

The computation of captured image is more challenging than performing the image acquisition. To achieve the computational features with low power, some image sensors started to use memory-in-pixel scheme [1]. A pixel with multiple analog memories are called as multi-tap or multi-bucket pixel. The operation of charge modulation and readout of multi-tap pixels is different from that of a conventional sensor. In conventional sensor, the acquisition of frames is performing sequential in manner. But in multi-tap pixels, the photo-generated charges in the photodiode (PD) are transferred and accumulated in the pixel-in memory. By this approach, the charge modulation and readout operations are performed separately. So that, multiple frames can be acquired simultaneously.

The concept of Multi-tap or multi-bucket CMOS image sensors are applied in this paper to elude the redundancy of sampling data points and to bridge the gap between 30fps and 1000fps while not suffering from inter-frame delay in exposure [2] [3]. A lateral electric field charge modulator (LEFM) developed at Shizuoka University is capable of implementing a pixel with multiple pieces of charge storage and has advantages such as high-speed and loss-less complete charge transfer and suppressed charge back-flow from the storage to the photodiode. Lateral-Electric-Field Charge Modulators, so-called LEFM, is possible to realize high-speed charge transfer, and easy to implement multiple taps. To simplify the explanation of LEFM, two-tap LEFM with a Drain, at first is explained. It is shown in Fig. 3.2.

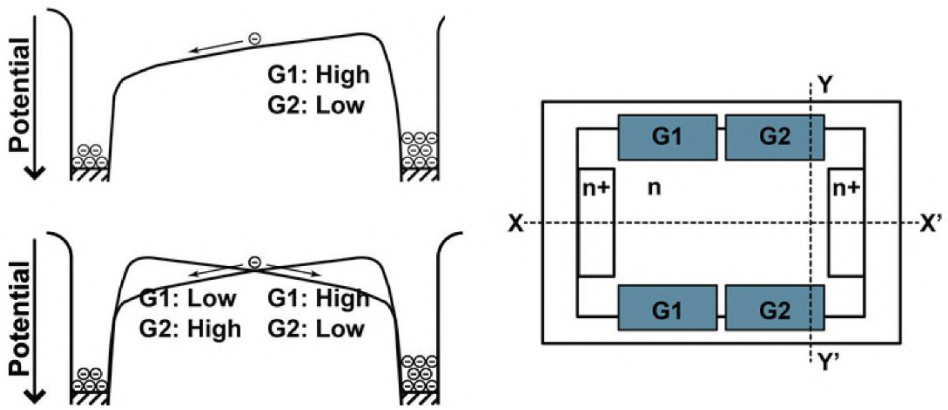

Fig. 3.2. Basic operation of the two-tap LEFM

The principle of the two-tap modulator is presented by our group at IISW 2013 [4]. The basic principle of the LEFM is used in the laboratory-developed four-tap pixel structure. In two-tap modulator, three sets of gates G1 and G2 are used for controlling electric field of Y-Y' direction as in Fig. 3.2. By changing the applied voltage of the gate, the potential of the photodiode is also changed. By using these potential change of photodiode, the electric field is controlled and the charge generated in photodiode can be transferred at very high speed. And when applying a high potential to the gate, leakage from channel to gate does not occur. For example, when G1 is HIGH and G2 is LOW, photoelectrons generated in the aperture region to be transferred to the left side. when G2 is HIGH and G1 is LOW, photoelectrons generated in the aperture region to be transferred to the right side. By using this technique, multiple-tap LEFM for TOF Range Image Sensor was developed in the laboratory. We utilized the laboratory-developed multi-tap charge modulation pixels [5], [6] [7] to build the MELSCI system to monitor the flow speed changes of the moving scatterers at about the video rate.

Fig. 3.3 and Fig. 3.4 shows an example of layout, equivalent schematic, and timing chart of 4-tap pixel based on LEFM. The pixel of this image sensor consists of photodiode (PD), four charge storage diodes (FD1-4) and drain. Although the charge storage is embodied as a floating diffusion (FD) in this figure, two-step charge transfer structures to suppress reset noise have been developed [8] [9]. The photo-generated charges in the PD are quickly transferred to one of the storage diodes and the drain by the 5 sets of controllable gates (G1-4 and GD).

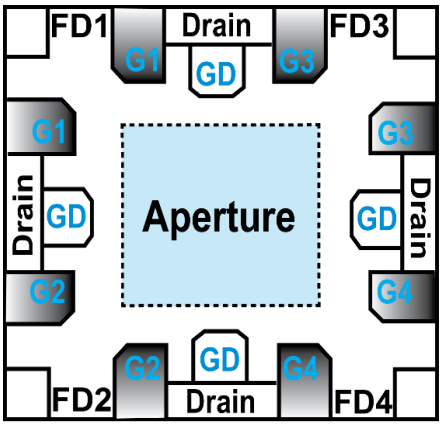

Fig. 3.3. A layout of 4-tap charge modulation pixels

While G1 is activated and the other gates are deactivated, the photoelectrons generated in the photodiode region are transferred to FD1. This operation is repeated for the gates G2, G3 and G4 and the charges are integrated into the corresponding FDs. Thus, arbitrary exposure is implemented by programming the GX (X = 1-4) signals. GD is a gate which drains the charges in the photodiode. During the image readout, the photo-charges should not be transferred to any FD, so that GD is activated and the other gates are deactivated. This image sensor can sample the charges efficiently at the higher modulation frequency than video rate to detect rapid fluctuation in speckle movement and read out the images for different exposures simultaneously at around the video rate. In other words, the four images for sub-frame exposures, which are programmable, are read out. Because there is no dead time during the charge modulation, the problem of inter-frame delay does not occur.

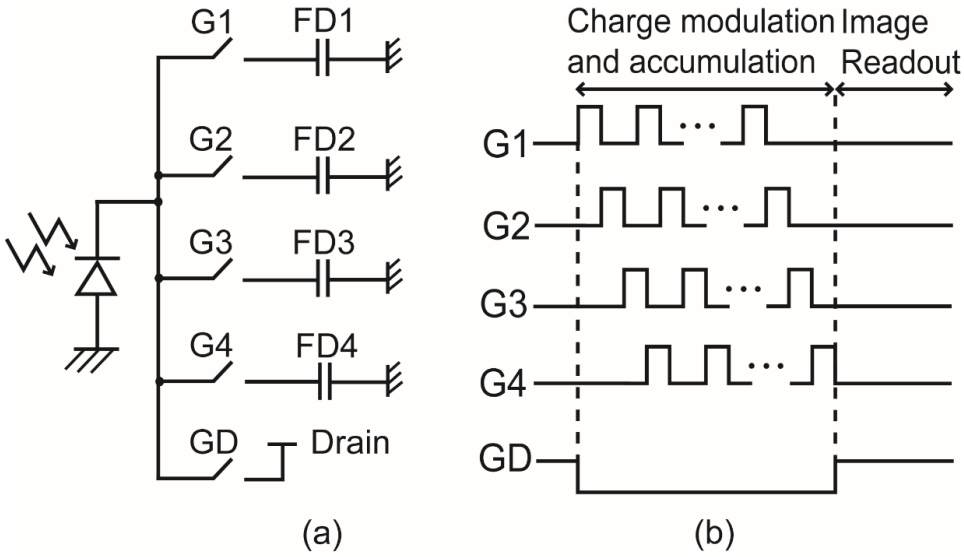

Fig. 3.4. A schematic diagram and operation timing chart of 4-tap pixel

3.2.2 Specifications of Multi-tap Sensor

The prototype chip with the 4 sets of charge modulator developed in our laboratory is used for this study [10]. The chip is fabricated in Dongbu HiTek 0.11um 1P4M CIS technology and the chip size is 9.3 × 7 mm^2. The unit size of the modulator is 11.2 × 11.2 um^2. In a unit pixel, 2 × 2 modulators are implemented, and those FDs are connected in parallel. The 4- tap pixel outputs are connected in parallel to 4 column ADCs each of which is 5.6 μm pitch. The entire chip consists of an array size of 132 × 84 pixels. The unit pixel size is 22.4 × 22.4 um^2. A single consists of 4 tap images. Therefore, to generate a flow map, 4 tap images are necessary.

Table. 3.2 Specification of 4-tap sensor

Process	Dongbu HiTek 0.11μm 1P4M CIS
Chip size	9.3 mm (H) × 7 mm (V)
Power supplies	1.5 V (Digital), 3.3 V (Analog, Digital)
Resolution	132 (H) × 84 (V)
Pixel size [μm^2]	22.4 × 22.4
Modulator size [μm^2]	11.2 × 11.2
ADC	Column-parallel folding integration/ Cyclic ADC
# of tap to make Flow map image	1 frame 4-tap

3.3 Exposure Patterns for 4-tap pixels

3.3.1 Coded Exposure Pattern

The coded exposure pattern designed for multi-tap CMOS image sensor to readout the images at about the video rate. The method is to have the same total accumulation time for all taps (G1-4) but variable effective exposure time for each tap. The ideology behind this pattern is to achieve the equal photon shot noise in each tap, effectively. By employing this pattern, the brightness of the raw speckle images obtained at different exposure time is identical. Therefore, the speckle contrast obtained from the different exposure time can be evaluated in the same light condition. A pixel value using a coded exposure pattern for tap-*i* is expressed in the following equation:

$$G_i = \sum p_i(t) \times w_i(t) \qquad 3.1$$

$$w_i(t) = \{0 \; or \; 1$$

where G_i is a pixel value at a tap-*i*. $p_i(t)$ and $w_i(t)$ are the generated charges in the photodiode at time *t* and a time window function for tap-*i*, respectively. The window

functions are shown is shown in Fig. 3.5. The effective exposure time is defined by the period from the beginning of the pulses to the end of the pulses. The duty ratio becomes smaller for longer exposure time to realize the equal photon shot noise at each tap.

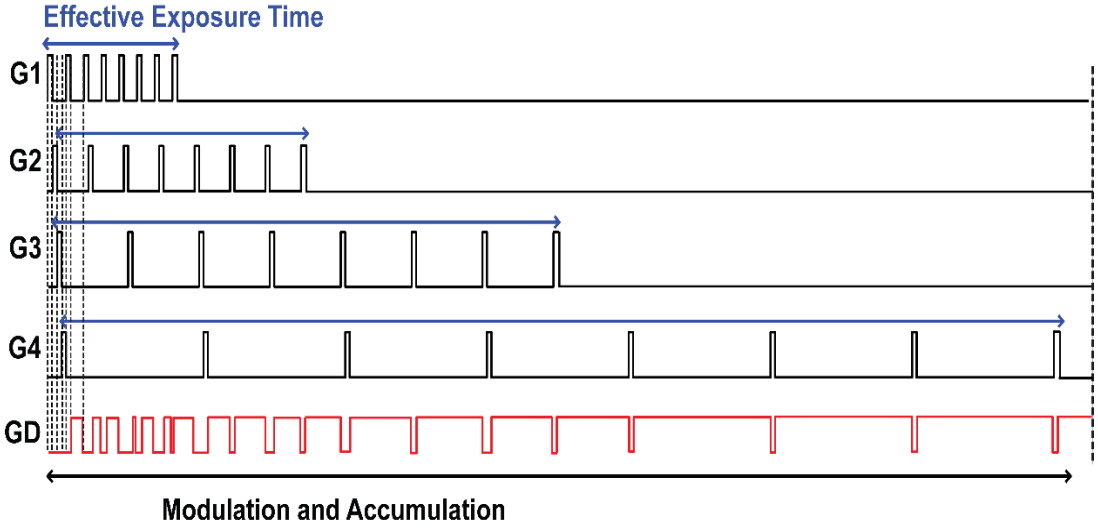

Fig. 3.5. Coded shutter pattern

The proposed coded shutter pattern has the advantage of equal photon shot noise for different effective exposure time. The multiple exposure time can be implemented without the need for the acoustic optical modulator. This pattern is also useful to readout the images of multiple exposure time at about the video rate and it can contribute to achieve a low power sensor. However, there is a drawback of not energy efficient, since only a part of the light is used to observe the speckle movement.

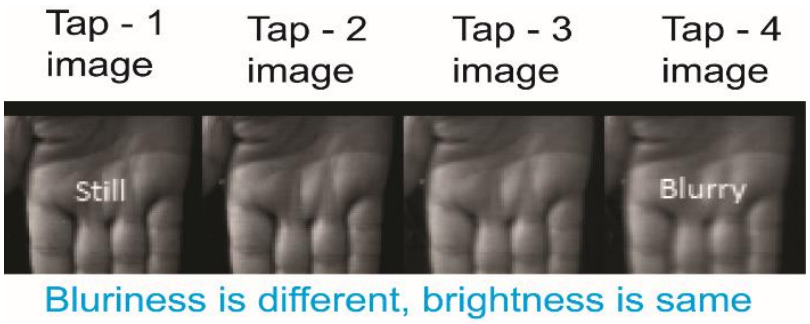

Fig. 3.6. Example of a captured image of moving hand

The example of the moving hand captured with 4-tap sensor is shown in Fig. 3.6. The exposure time in tap 1 and tap 4 are shortest and longest exposure time, respectively. The shortest and longest exposure time gives the still and blurry image, respectively. Because the contrast value is dependent on the exposure time.

3.3.2 Equal and Exponential Exposure Pattern

The equal and exponential exposure patterns designed for laboratory developed multi-tap charge modulation pixels are depicted in Fig. 3.7. and Fig. 3.8, respectively. Its efficiency to monitor the blood flow changes are explained. The unit exposure time or shortest exposure time to capture an image from each tap is represented by T_0. The ratio of exposure time between each tap is designed in the way of equal and exponential in nature. In other words, the ratio of shortest to longest exposure time is 1:4 (equal pattern) and 1:8 (exponential pattern). A frame is composed of four exposure images together. The effective exposure times are synthesized in offline mode with four images that are obtained with the exposure patterns G1-4.

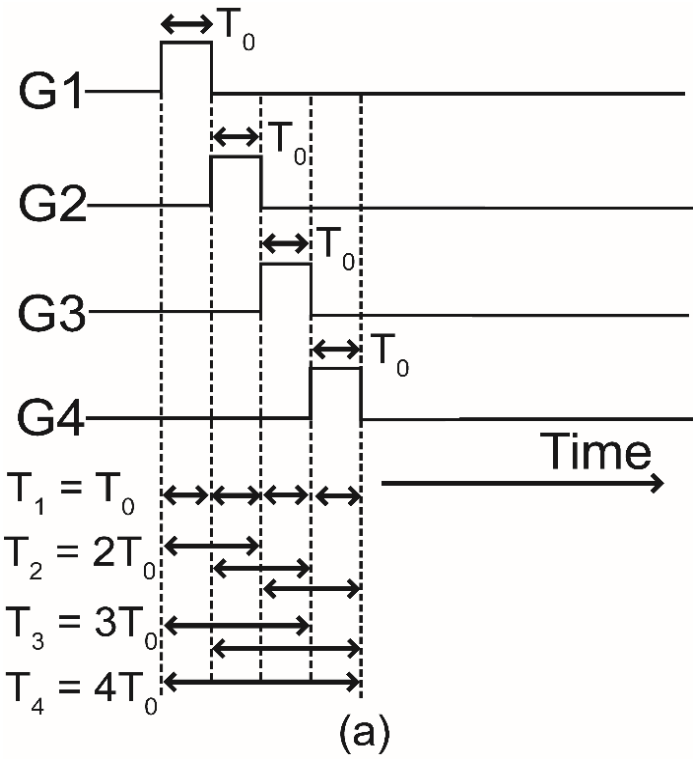

Fig. 3.7. Equal exposure pattern

During the exposure pattern design, the signal-to-noise-ratio (SNR) and wide flow speed range was considered. The equal exposure is designed in the way to give a high SNR and exponential pattern is expected to measure wide flow speed range. So, the trade-off exists between the better SNR and wide flow speed range in the design. To cover a wide range of flow speed, the ratio of the longest exposure to the shortest should be small.

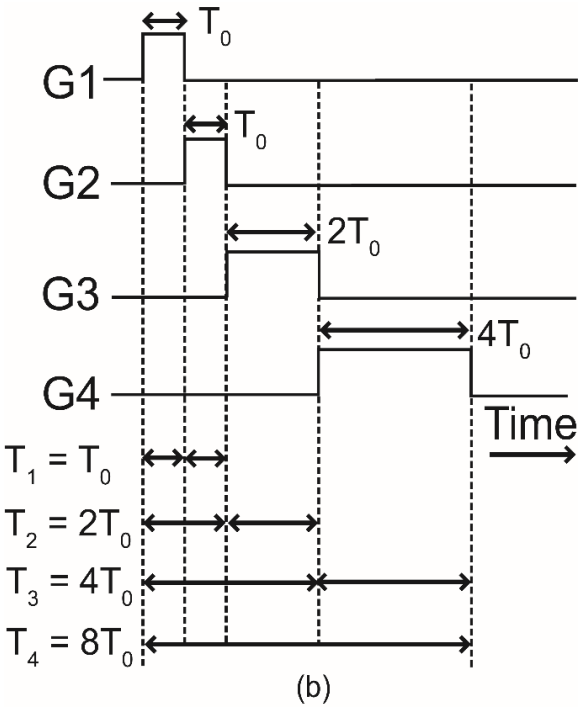

Fig. 3.8. Exponential exposure pattern

The SNR of the captured image for a shorter exposure time becomes worse. Therefore, it is effective to utilize multiple taps for the same exposure time and average the calculated contrast values among the taps. As depicted in Fig. 3.7, an effective exposure time, T_1, is given by the sum and averaging of four images of G_1, G_2, G_3, G_4. By this averaging approach, the standard deviation of the calculated contrast will be improved by a factor of 2. For example, to synthesize the effective exposure time $T_2 = 2T_0$, $T_3 = 3T_0$, three and two combinations of images, respectively, were used in equal case. But in contrast, the exponential case used two images (G_1 and G_2) to synthesize the effective exposure time, T_0. And, 2 combinations were used to synthesize the effective exposure of $T_2 = 2T_0$ in exponential case. But for $T_3 = 4T_0$ and $T_4 = 8T_0$, all the images were used effectively to synthesize the exposure time. It is clear the exponential pattern suffers from larger noise in comparison to equal case, because of the less effective synthesization of T_1 and T_2. But it suitable to extend the measurable flow speed range. On the other hand, the equal exposure is suitable to measure flow speed with higher SNR, because it effectively utilizes all tap images to perform the synthesization of exposure time.

Bibliography

[1] J. Nakamura, *IMAGE SENSORS and SIGNAL PROCESSING for DIGITAL STILL CAMERAS*. 2006.

[2] G. Wan, G. S. Member, X. Li, and G. Agranov, "CMOS Image Sensors With Multi-Bucket Pixels for," *Solid-State Circuits, IEEE J.*, vol. 47, no. 4, pp. 1031–1042, 2012.

[3] G. Wan, "Applications of Multi-Bucket Sensors to Computational Photography," *Stanford CG Lab Tech. Rep.*, pp. 1–9, 2012.

[4] S. Kawahito, G. Baek, Z. Li, S. M. Han, and M. W. Seo, "CMOS Lock-in Pixel Image Sensors with Lateral Electric Field Control for Time-Resolved Imaging," *Int. Image Sens. Work.*, vol. 2, pp. 3–5, 2013.

[5] S. M. Han, T. Takasawa, K. Yasutomi, S. Aoyama, K. Kagawa, and S. Kawahito, "A time-of-flight range image sensor with background canceling lock-in pixels based on lateral electric field charge modulation," *IEEE J. Electron Devices Soc.*, vol. 3, no. 3, pp. 267–275, 2015.

[6] T. TAKASAWA *et al.*, "A Time-of-Flight CMOS Range Image Sensor Using 4-Tap Output Pixels with Lateral-Electric-Field Control," *Electron. Imaging*, vol. 2016, no. 12, pp. 1–6, 2017.

[7] C. S. Bamji *et al.*, "IMpixel 65nm BSI 320MHz demodulated TOF Image sensor with 3μm global shutter pixels and analog binning," In Proceedings of the 2018 *IEEE International Solid-State Circuits Conference*, San Francisco, CA, USA, 11–15 February 2018; pp. 94–96.

[8] M. W. Seo *et al.*, "A 10 ps time-resolution CMOS image sensor with two-tap true-CDS lock-in pixels for fluorescence lifetime imaging," *IEEE J. Solid-State Circuits*, vol. 51, no. 1, pp. 141–154, 2016.

[9] M. W. Seo, Y. Shirakawa, Y. Kawata, K. Kagawa, K. Yasutomi, and S. Kawahito, “A time-resolved four-tap lock-in pixel CMOS image sensor for real-time fluorescence lifetime imaging microscopy,” *IEEE J. Solid-State Circuits*, vol. 53, no. 8, pp. 2319–2330, 2018.

[10] K. Kondo *et al.*, “A Built-in Drift-field PD Based 4-tap Lock-in Pixel for Time-of-Flight CMOS Range Image Sensors,” Int'l Conf. on Solid State Devices and Materials, J-7-03, pp. 5–6, 2018.

Chapter 4

Simulation of Multi-Tap Charge Modulation CMOS Image Sensor with High-Speed Camera Data

4.1 Introduction

For blood flow studies with laser speckle contrast imaging, the detector which can efficiently monitor the movement of speckle movement is essential. The recent high-speed cameras can able to monitor the blood flow movement and reproduce the flow map. But it requires huge processing power and large memory to process the data on chip. So, it will require more power to operate a chip and it is not energy efficient. The huge memory leads to large and expensive hardware and it is not cost efficient. The laboratory-developed multi-tap CMOS image sensor for ToF range imaging, is expected to sample the fast changes of speckle pattern efficiently with no inter-frame delays and it readout of shorter and longer exposure time images simultaneously at the frame rate of about a video-rate. So, this kind of approach can help to achieve low power and cost effective MELSCI system to monitor blood flow. The exposure patterns were designed to implement with 4-tap image sensor. In order to evaluate the effectives of the proposed method and to find the suitable exposure pattern for monitoring blood flow changes, the simulation is necessary.

4.2 Measurement setup of High-Speed Camera and its Signal Processing

4.2.1 Data Acquisition with High-Speed Camera

The multi-tap charge modulation CMOS image sensor to measure the flow speed and to observe the flow speed changes has been developed in the laboratory. At first, reference high-speed camera data were used to investigate the applicability of multi-tap charge modulation pixels for blood flow studies. The different exposure patterns such as equal exposure, exponential exposure and coded exposure pattern were designed to implement with multi-tap charge modulation CMOS image sensor. The effectiveness of the proposed exposure patterns was verified by the simulation of measured high-speed camera data. The simulation was performed out in MATLAB R2014b after acquiring the raw speckle data. The phantom of solid and fluid mediums was adopted to carry out the MELSCI measurement with high-speed camera as shown in Fig. 4.2. For solid and fluid scatter medium, the ground glass plate (Edmund Optics, 45-656, 220 grits, 100 x 100 mm dimension and thickness of 1.60 mm) and Intralipose (Otsuka Pharmaceutical Co., Ltd., 20% concentration) were used, respectively. The Intralipose was used to mimic the blood flow. The ground glass plate was placed on a motorized stage and CW laser beam (ONDAX RO-USB-785-PLR-100-1, power = 100 mW, spatial single mode, polarization = 100:1, linewidth ($\Delta\lambda$) = 50 MHz) at the wavelength (λ) of 785nm was used as a light source with linear polarization. The laser power of 8 mW and diameter of 10 mm were illuminated on the phantom of ground glass plate and Intralipose. The motorized stage (OptoSigma, OSMS20-85) movement was operated manually from computer by using GSC-01 controller. The motorized stage speed varied manually from 1-5 mm/s with an incremental step size of 1 mm/s. To validate the blood flow movement with the fluid setup, we have used the phantom of capillary tube filled with Intralipose fluid pushed by a syringe pump (YMC, Japan, YSP-101 Pump). The inner diameter of the capillary tube is 1 mm. The velocity of the fluid was set from the range of 0.047 ml/min to 0.235 ml/min which corresponds to a linear velocity of 1-5 mm/s (1 mm/s incremental step size). A C-Mount convex lens (Edmund Optics, #67-715) operates in a near-infrared visible region with the focal length of 25mm was used to forms a raw speckle image of the ground glass plate and

Intralipose on the high-speed CMOS global shutter camera (Mikrotron, Model MC1362). To remove the non-scattered surface reflection of the laser illumination, an analyzer was placed in front of the imaging lens. F/# of the imaging lens was optimized to give the highest contrast value [1].

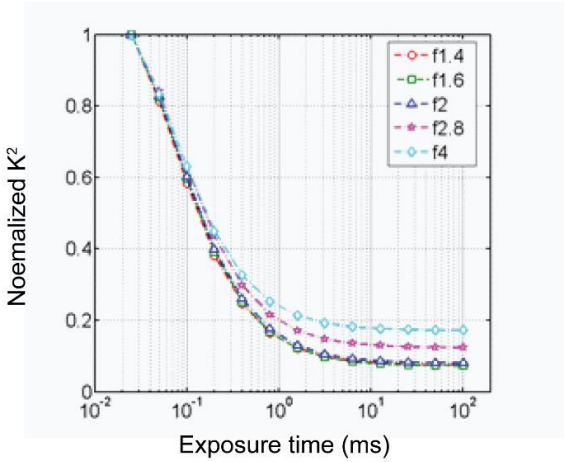

Fig. 4.1 Exposure contrast curve for various F/# for high-speed camera

From Fig. 4.1, it was observed that the F/# 2 gives the highest contrast change in correspondance to the shortest to longest exposure time. F/# 2 was used to capture speckle images with high-speed camera.

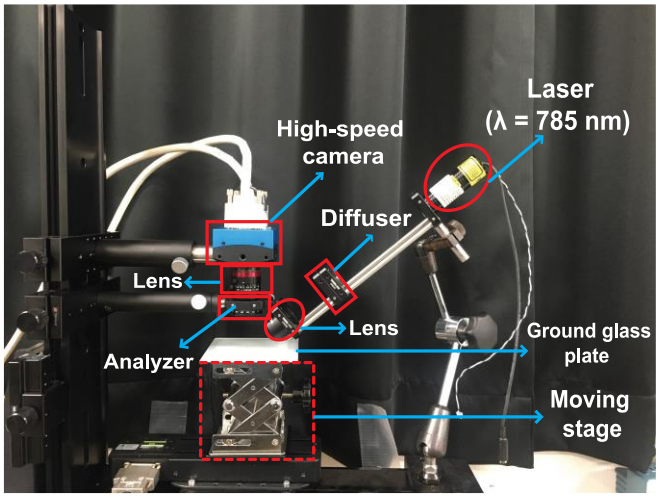

Fig. 4.2 Experimental set up of Mikrotron high-speed camera

4.2.2 Raw Data Processing of High-Speed Camera

The experiment was carried out for the total duration of 2s to acquire 80000 raw speckle images. The temporal resolution or exposure time is 25 μs for each raw speckle image. The

raw speckle images captured from the high-speed camera was stored and processed in the offline mode in MATLAB R2014b. During image capture, the total of 800 frames were captured and each buffered frame consists of 100 sub-frames (raw speckle images). At first, the sub-frames are extracted from captured frames to prepare 80000 raw speckle images as shown in Fig. 4.3.

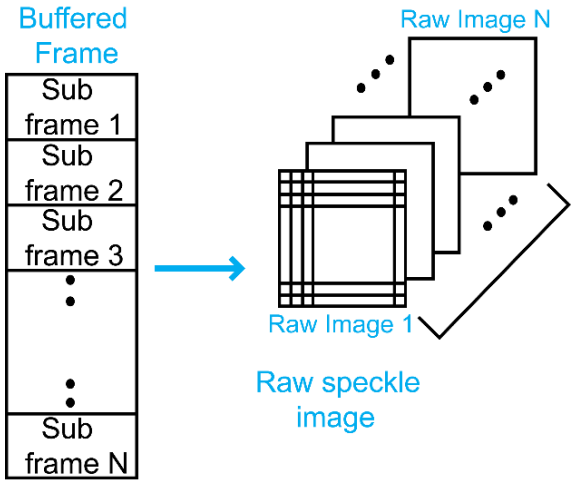

Fig. 4.3 Dataset preparation of high-speed camera

The raw speckle data of Ground glass plate and Intralipose captured by the high-speed camera with F/# of 2 is shown in Fig. 4.4 (a) and (b), respectively.

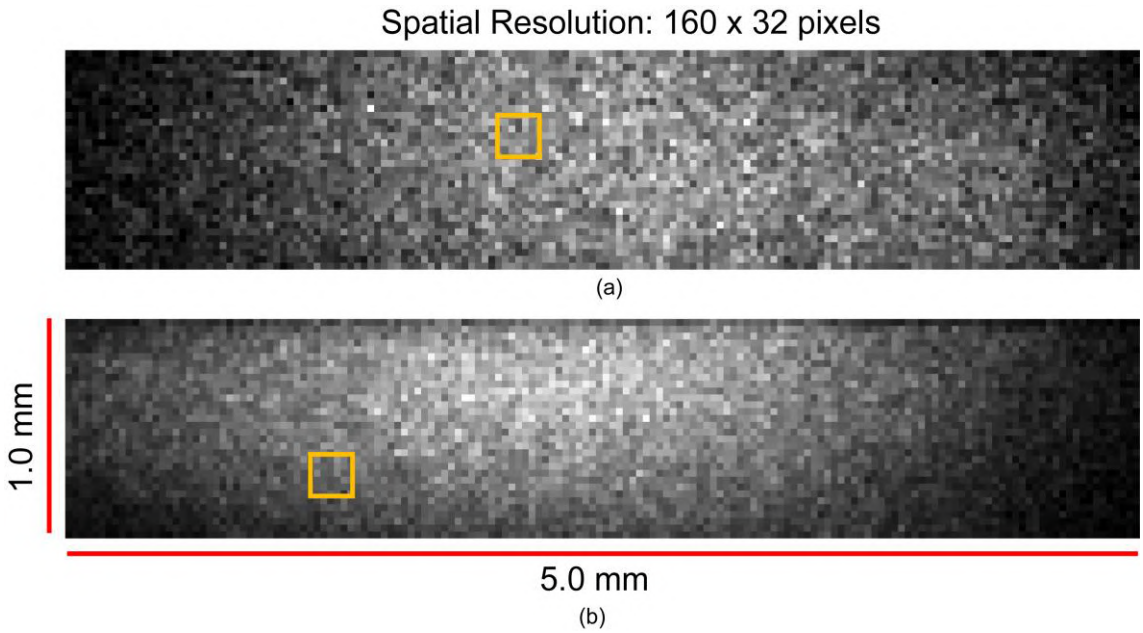

Fig. 4.4 Raw data of reference high-speed camera. (a) Ground glass plate (b) Intralipose

The preparation of datasets was done before performing the data analysis. From the total of 80000 raw speckle images, 19 datasets were generated. Each datasets consists of 4096 speckle images with a total exposure duration of 102.4 ms. From the shortest exposure time (25μs), the combination of longer exposure times was synthesized based on binary tree structure [2] as shown in Fig. 4.5. The longest exposure time of 102.4 ms was obtained by summing up a total of 4096 speckle images. A set of 4096 images were divided into pairs of successive images. The corresponding pixel values in both images were added together to generate a single image to double the exposure time. This process is iteratively repeated to generate exposure times of 25 μs, 50μs, and so on. Note that multiple images are obtained for each effective exposure time except the longest exposure. For example, 4096 images for 25μs, 2048 images for 50μs, etc.

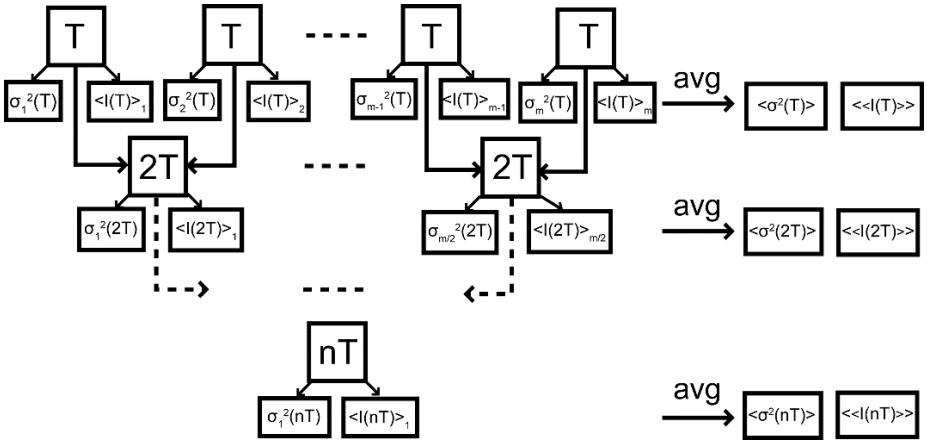

Fig. 4.5 Binary tree averaging algorithm

In total, this binary tree algorithm generates 8191 images with 13 different exposure times. It made sure that all images were utilized for each exposure time. For each image, the variance (σ^2) and average mean intensity was calculated over the ROI of 7 × 7 pixels. The mean variance and mean average intensity for each exposure time is calculated as follows:

$$\langle \sigma^2(T) \rangle = \frac{1}{N} \sum_{m=1}^{N} \sigma_m^2(T) \qquad 4.1$$

$$\langle\langle I(T) \rangle\rangle = \frac{1}{N} \sum_{m=1}^{N} \langle I(T) \rangle_m , \qquad 4.2$$

where N is the number of images for exposure time T (4096 images for 25 μs, 2048 images for 50 μs, etc..).

The speckle contrast-squared value is notated by K^2 in the remaining part of this thesis. K^2 value was calculated for each synthesized image, and the K^2 values for the same effective exposure time were averaged to reduce the variation and to improve the SNR. Thus, a dense K^2 curve that consisted of 13 exposure times (25μs – 102.4ms) was obtained and K^2 is expressed as:

$$K^2 = \frac{\langle \sigma^2(T) \rangle}{\langle \langle I(T) \rangle \rangle}, \tag{4.3}$$

It is important to note, the measured contrast-square is the raw value and no calibrations were applied. After calculate the K^2 value, the flow speed map was mapped. These operation was repeated for remaining 19 data sets as shown in Fig. 4.6. The squared contrast value, K^2, for each exposure time was calculated for each data set. K^2 and speed were obtained by further averaging of the 19 data sets.

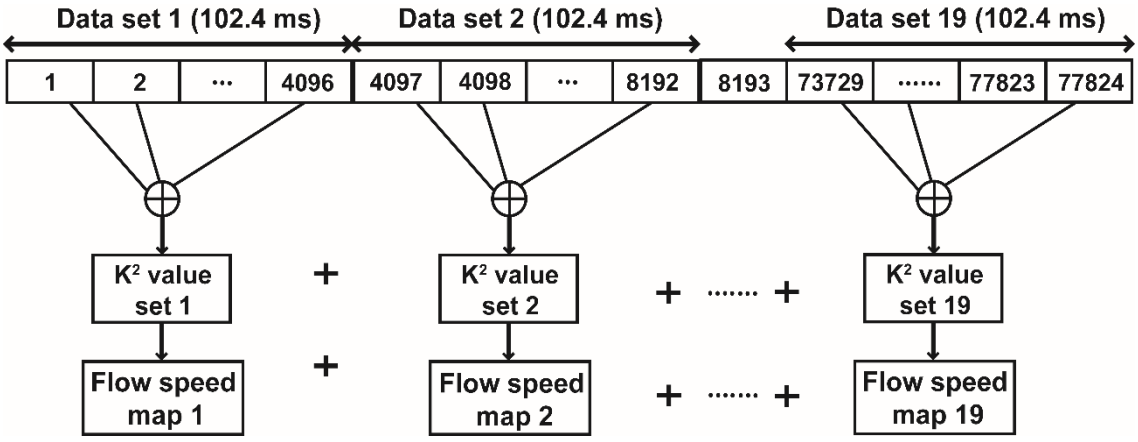

Fig. 4.6 Processing of high-speed camera data

The efficiency of binary-tree algorithm was verified by plotting the exposure - K^2 curve as shown in Fig. 4.7. The K^2 curve of Ground glass plate and Intralipose was plotted with and without averaging operation. The results suggested that, averaging helps to reduce the variation in the measured K^2 value. Particularly, at shorter exposure time of 25 μs to 1 ms, the averaging algorithm improved the calculation of K^2 value. Because at shorter exposure time, the SNR is not so high because of low light and it need the help of averaging to improve the SNR.

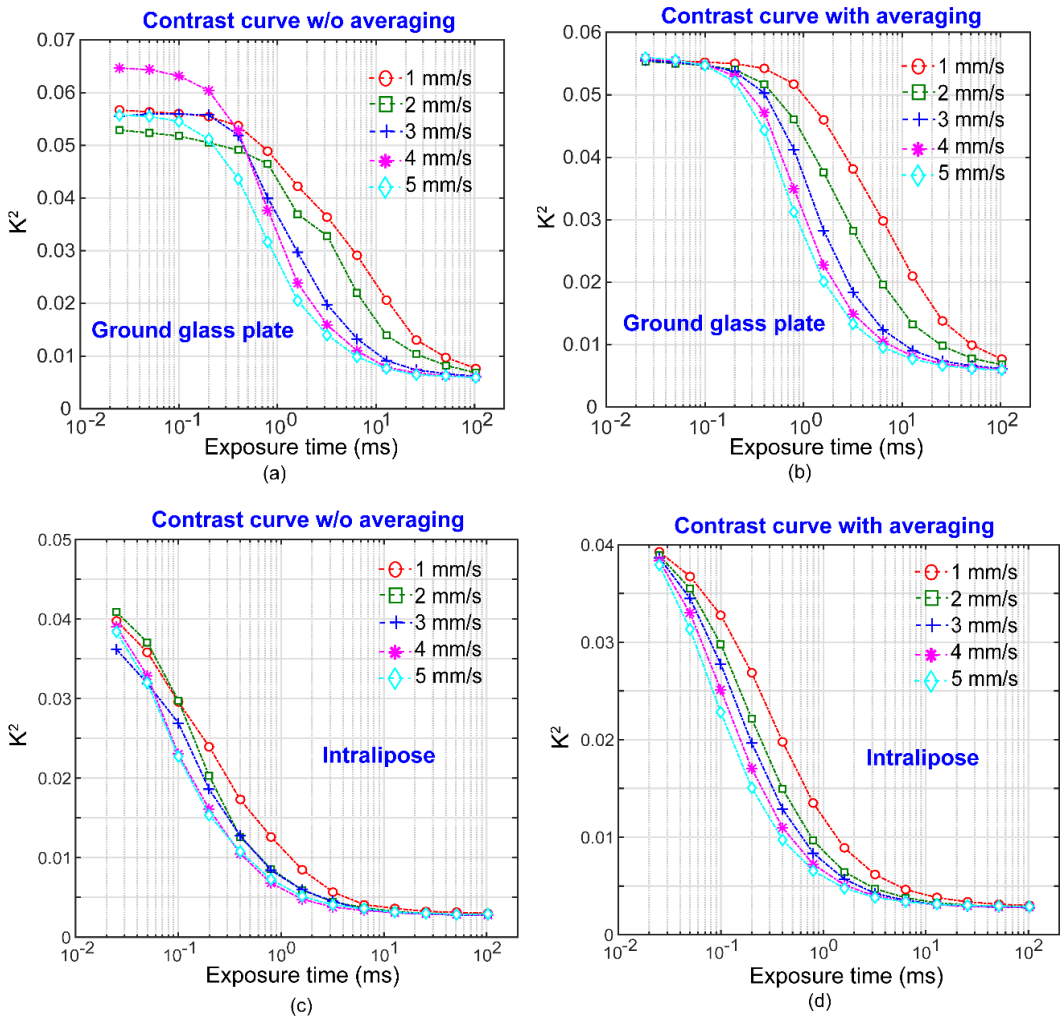

Fig. 4.7 Comparison of exposure contrast curve (a) (b) without and with averaging for Ground glass plate (c) (d) Without and with for Intralipose

4.3 Verification of Multi-Tap Charge Modulation Pixels with Reference High-Speed Camera Data

4.3.1 Simulation of Multi-Tap Charge Modulation Pixel

The implementation of designed exposure patterns with the measured high-speed camera data are discussed here. The verification of multi-tap charge modulation pixels with the reference high-speed camera data will help to confirm the applicability of 4-tap for blood flow monitoring and also help to evaluate the performance of exposure patterns. The

images for each tap are generated from the measured high-speed camera data. Multi-tap images $\{I^i(x, y)\ (i = 1\text{-}4)\}$ were emulated as follows:

$$I^i(x,y) = \sum_{n=0}^{N-1} I(x,y;nT_{\min})\, G_i(nT_{\min}), \quad 4.4$$

where (x, y) denotes the pixel position. i is the index of tap. $I(x, y; t)$ represents captured high-speed images. $G_i(t)$ is an exposure pattern function for tap-i. T_{min} and T_0 were 25μs and unit or lowest exposure time, respectively, in simulation. N is the total number of frames (N = 4096).

After image acquisition from each tap (G1-G4), the synthesization was done to get the effective exposure time for each tap (T_1-T_4). The synthesization of effective exposure time in equal and exponential exposure pattern case are shown in Fig. 4.8 and Fig. 4.9, respectively. The ratios of the shortest to the longest exposure times are 1:4 (equal pattern) and 1:8 (exponential pattern). The images for multiple exposure times are synthesized by summing up the images of adjacent exposure time windows. For example, the synthesization of exposure time T_1 and T_2 generates 4 and 3 combination of images. The variance and mean intensity value was calculated for each image in the same region which used for high-speed camera data and the ROI of 7 × 7. The K^2 calculated from the ratio of variance to the mean intensity value for each image. Finally, the K^2 value from each image are sum and average together to obtain the averaged K^2 value at exposure time of T_1-T_4. The averaged K^2 for each exposure time value is expressed as follows:

$$K^2_{avg}(T_i) = \frac{1}{N} \sum_{count=1}^{N} K^2_{count}(T_i), \quad 4.5$$

where count represents the number of combinations for each effective exposure time (T_i). i represents the index of the exposure time. By performing these synthesization, the different exposure times were realized and averaging helps to improve the SNR of the raw speckle images which are used to compute the K^2 value.

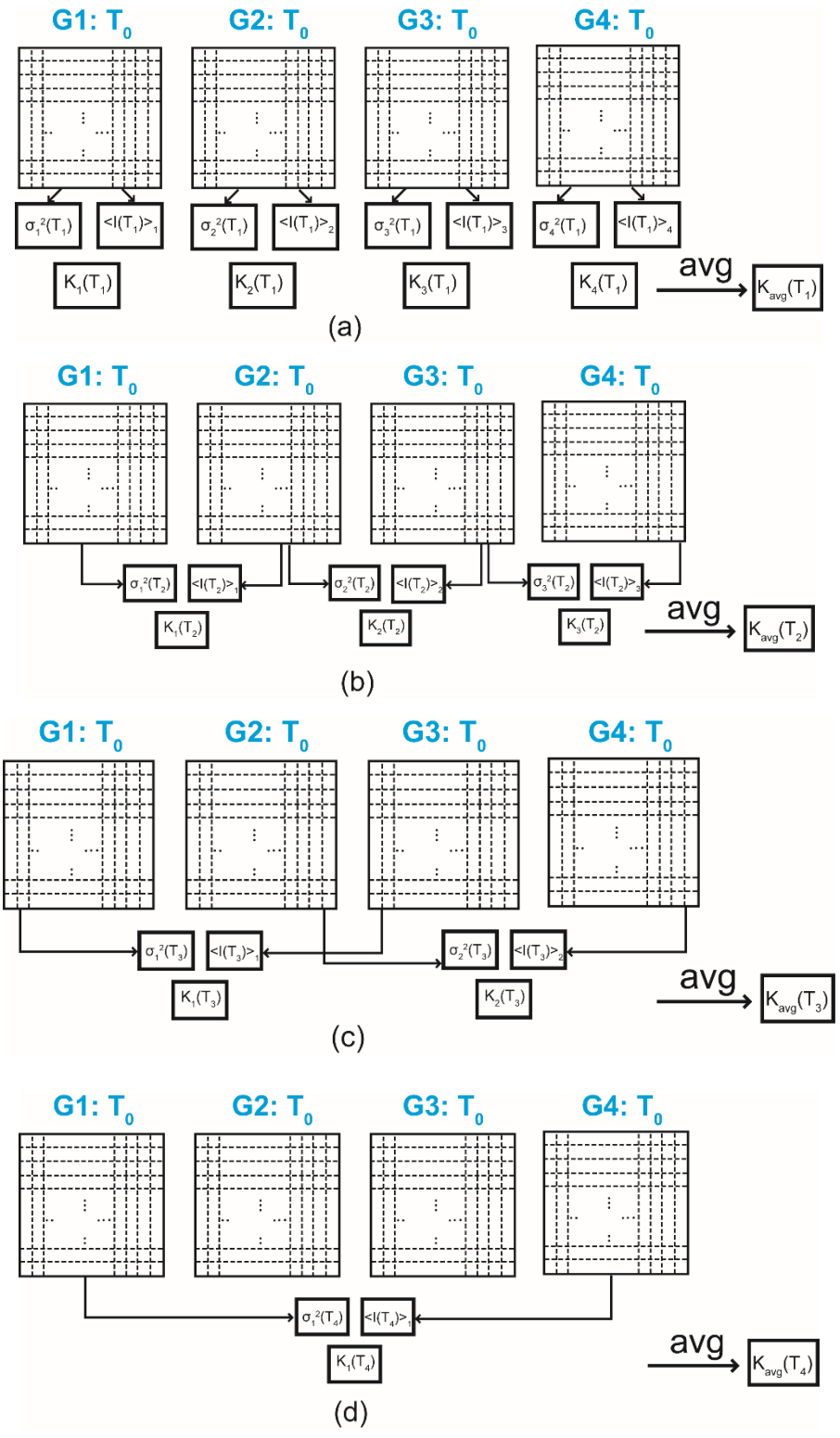

Fig. 4.8 Synthesization of effective exposure time in equal exposure pattern and calculation of contrast value for each exposure time (a) (b) (c) (d)Tap 1-4

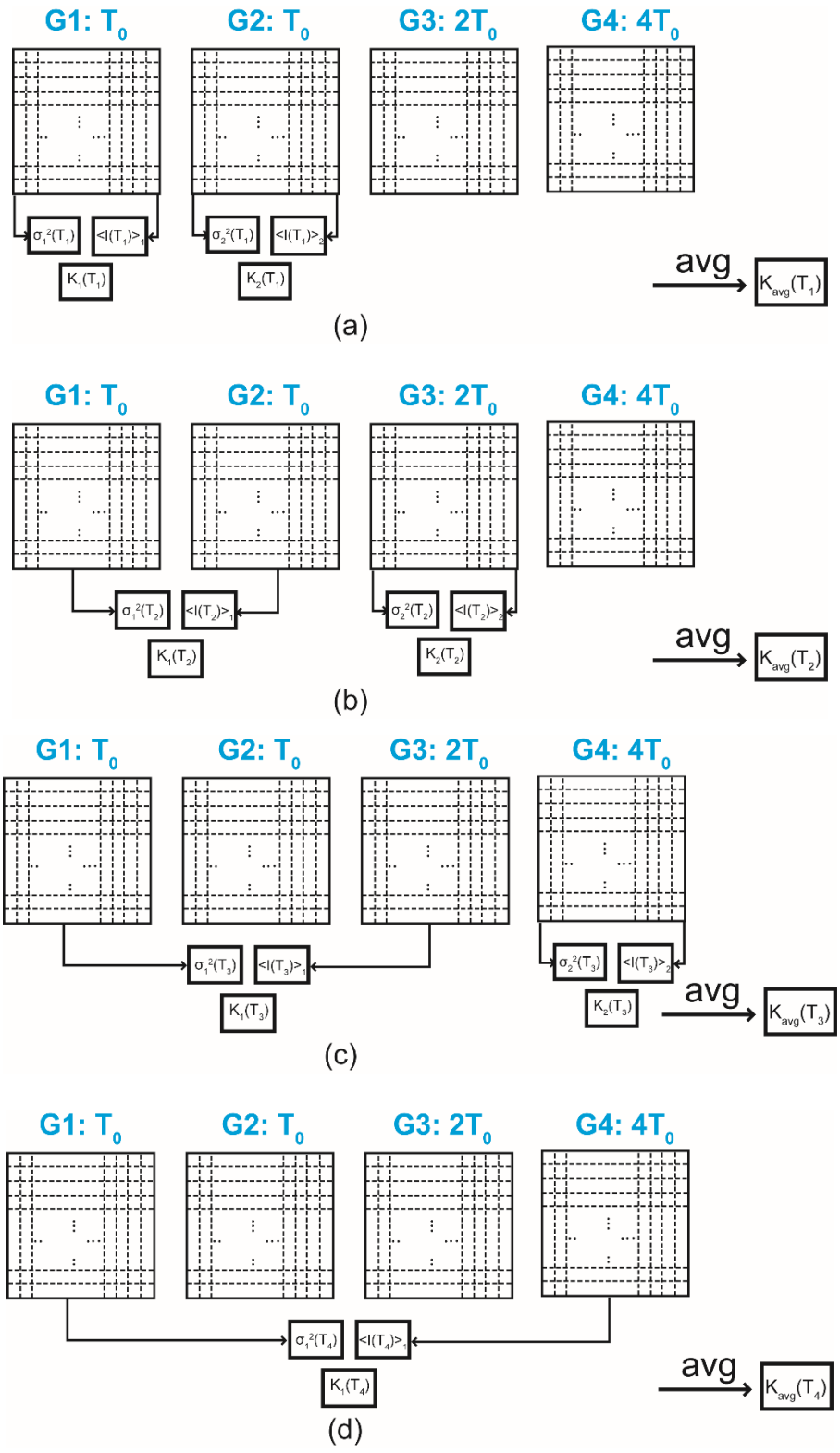

Fig. 4.9 Synthesization of effective exposure time in exponential exposure pattern and calculation of contrast value for each exposure time (a) (b) (c) (d) Tap 1-4

The flow of simulating the multi-tap pixel with the reference high-speed camera data is depicted in Fig 4.10. After calculating the K^2 value, the calculated K2 value was compared with reference high-speed K^2 curve. It was confirmed that, the calculated K^2 value was exactly matched with measured K^2 value. Then, fitting was performed with the speckle model to estimate the correlation time (τ_c). From the estimated τ_c, the flow speed (v) was estimated. The estimated flow speed was compared with measured flow speed by high-speed camera. This comparison will help to confirm that the designed exposure pattern can measure the flow speed accurately and can implement with multi-tap pixels in real time.

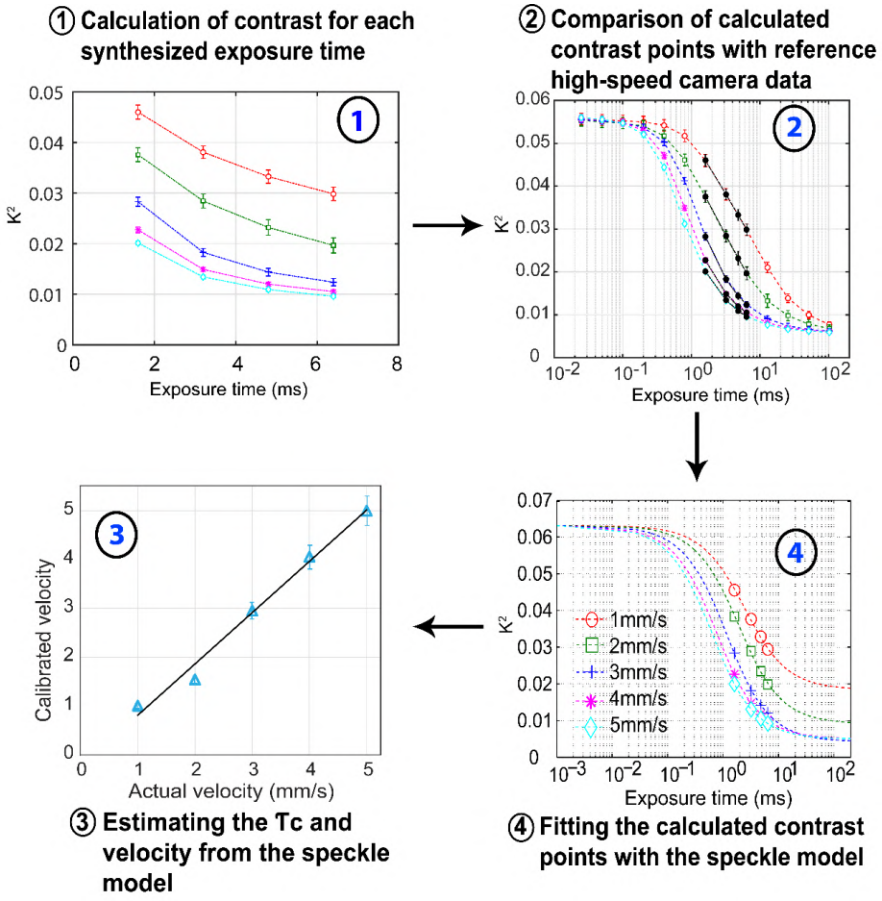

Fig. 4.10 Simulation flow of multi-tap charge modulation pixels

4.3.2 Simulation Results of Coded Exposure Pattern

The coded exposure pattern was designed and simulated with high-speed camera data (Ground glass plate and Intralipose). The simulation was carried out for several unit exposure time (T_0) under the constraint that the longest exposure time is less than 33 ms (one frame period for the video rate). T_0 of (0.2, 0.8, 1.6, and 3.2 ms) and T_0 of (0.2, 0.4,

0.8 and 3.2 ms) were simulated for Ground glass plate and Intralipose, respectively, as shown in Fig. 4.11. By choosing these set of unit exposure time (T_0) helped to sample each part of K^2 curve and the optimized T_0 can be found out. The ratio of exposure time (T) between each tap (G1- G4) is [1 2 4 8].

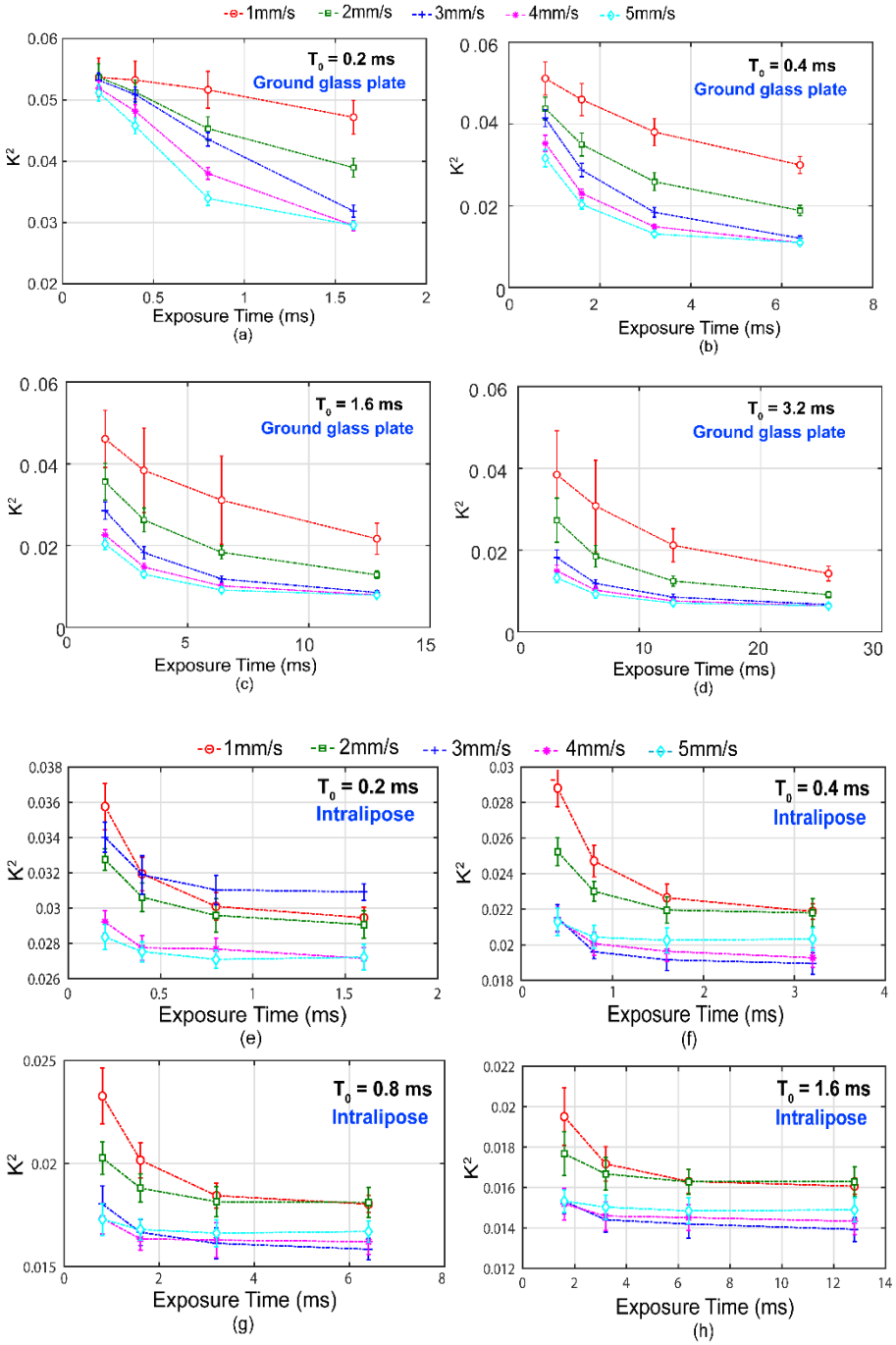

Fig. 4.11 Simulation of K^2 of coded exposure pattern

4.3.3 Simulation Results of Equal Exposure Pattern

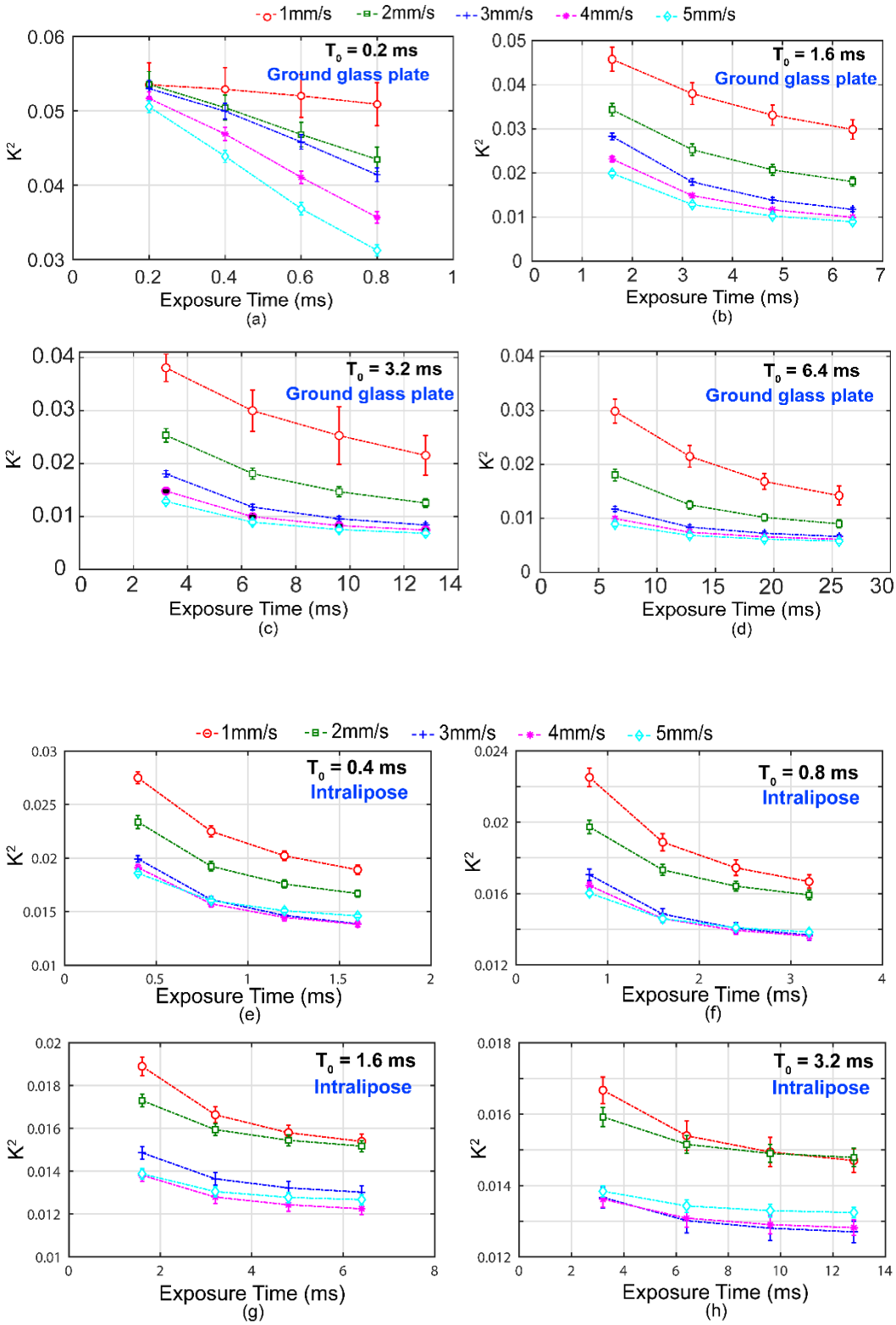

Fig. 4.12 Simulation of K^2 of equal exposure pattern

4.3.4 Simulation Results of Exponential Exposure Pattern

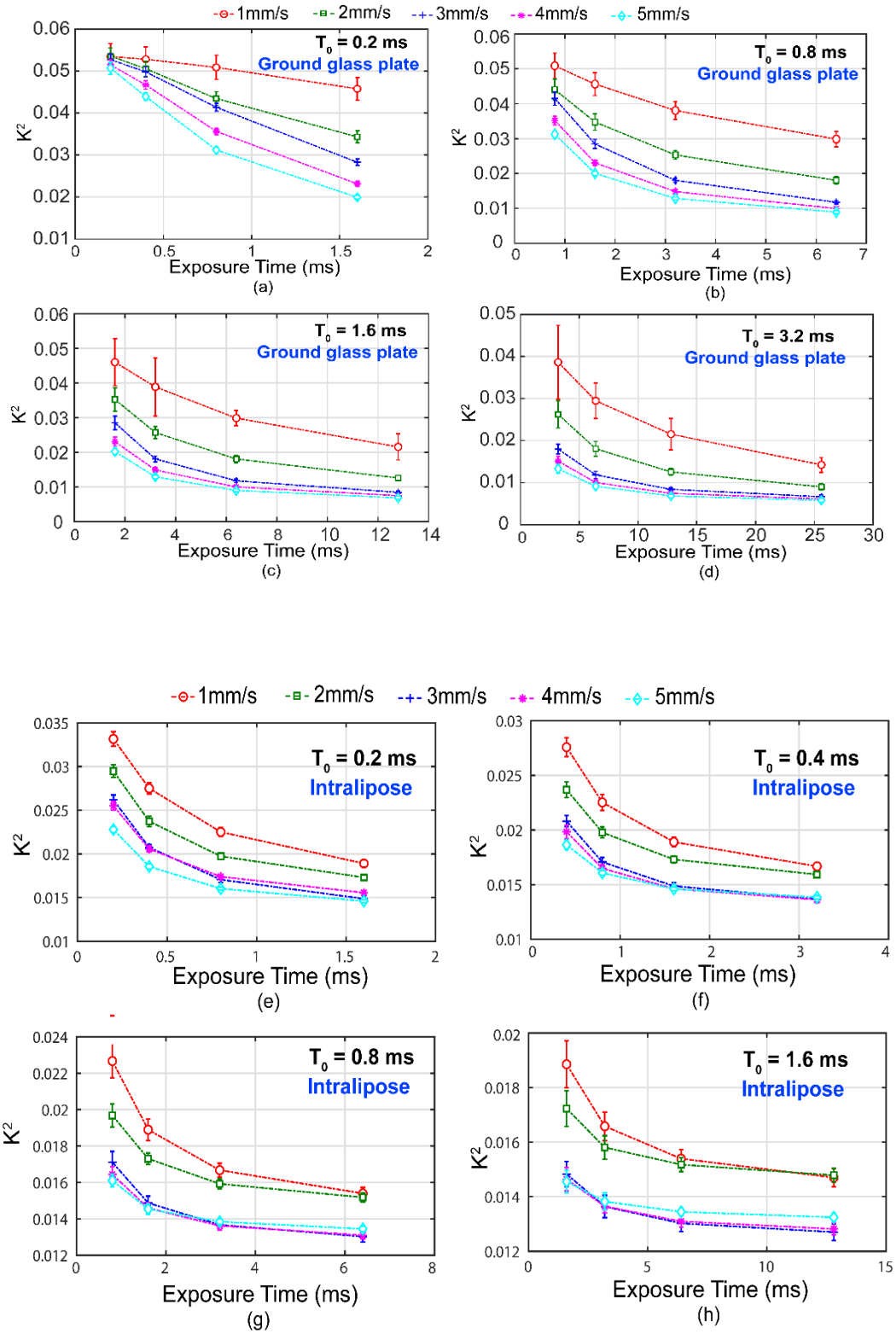

Fig. 4.13 Simulation of K^2 of exponential exposure pattern

From the K^2 curve, the change in K^2 value in correspondence to the shortest and longest exposure time was observed. For higher flow speed of 4mm/s and 5 mm/s, the shortest T_0 of 0.2 ms and 0.8 ms (coded exposure) in Fig. 4.11, 0.2 ms and 1.6 ms (equal exposure) in Fig. 4.12, and 0.2 ms and 0.8 ms (exponential exposure) in Fig. 4.13 gives the larger K^2 value (ground glass plate) change in correspondence to the shortest and longest exposure time. For high flow speed, the speckles fluctuate at fast rate and shorter exposure time is satisfactory to observe these speckle changes. In contrast the longer exposure time is essential to observe the slow moving scatterers. Another observation is, from K^2 curve it is expected that, the equal exposure gives better flow speed to noise ratio. Because, the error rate in the calculated K^2 value at the shortest effective exposure time of T_1 and T_2 is higher in exponential and coded exposure case in comparison to the equal exposure case. These outcome of results are expected one because, the equal exposure has 4 and 3 combinations of images to synthesize the shorter exposure time T_1 and T_2, respectively. In contrast, the exponential exposure case used only 2 combination of images to synthesize T_1 and T_2.

4.4 Comparison of High-Speed Camera with Multi-Tap Sensor

4.4.1 Laser Speckle Model without the Effect of ρ

The comparison of high-speed camera with the laboratory developed 4-tap CMOS image sensor was carried out here. The measured flow speed by high-speed camera compared with an estimated flow speed by 4-tap sensor.

Table. 4.1. Comparison of high-speed camera with 4-tap sensor

Parameters	**Mikrotron high-speed camera**	**4-tap CMOS image sensor**
Pixel size (μm)	14 × 14	22.4 × 22.4
Total pixel count	1280 × 1024	132 × 88
Effective pixel count used in the measurement	160 × 32	132 × 84

Imaging area (mm^2)	5.0 × 1.0	15.0 × 10.0
Maximum frame rate (fps)	120k	100
Effective frame rate used in the measurement (fps)	40k	~30

The K^2 obtained from the simulation of reference high-speed camera data was fitted with two speckle models and discussed its own advantages and limitations. By fitting the K^2 with the speckle model, the correlation time (τ_c) of the particle which moves with different flow speed can be obtained. From the correlation time, the flow speed (v) of the moving particle can be estimated. But the estimated flow speed is not actual flow speed which the particle is moving. Some calibrations are essential to find out the flow speed [3] [4].

By assuming that the particle is moving in an unordered motion, the Lorentzian velocity profile is considered in this study to estimate the flow speed. Primarily, speckle model with and without the effect of static scatterers have been considered to estimate the flow speed. First of all, the speckle model without the effect of static scatterers have been discussed with results. The speckle model without the presence of static scatterers can be expressed as follows [5]:

$$K^2 = \frac{\langle (I - \langle I \rangle)^2 \rangle}{\langle I^2 \rangle} = \beta \left(\frac{1}{2x^2} [e^{-2x} - 1] + \frac{1}{2x} \right) + v_n, \qquad 4.6$$

where β is for speckle averaging effect, which is same for all the flow speeds. v_n is an instrumental noise. The ρ is the parameter which defines for the amount of light which are dynamically scattered. In this case, ρ is considered as 1, which means that, all the lights are Doppler-shifted or scattered by the dynamic object and therefore, static scatter objects are not present.

The fitting was carried out in the MATLAB R2014b with the fminsearch function. For high-speed camera case, three parameters β, $x = T/\tau_c$, and v_n were estimated by fitting 13 calculated contrast points (K^2) with the above speckle model. Whereas, for the

simulation of 4-tap case, two parameters of $x = T/\tau_c$, and v_n were estimated. The speckle averaing paramter β, was considered as the assumption. The β was assumed as 0.0670. The value of 0.0670 was obtained from the measurement of static ground glass plate at the exposure time of 25μs [6]. The assumption of β was needed, because estimating 3 parameters from 4 data points is difficult.

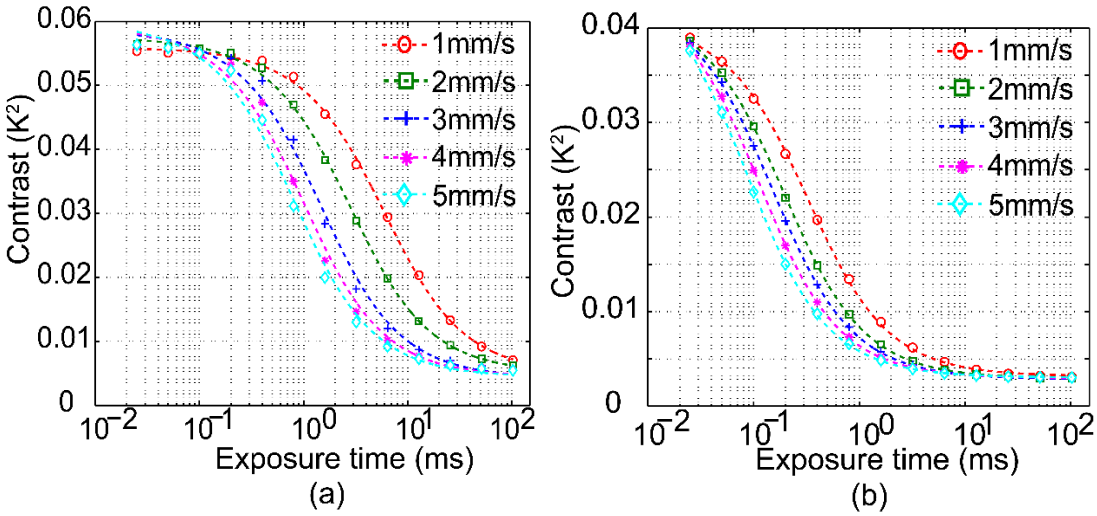

Fig. 4.14 Fitted K^2 curve of high-speed camera

Table. 4.2. Extracted fitting parameters of high-speed camera

Ground Glass Plate				**Intralipose**			
Velocity (mm/s)	**β**	**v_n**	**τ_c (ms)**	**Velocity (mm/s)**	**β**	**v_n**	**τ_c (ms)**
1	0.0506	0.0056	4.5811	1	0.0383	0.0031	0.2498
2	0.0507	0.0057	2.0914	2	0.0404	0.0028	0.1466
3	0.0553	0.0048	1.1203	3	0.0415	0.0028	0.1135
4	0.0541	0.0049	0.7696	4	0.0430	0.0028	0.0841
5	0.0546	0.0049	0.6243	5	0.0445	0.0029	0.0654

The speckle model fits well with K^2 curve and it is depicted in Fig. 4.14. The estimated parameters from the fitting is shown in Table 4.2. From the table it

is understood that, the assumed β value is almost to the similar to the measured β value in Ground glass and Intralipose. The β value should be uniform for different flow speeds, because it is a calibration factor which accounts for speckle averaging. β value for different flow speeds was verified. Fig. 4.15. shows the normalized measured speed of Ground glass plate and Intralipose with high-speed camera data. As LSCI cannot quantitatively measure the absolute flow speed, the normalization was done. The measured flow speed was normalized to the slowest flow speed (1 mm/s).

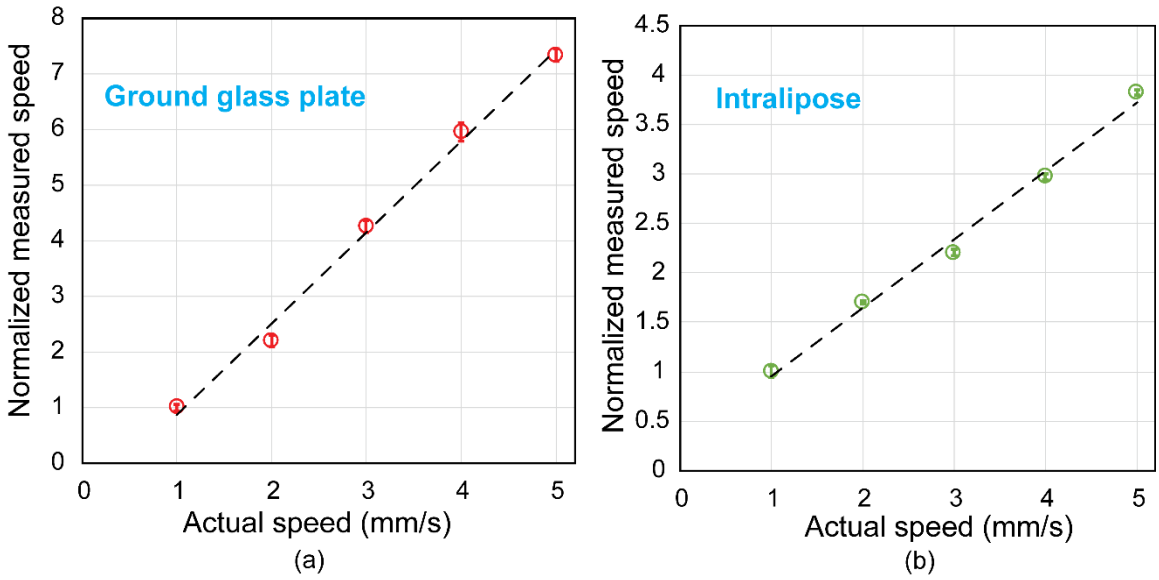

Fig. 4.15 Flow speed profile of high-speed camera. (a) Ground glass plate (b) Intralipose

The fitted K^2 curve of 4-tap sensor with the speckle model assuming $\rho = 1$ is shown Fig. 4. 16. The speckle model fits well with 4 estimated K^2 value. Although, τ_c and v_n were estimated, the fitting curve doesn't converge at shorter exposure times. When the noise factor v_n is zero, the K^2_{max} approaches β value for the limit of exposure time T→ 0 [7]. But the estimated v_n was not zero and it has some finite value. So at T → 0, the K^2_{max} doesn't converge to β. When v_n is finite, K^2_{max} becomes $K^2_{max} = \beta + v_n$. In order to converge the curve or solve this contradiction, an additional term v_n was added. In other words the offset correction was done. The modified speckle model is derived as follows:

$$K^2 = \frac{\langle (I - \langle I \rangle)^2 \rangle}{\langle I^2 \rangle} = (\beta - v_n)\left(\frac{1}{2x^2}[e^{-2x} - 1] + \frac{1}{2x}\right) + v_n, \qquad 4.7$$

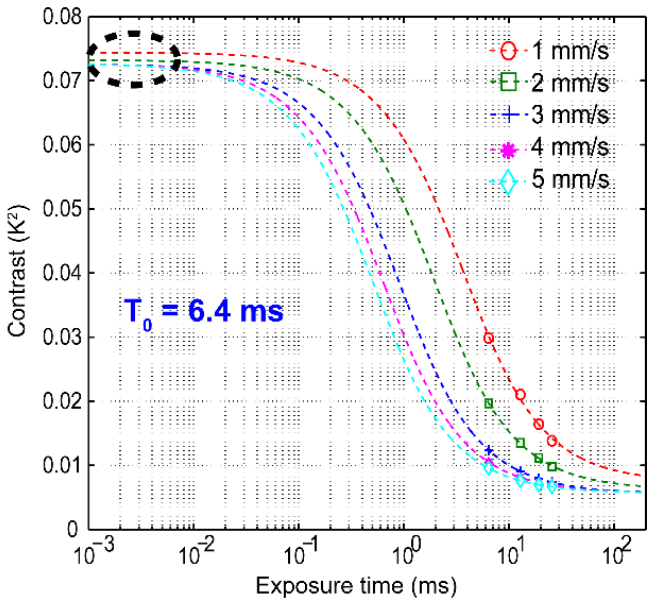

Fig. 4.16 Fitted K^2 curve of 4-taps sensor with speckle model (ρ = 1)

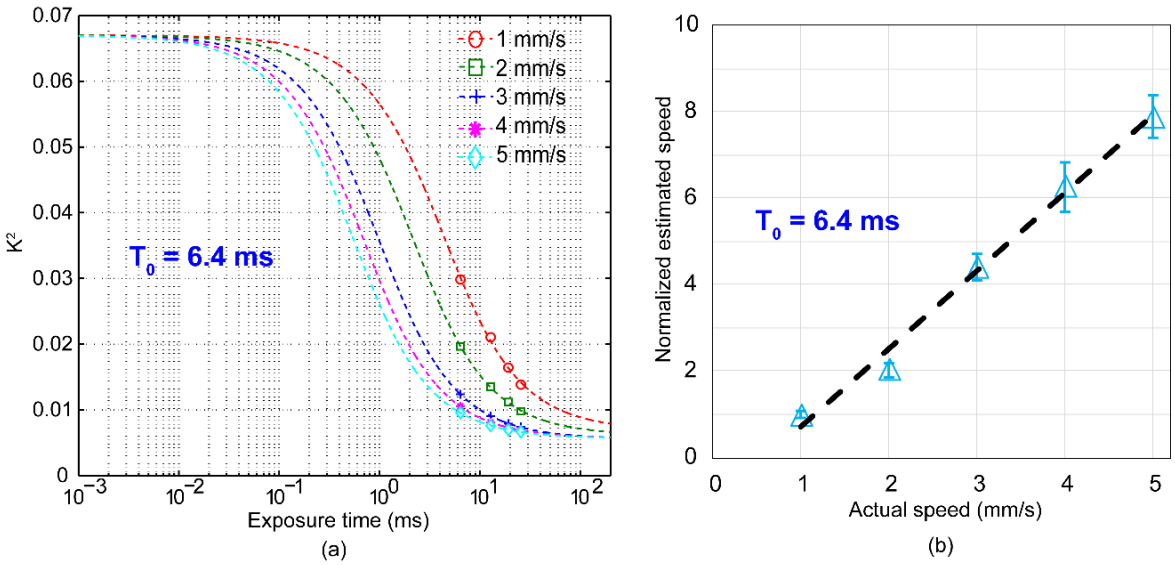

Fig. 4.17 Fitted K^2 curve of 4-taps sensor with modified speckle model (ρ = 1)

From Fig. 4.16 it was understood that, the K^2_{max} approaches β value for the limit of exposure time T→ 0. In the simulation, β was 0.0670, which was defined for the static ground glass plate at the shortest exposure time of 25 µs. The fitting was performed with the modified speckle model for all exposure patterns. The flow speed was estimated for each unit exposure time (T_0) and the comparison was performed to find the optimum exposure time. The fitted curve for the longest unit exposure time more resemble those of

the high-speed camera K^2curve as shown in Fig. 4.14. However, these speckle model doesn't consider the effect of static scatterers and it may affect the estimation of flow speed accuracy.

4.4.2 Laser Speckle Model with the Effect of ρ

The speckle models discussed earlier are based on some assumption and it does not include the presence of static scatterers in the scattering medium it observes. However, static scatterers will produce a speckle contrast component that remains constant when the imaging system exposure time increases. The laser light that is back-scattered by the static scatterers can underestimate the dynamics of the flowing system. That is, the amount of speckle contrast value increases. In this section, the speckle model with the effect of static scatterers is discussed and it is expressed as follows [8,9] [10] [11]:

$$K^2 = \frac{\langle (I - \langle I \rangle)^2 \rangle}{\langle I^2 \rangle} = \rho^2 \frac{e^{-2x} - 1 + 2x}{2x^2} + 4\rho(1-\rho)\frac{e^{-x} - 1 + x}{x^2} + v_n, \qquad 4.8$$

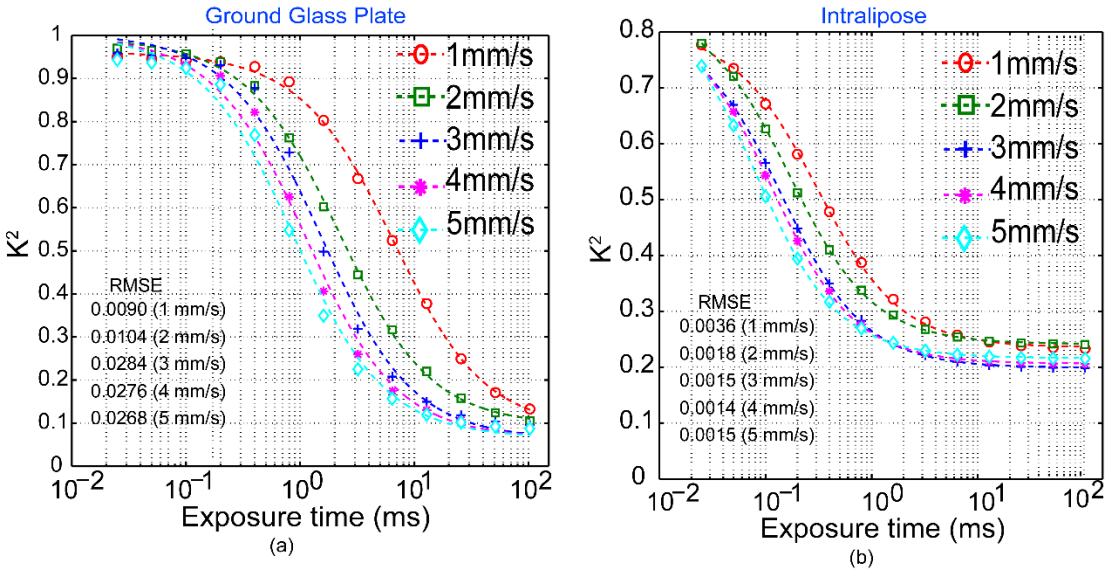

Fig. 4.18 Fitted K^2 curve of high-speed camera with improved speckle model

In the original speckle model, the parameter β is present. But in this case, β was considered as a normalization factor to calibrate the measured K^2 value by the K^2 value measured from the static ground glass plate. Therefore, β was excluded from the speckle model and virtually used as a scaling factor.

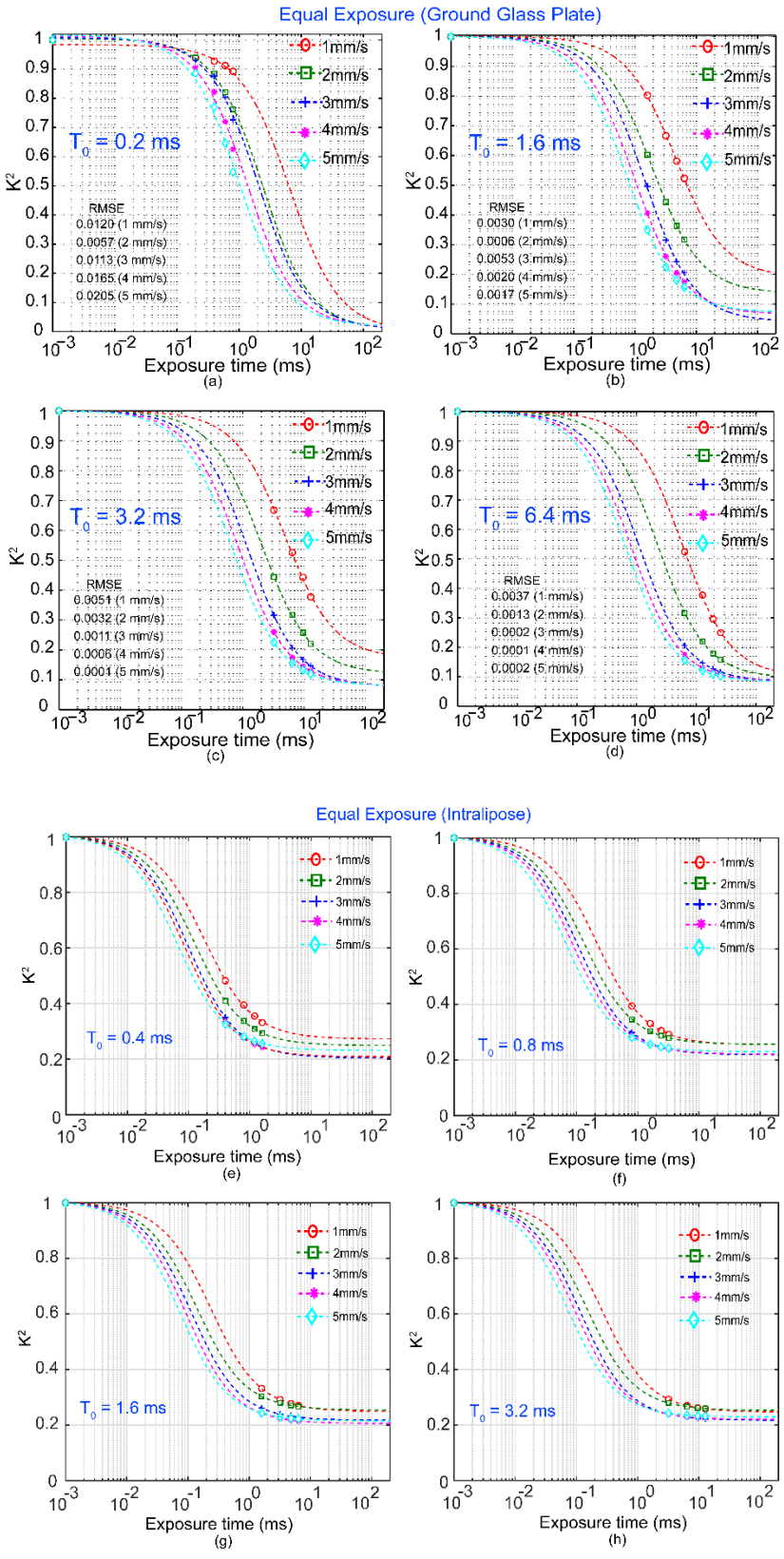

Fig. 4.19 Fitted K^2 curve of 4-tap sensor with improved speckle model (Equal exposure)

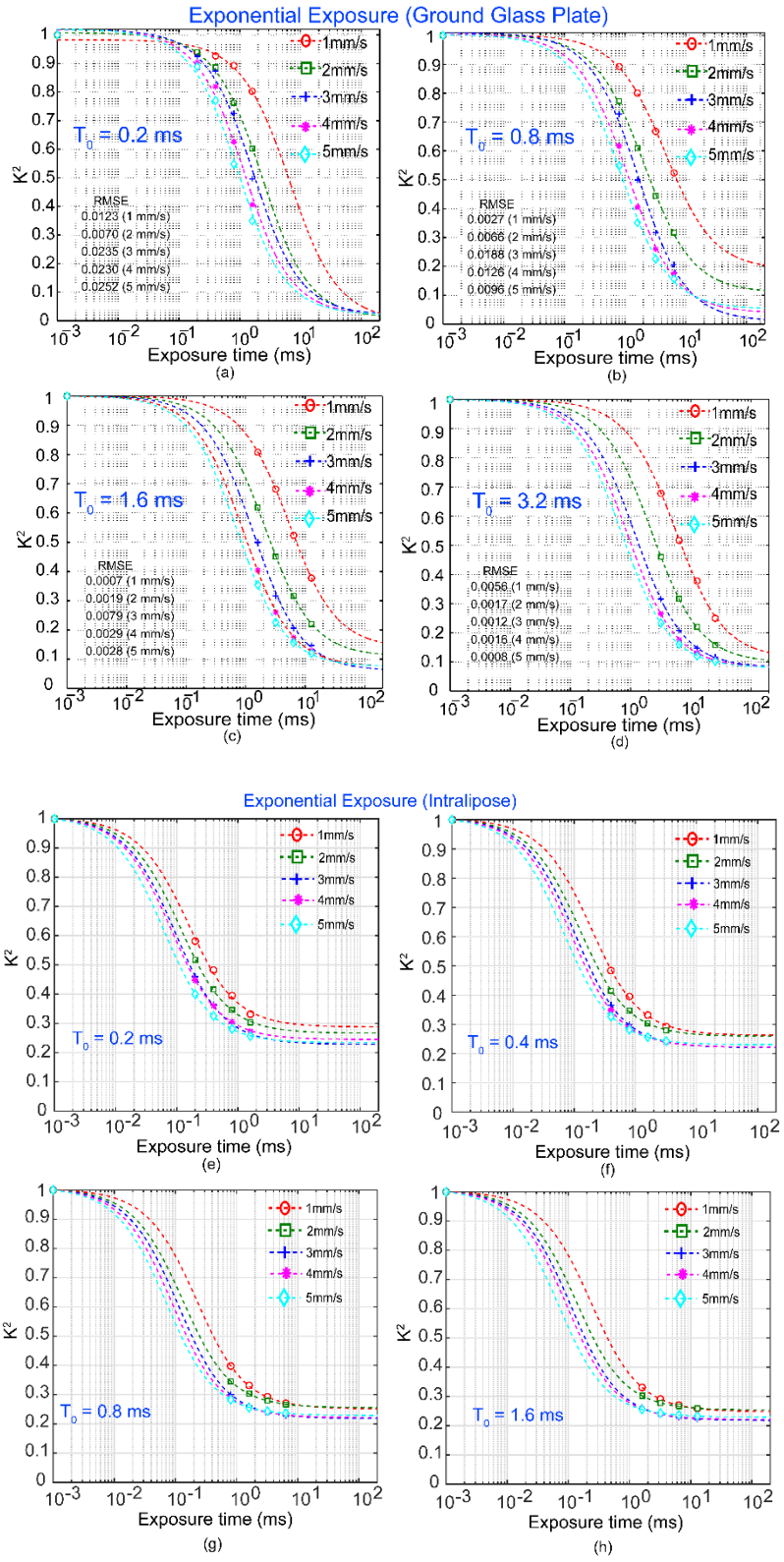

Fig. 4.20 Fitted K^2 curve of 4-tap sensor with improved speckle model (Exponential exposure)

The fitting was performed with the "fminsearchbnd" function available from MathWorks File Exchange. Three parameters, ρ, $x = T/\tau_c$, and v_n were estimated by fitting under the condition $[0 < \rho < 1, 0 < v_n < \infty, 0 < \tau_c < \infty]$. The K^2 values for the Intralipose in high-speed camera data are smaller than those for the ground glass. It is majorly due to increased Brownian motion associated with Intralipose.

In fitting the 4-tap data, one more additional point was considered with an assumption that the normalized K^2 value becomes unity for a sufficiently short exposure time. It is because to estimate three parameters from only 4 data points were not satisfactory from fitting. The short exposure time of 1 μs was used in this study. The K^2 value at the exposure time of 1 μs is considered as 0.0570 which was a measured K^2 value of static ground glass plate. The estimated K^2 value from the simulation was normalized with measured K^2 value. Fig. 4.19 and 4.20 show the fitted curves (Ground glass plate and Intralipose) for the equal exposure pattern and the exponential exposure pattern, respectively. In each figure, several unit exposure times were given under the constraint that the longest exposure time is less than 33ms (one frame period for the video rate). The extracted parameters from the fitting is shown in Table. 4.3. It is understood, by including the static scatterers in the speckle model gives the accurate the estimation of ρ, instead of assuming $\rho = 1$. The accurate ρ value estimation leads to the improved estimation of flow speed (v). The ρ value of Intralipose keeps on increases with increase in flow speed. The reason may be high flow speed has more dynamic scatters.

Table. 4.3. Extracted fitting parameters of 4-tap sensor with improved speckle model

Ground Glass Plate				**Intralipose**			
Velocity (mm/s)	**ρ**	**v_n**	**τ_c (ms)**	**Velocity (mm/s)**	**ρ**	**v_n**	**τ_c (ms)**
1	**0.6520**	0.0890	3.4679	1	**0.3497**	0.2351	0.1356
2	**0.6834**	0.0951	1.2159	2	**0.3787**	0.2413	0.0751
3	**0.7567**	0.0631	0.9140	3	**0.3917**	0.1987	0.0635
4	**0.7478**	0.0650	0.6609	4	**0.4043**	0.2062	0.0511
5	**0.7515**	0.0657	0.5218	5	**0.4354**	0.2162	0.0363

4.4.3 Comparison of Estimated Flow Speeds of High-Speed camera with 4-tap CMOS Image Sensor

The estimated speeds by the high-speed camera and the simulated 4-tap CMOS image sensor were compared. Because it is difficult to quantify the absolute value of speed using the MELSCI system due to several hindrances such as improper statistical model and interpretation of inferred correlation time, τ_c, and the speed, v, the estimated speed ($1/\tau_c$) was normalized to the slowest flow speed (1mm/s). A linear fit is also shown in the plots for the unit exposure time associated with the highest sensitivity, as determined by the steepest slope.

As shown in Fig. 4.20, a longer exposure time mostly resulted in higher sensitivity. The quality of the estimated speed was evaluated by the flow speed-to-noise ratio (FNR), which was defined as the quotient of the mean estimated speed to the standard deviation of estimated speed. The FNRs for the different T_0 for ground glass and Intralipose over various exposure patterns were compared in Table 4.4 to Table 4.9. Based on the highest sensitivity or FNR, the T_0 was optimized for ground glass plate and Intralipose in each exposure patterns.

Overall, the equal exposure pattern provided higher FNR than the exponential pattern. One possible reason is that the variation of the estimated speed is significantly affected by the K^2 for the shortest exposure time in exponential exposure case. As discussed earlier about synthesization, the number of averaged data for the shortest exposure were 2 and 4 for the equal and exponential exposure patterns, respectively. The results suggest that the estimated speed for the exponential exposure fluctuates more than that of the equal exposure.

In conclusion, the equal exposure pattern is suitable to observe flow speeds with higher FNR. The optimized unit exposure time (T_0) for Ground glass plate and Intralipose with equal exposure case is 6.4 ms and 0.8 ms, respectively.

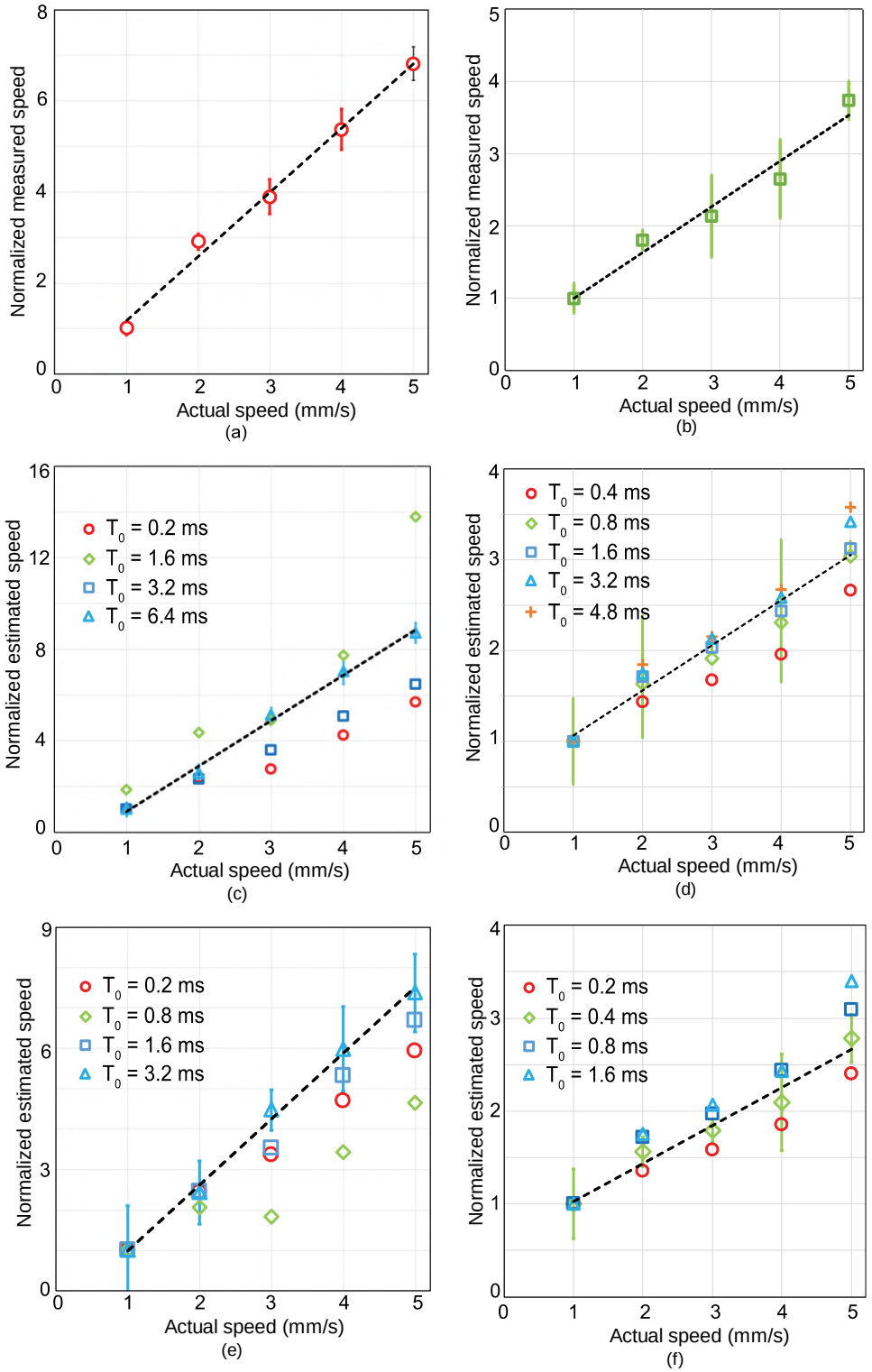

Fig. 4.21 Flow speed of high-speed camera and 4-tap sensor obtained with improved speckle model. Pattern: (a)(b) High-speed camera (c)(d) Equal exposure (e)(f) Exponential exposure. Measured object: (a)(c)(e) Ground glass plate, (b)(d)(f) Intralipose

Table. 4.4. Flow speed to noise ratio of equal exposure (Ground glass plate)

Ground glass plate	**Flow Speed to Noise Ratio (FNR)**			
Velocity (mm/s)	**T_0 = 0.2 ms**	**T_0 = 1.6 ms**	**T_0 = 3.2 ms**	**T_0 = 6.4 ms**
1	2.02	2.16	2.13	**6.43**
2	6.04	4.55	7.09	**8.83**
3	16.14	9.01	10.31	**19.21**
4	20.95	8.50	14.41	**14.66**
5	22.43	6.28	7.73	**22.33**

Table. 4.5. Flow speed to noise ratio of exponential exposure (Ground glass plate)

Ground glass plate	**Flow Speed to Noise Ratio (FNR)**			
Velocity (mm/s)	**T_0 = 0.2 ms**	**T_0 = 0.8 ms**	**T_0 = 1.6 ms**	**T_0 = 3.2 ms**
1	3.78	1.38	0.76	**1.44**
2	8.22	2.67	3.65	**3.87**
3	22.66	6.14	6.17	**10.09**
4	30.33	6.73	7.04	**6.28**
5	35.41	6.84	7.01	**8.27**

Table. 4.6. Flow speed to noise ratio of coded exposure (Ground glass plate)

Ground glass plate	**Flow Speed to Noise Ratio (FNR)**			
Velocity (mm/s)	**T_0 = 0.2 ms**	**T_0 = 0.8 ms**	**T_0 = 1.6 ms**	**T_0 = 3.2 ms**
1	7.46	1.19	**0.71**	0.50
2	3.20	2.73	**2.49**	2.94
3	26.23	4.14	**5.26**	5.10
4	10.01	5.06	**7.56**	5.79
5	4.21	6.37	**6.45**	6.01

Table. 4.7. Flow speed to noise ratio of equal exposure (Intralipose)

Intralipose	**Flow Speed to Noise Ratio (FNR)**			
Velocity (mm/s)	**T_0 = 0.4 ms**	**T_0 = 0.8 ms**	**T_0 = 1.6 ms**	**T_0 = 3.2 ms**
1	0.80	**1.70**	7.61	0.26
2	1.52	**1.71**	2.05	0.52
3	2.17	**21.43**	21.78	3.06
4	3.09	**2.31**	3.16	2.82
5	2.54	**32.34**	3.40	11.37

Table. 4.8. Flow speed to noise ratio of exponential exposure (Intralipose)

Intralipose	**Flow Speed to Noise Ratio (FNR)**			
Velocity (mm/s)	**T_0 = 0.2 ms**	**T_0 = 0.4 ms**	**T_0 = 0.8 ms**	**T_0 = 1.6 ms**
1	0.93	**1.18**	4.04	2.34
2	1.36	**6.26**	2.42	2.04
3	1.87	**9.89**	2.61	3.58
4	1.65	**6.65**	3.14	1.99
5	2.17	**6.61**	6.13	1.93

Table. 4.9. Flow speed to noise ratio of coded exposure (Intralipose)

Intralipose	**Flow Speed to Noise Ratio (FNR)**			
Velocity (mm/s)	**T_0 = 0.2 ms**	**T_0 = 0.4 ms**	**T_0 = 0.8 ms**	**T_0 = 1.6 ms**
1	2.70	**3.94**	5.06	3.30
2	3.53	**2.48**	1.70	0.22
3	0.30	**2.72**	0.56	1.72
4	0.71	**2.57**	0.50	0.27
5	0.53	**0.54**	0.48	0.61

For different T_0's, the value of mean FNR was calculated as shown in Fig. 4.22. The clear trend of two peaks was observed in mean FNR vs T_0 plot for equal and exponential exposure patterns (ground glass plate and Intralipose). Because of Brownian motion associated with Intralipose, the fitted K^2 curve does not have flat part at shorter exposure time. Therefore, the shorter T_0 can estimate the flow speed with the better mean FNR as shown in Fig. 4.22 (b) and (d).

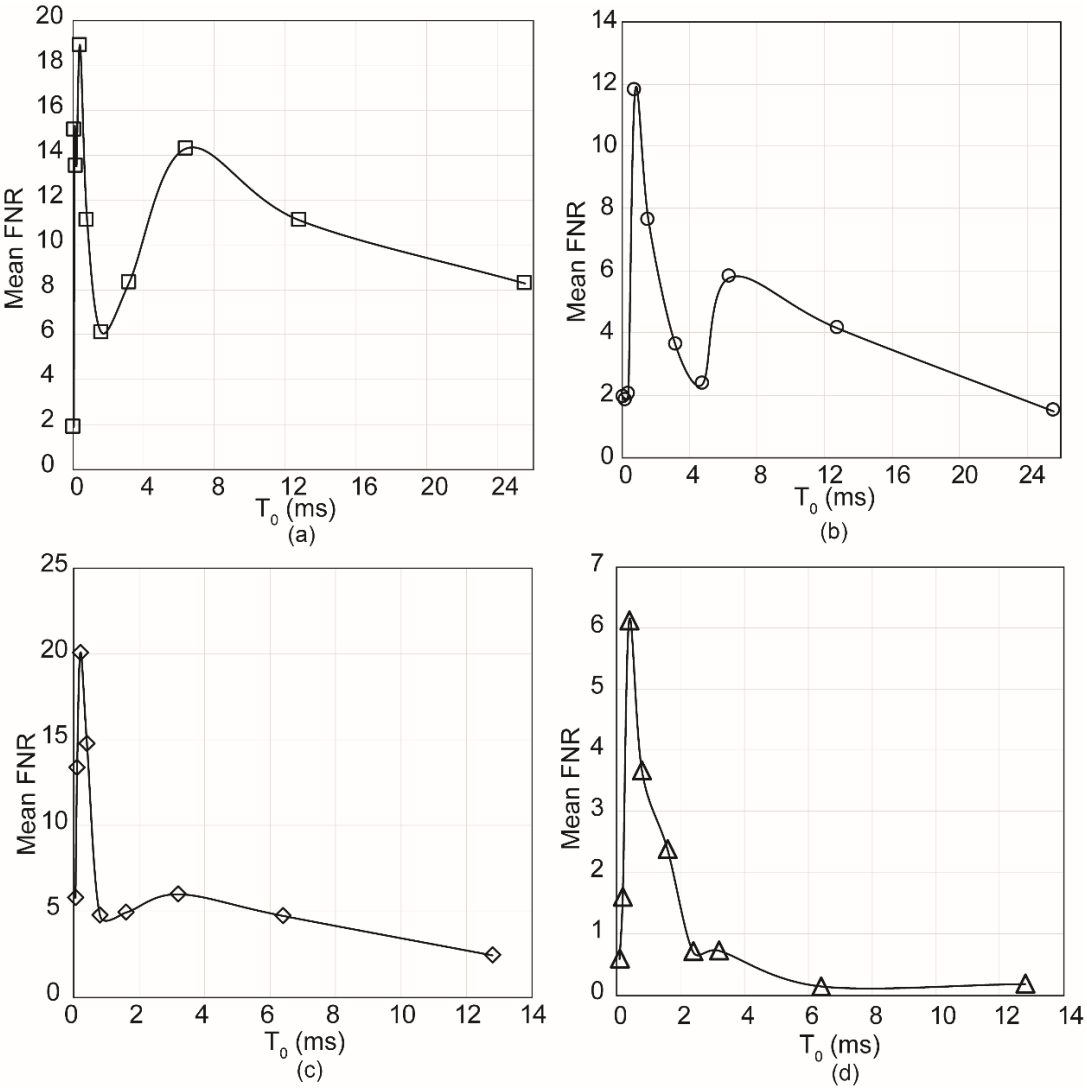

Fig. 4.22. Mean FNR vs. T_0 (ms). Exposure pattern: (a)(b) Equal exposure pattern. Exposure pattern: (c)(d) Exponential exposure pattern. Measured object: (a)(c) Ground glass plate, (b)(d) Intralipose.

The estimated FNR of optimized exposure conditions (T_0's) for different patterns (Ground glass plate and Intralipose) is compared with the measured FNR of high-speed camera and summarized in Table. 4.10.

Table. 4.10. Flow speed to noise ratios for high-speed camera, equal and exponential exposure patterns

Actual speed (mm/s)	Flow speed to noise ratio (Ground glass)			Flow speed to noise ratio (Intralipose)		
	High-speed camera	Equal exposure (T_0 = 6.4 ms)	Exponential exposure (T_0 = 3.2 ms)	High-speed camera	Equal exposure (T_0 = 0.8 ms)	Exponential exposure (T_0 = 0.4 ms)
1	10.77	6.43	1.44	3.29	1.70	1.18
2	18.93	8.83	3.87	10.80	1.71	6.26
3	11.48	19.21	10.09	3.21	21.43	9.89
4	13.02	14.66	6.28	4.30	2.31	6.65
5	19.71	22.33	8.27	12.99	32.34	6.61
Mean FNR	14.78	14.29	5.99	6.92	11.89	6.11

The feasibility of the 4-tap sensor to evaluate the flow speed of the moving blood can be given by relative estimation error. The relative estimation error is expressed as:

$$\text{Relative estimation error (\%)} = \frac{\text{Estimated speed} - \text{Actual speed}}{\text{Actual speed}} \text{ x } 100 \qquad 4.9$$

While the flow speed to noise ratio (FNR) has been evaluated for different exposure conditions, the estimation error related to the actual speed for optimized T_0 is summarized in Table. 4.11.

Table. 4.11. Relative estimation error for high-speed camera, equal and exponential exposure patterns

Actual speed (mm/s)	Relative estimation error (%) (Ground glass)			Relative estimation error (%) (Intralipose)		
	High-speed camera	Equal exposure (T_0 = 6.4 ms)	Exponential exposure (T_0 = 3.2 ms)	High-speed camera	Equal exposure (T_0 = 0.8 ms)	Exponential exposure (T_0 = 0.4 ms)
1	-12.5	4.49	0.29	-0.36	-5.87	-6.15
2	11.49	-8.19	-5.82	13.57	13.71	15.21
3	-2.41	4.09	4.53	-6.85	-4.76	-4.59
4	-0.50	1.88	1.53	-9.76	-7.60	-9.76
5	0.08	-1.45	-1.73	6.53	4.60	5.71

The positive and negative signs show the over estimation and under estimation of flow speed, respectively. From the relative estimation error analysis, it is evident that 4-tap sensor has the capability to monitor the flow speeds with acceptable errors.

4.5 Summary

The measurement setup of high-speed camera was discussed and the data acquisition was done at the sampling frequency of 40 kHz with a temporal resolution of 25 μs. The data processing of measured high-speed camera data was done using binary tree averaging algorithm. It was verified that averaging algorithm improves the calculation of K^2 value with higher SNR. The simulation of multi-tap pixels was carried out with reference high-speed camera data to verify the feasibility of the proposed method and to evaluate the performance of the proposed exposure patterns. The various exposure patterns were simulated with the reference data. The fitting was performed with both speckle models (with and without the effect of static scatterers) to estimate the flow speed. It was understood that, considering the effect of static scatterers in the speckle model can help to improve the accuracy of flow speed estimation. The measured flow speed was compared with the estimated flow speed. The flow speed was estimated with several unit exposure time (T_0) and the longer exposure time resulted in higher sensitivity. The excellence of the estimated flow speed was evaluated by flow-speed-to-noise ratio (FNR). From the comparison of FNR between exposure patterns, the equal exposure presented the highest FNR in comparison to exponential and coded exposure pattern. From the simulation, it was verified that equal exposure pattern is better to suitable to monitor blood flow changes and exponential exposure pattern use to achieve wide flow speed range.

Bibliography

[1] A. Fuentes-Garcia, J. C. Ramirez-San-Juan, N. Salazar-Hermenegildo, B. Choi, R. Ramos-Garcia, and E. Mendez-Aguilar, "Effects of speckle/pixel size ratio on temporal and spatial speckle-contrast analysis of dynamic scattering systems: Implications for measurements of blood-flow dynamics," *Biomed. Opt. Express*, vol. 4, no. 10, p. 1883, 2013.

[2] M. Hultman, I. Fredriksson, M. Larsson, A. Alvandpour, and T. Strömberg, "A 15.6 frames per second 1-megapixel multiple exposure laser speckle contrast imaging setup," *J. Biophotonics*, vol. 11, no. 2, pp. 1–9, 2018.

[3] D. D. Duncan and S. J. Kirkpatrick, "Can laser speckle flowmetry be made a quantitative tool?," *J. Opt. Soc. Am. A*, vol. 25, no. 8, p. 2088, 2008.

[4] S. Sun, B. R. Hayes-Gill, D. He, Y. Zhu, N. T. Huynh, and S. P. Morgan, "Comparison of laser Doppler and laser speckle contrast imaging using a concurrent processing system," *Opt. Lasers Eng.*, vol. 83, pp. 1–9, 2016.

[5] D. A. Boas and A. K. Dunn, "Laser speckle contrast imaging in biomedical optics," *J. Biomed. Opt.*, vol. 15, no. 1, p. 011109, 2010.

[6] M. Chen *et al.*, "Improving the estimation of flow speed for laser speckle imaging with single exposure time," *Opt. Lett.*, vol. 42, no. 1, pp. 57-60, 2016.

[7] L. M. Richards, S. S. Kazmi, K. E. Olin, J. S. Waldron, D. J. Fox, and A. K. Dunn, "Intraoperative multi-exposure speckle imaging of cerebral blood flow," *J. Cereb. Blood Flow Metab.*, vol. 37, no. 9, pp. 3097–3109, 2017.

[8] P. Zakharov *et al.*, “Dynamic laser speckle imaging of cerebral blood flow.,” *Opt. Express*, vol. 17, no. 16, pp. 13904–17, 2009.

[9] W. J. Tom, X. Zhang, A. Gopal, A. B. Parthasarathy, and A. K. Dunn, “Robust flow measurement with multi-exposure speckle imaging,” *Opt. Express*, vol. 16, no. 3, p. 1975, 2008.

[10] S. M. S. Kazmi, A. B. Parthasarthy, N. E. Song, T. A. Jones, and A. K. Dunn, “Chronic imaging of cortical blood flow using Multi-Exposure Speckle Imaging,” *J. Cereb. Blood Flow Metab.*, vol. 33, no. 6, pp. 798–808, 2013.

[11] A. B. Parthasarathy, S. M. S. Kazmi, and A. K. Dunn, “Quantitative imaging of ischemic stroke through thinned skull in mice with Multi Exposure Speckle Imaging,” *Biomed. Opt. Express*, vol. 1, no. 1, p. 246, 2010.

Chapter 5

Implementation of Multi-Exposure Laser Speckle Contrast Imaging with Multi-Tap Charge Modulation CMOS Image Sensor

5.1 Introduction

The blood flow changes generally happen during each cardiac cycle. The frequency of each cardiac cycle is 0.8 seconds or about 1 Hz. So in practical, to observe the blood flow change the high-speed MELSCI system are not necessary. But to observe the speckle fluctuation caused by moving scatterers like red blood cells (RBCs), the high-speed sensor is essential. Therefore, monitoring the blood flow using high-frame rate systems which operate at 20 kHz is consequential. The usage of high-frame rate system means, the redundant sampling of slow hemodynamics signals. In other words, using the high-frame rate sensor for inefficient sampling is not a good idea. This makes high-frame rate sensor an energy inefficient and high cost system. The laboratory-developed sensor has different modulation frequency and readout frequency. This multi-tap senor can efficiently sample the charges at high modulation frequency and readout the different exposure time images at a video rate. It believes that, this kind of approach can help to develop MELSCI system with low

power requirement and cost-effective. It presents the unique dimension to monitor the blood flow changes and bring the MELSCI system next step forward.

5.2 Implementation of Multi-Exposure Laser Speckle Contrast Imaging System

5.2.1 Multi-Exposure Laser Speckle Contrast Imaging System with 4-tap Pixel

The prototype chip with the charge modulator developed in our laboratory is used for this study [1]. The chip is fabricated in Dongbu HiTek 0.11um 1P4M CIS technology and the chip size is 9.3 × 7 mm^2. The unit size of the modulator is 11.2 × 11.2 um^2. In a unit pixel, 2 × 2 modulators are implemented, and those FDs are connected in parallel. The 4- tap pixel outputs are connected in parallel to 4 column ADCs each of which is 5.6 μm pitch. The entire chip consists with an array size of 132 × 84 pixels. The unit pixel size is 22.4 × 22.4 um^2.

5.2.2 Timing Diagram and its Operation

The timing diagram for 4-tap charge modulator pixels is depicted in Fig. 5.1. The back-scattered laser speckle signals from the specimen are sampled by the four sets of controlling gates G1-4. The image readout period is separated from the charge modulation and accumulation operation, as the laboratory-developed image sensor operates in the global shutter mode. Each cycle composed of charge modulation and accumulation and readout operation and these operations completes capturing of one frame. During modulation, the speckle fluctuated signals are sampled at high frequency by programming controllable FPGA signal, G1-4. During the readout period, the images of various exposure time are readout simultaneously at about the video rate. The exposure time (T_0) of each gate is determined by the shutter pattern and the readout period was fixed and it is about 2.8 ms. For example, the exposure time (T_0) of 4.8ms for each tap corresponds to the total modulation period of 19.2ms and readout time of roughly 2.8ms. Therefore, the time required to acquire a frame with four exposure images is about 22ms. With this operation,

it is confirmed that, the flow speed changes can be monitored efficiently at the frame rate of 45fps which is about the video rate.

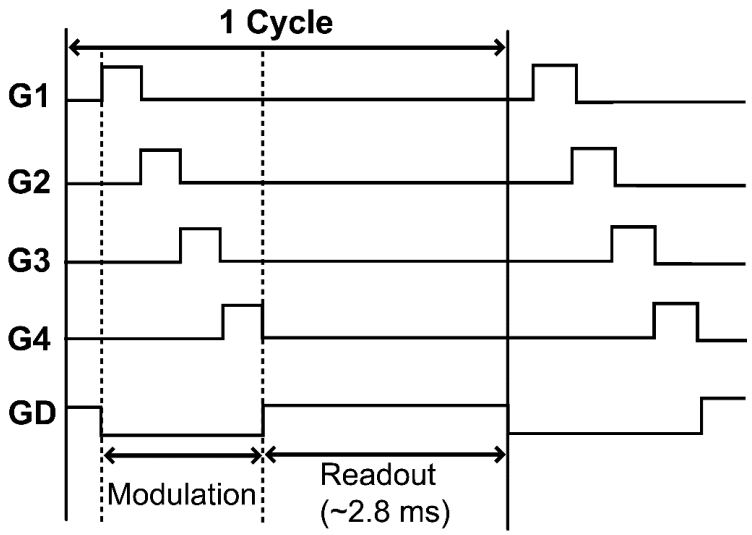

Fig. 5.1 Timing-chart of multi-tap CMOS image sensor

5.2.3 Measurement Setup of Multi-Exposure Laser Speckle Contrast Imaging System

Fig. 5.3. shows the measurement setup to build the MELSCI system with the multi-tap charge modulation pixels. To validate the multi-tap charge modulator pixels with designed exposure patterns for Multi-Exposure Laser Speckle Contrast Imaging (MELSCI), the sample of Ground glass plate and phantom of Intralipose solution (20% concentration) was used. The purpose of this experiments is to present the eminence of multi-tap charge modulator pixels to monitor the blood flow movement at low frame rate requirement, in comparison to high-speed camera. So, we emulate the reference high-speed camera experimental setup for comparison. But it is impossible to use the same measurement conditions as reference high-speed camera. The *f*-number for reference high-speed camera is 2. But the *f*-number of 11 was used for multi-tap charge modulation image sensor. Because of different pixel size in both cameras, it is important to choose the suitable *f*-number for multi-tap CMOS image sensor to obtain the speckle size which gives higher contrast value and better contrast to noise ratio (CNR). The imaging area for reference camera was limited to 5.0 × 1.0 mm to achieve high frame rate of 40kfps with the spatial

resolution of 160 × 32 pixels. But in laboratory-developed sensor, the raw speckle images were captured with an imaging area of 15 × 10 mm with the spatial resolution of 132 × 84 pixels.

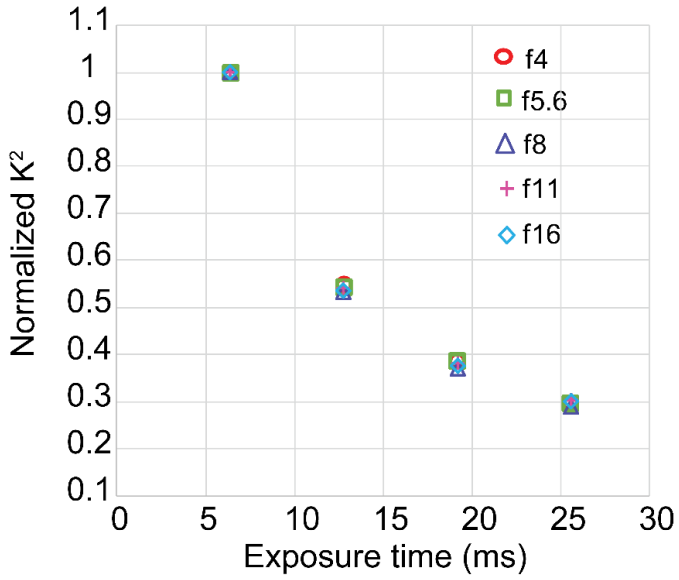

Fig. 5.2 Normalized exposure contrast curve at various f#

Table 5.1 Comparison of contrast to noise ratio at various f#

	Contrast to Noise Ratio (CNR)				
Exposure Time (ms) T_0	***f*# 4**	***f*# 5.6**	***f*# 8**	***f*# 11**	***f*# 16**
6.4	16.9	18.1	18.0	**21.9**	13.9
12.8	10.9	13.1	12.6	**14.4**	10.3
19.2	9.3	10.5	10.6	**11.3**	10.1
25.6	8.5	8.4	9.3	**8.0**	9.5

From Fig. 5.2 it is understood that, the exposure-contrast curve (normalized) for different f# gives the same contrast value in correspondence to shorter and longer exposure time. So it is difficult to choose the optimum f# from the exposure-contrast curve. The contrast to noise ratio (CNR) for each exposure time was estimated. CNR is given by:

$$CNR = \frac{Mean\ K^2}{standard\ Deviation\ of\ K^2} \qquad 5.1$$

The total frame count of 20 was used to obtain the mean and standard deviation of K^2. The measured CNR was compared between different f#'s and f# which gives the better CNR can be optimized. Based on the CNR analysis the f# - 11 was optimized to obtain the raw speckle images with multi-tap CMOS image sensor. The speckle size which given by f# - 11 was calculated. The speckle size can be estimated by the following equation [2].

$$d = 1.2\ (1 + M) f\#\ \lambda \qquad 5.2$$

where M is the optical magnification of the camera system and λ is the wavelength of the laser source used. The optical magnification of the system is calculated as 0.224. Based on this, speckle size generated by the multi-tap sensor is about 12.6 μm with the configured f# - 11. The speckle to pixel ratio is about 0.5765.

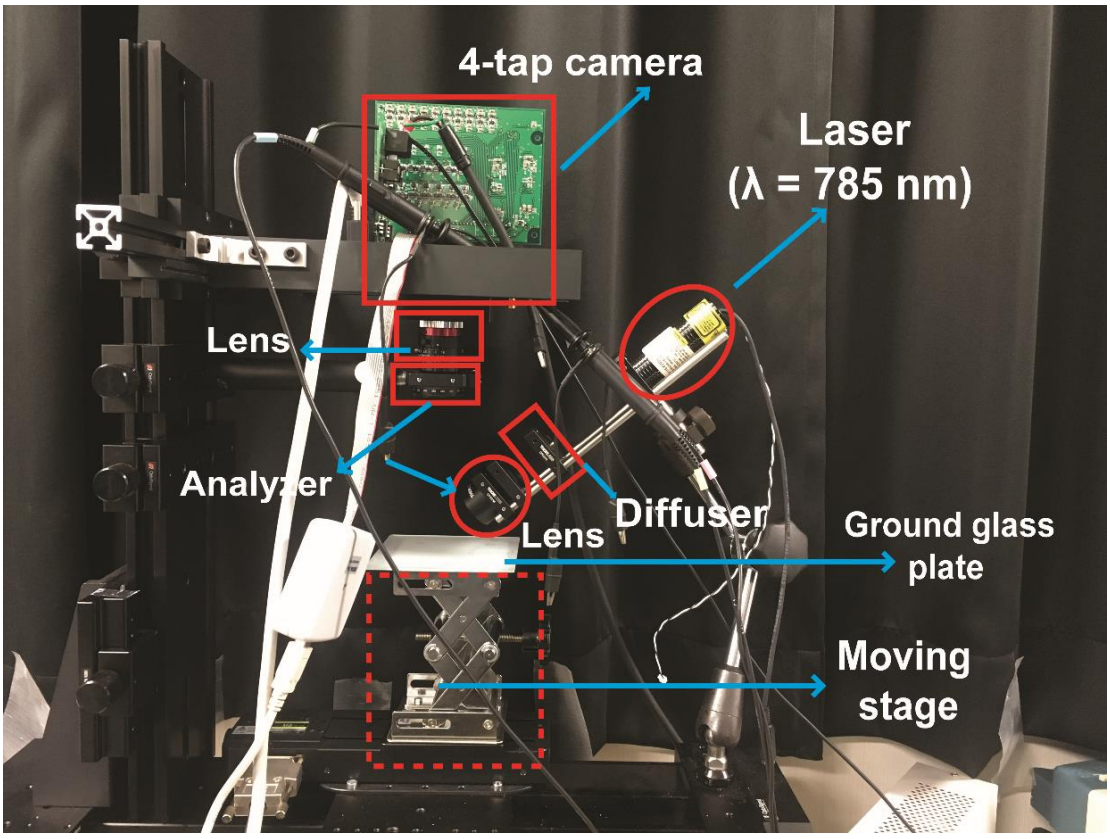

Fig. 5.3 Measurement set-up of multi-tap charge modulation CMOS image sensor

5.3 Basic Characterization of 4-tap Sensor

The basic capability of 4-tap sensor to distinguish different flow speeds has been demonstrated by the specimens of Ground glass plate and Intralipose. The flow speed of both specimen was controlled from 1mm/s to 5mm/s with the incremental step size of 1mm/s. The programmable exposure patterns of equal and exponential exposure case were implemented with 4-tap sensor. The performance of exposure patterns was compared in terms of flow speed to noise ratio (FNR).

5.3.1 Equal Exposure Pattern

At first, the measurement was carried out with equal exposure pattern. The signals to each tap (G1-4) which are controlled programmatically by FPGA is shown in Fig. 5.4.

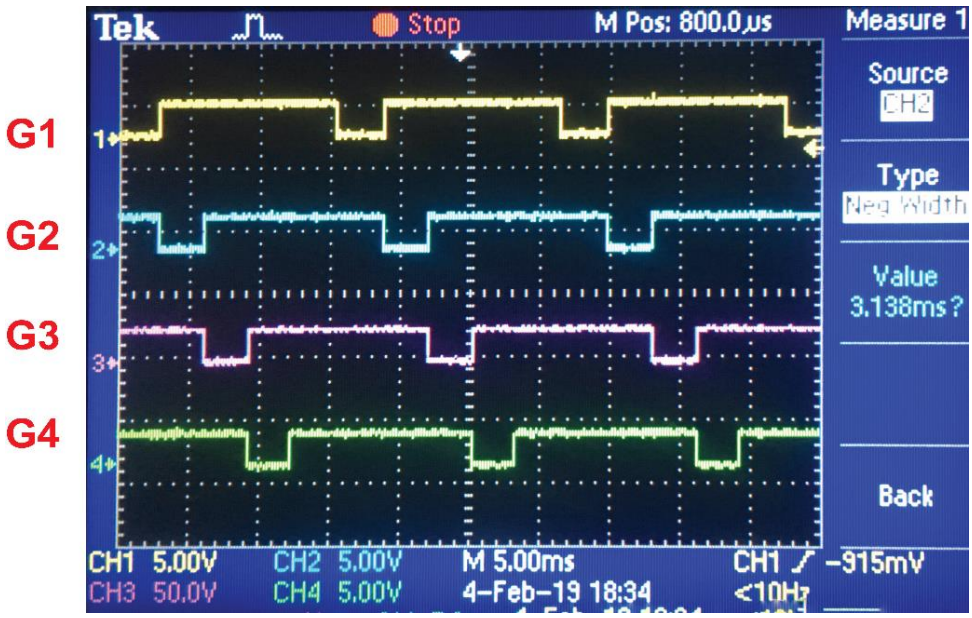

Fig. 5.4 FPGA controllable signals to 4-tap (Equal exposure)

The ratio of shortest to longest exposure time is 1:4 and the unit exposure time (T_0) is same in each taps. The measurement was carried out for the unit exposure time (T_0) of 3.2 ms and 6.4 ms for Ground glass plate. For Intralipose, the T_0 of 3.2 ms and 4.8 ms was used. By comparing the wide range of flow sensitivity and better flow speed to noise ratio (FNR), the suitable unit exposure time (T_0) was optimized.

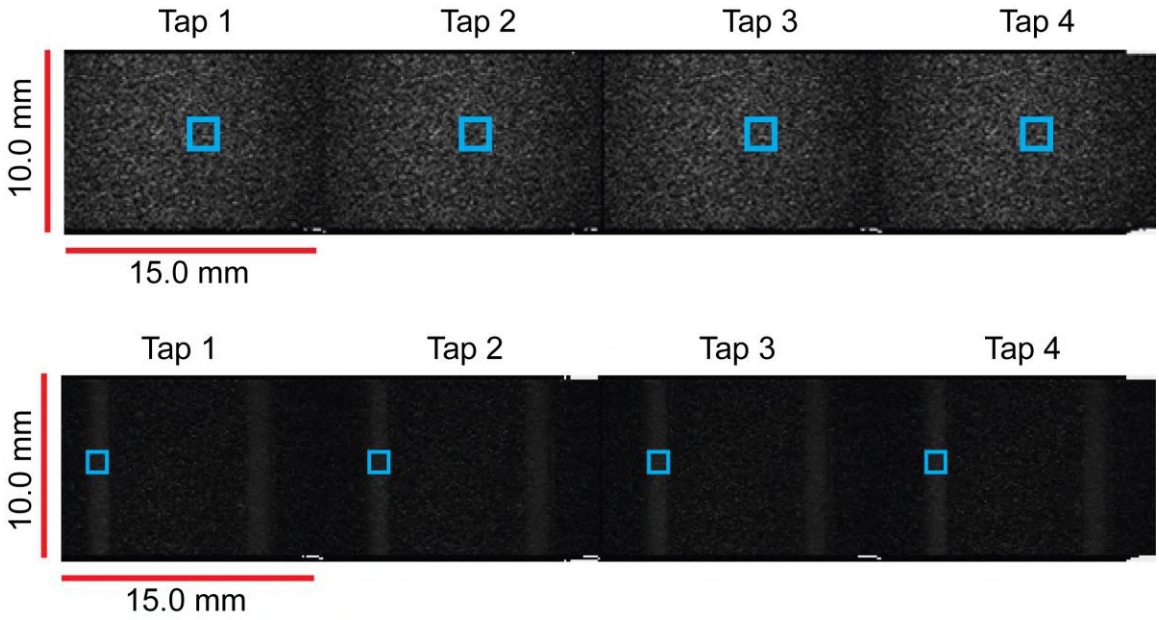

Fig. 5.5 Equal exposure raw speckle images. (a) Ground glass plate (b) Intralipose

The raw speckle images for different exposure time captured by 4-tap CMOS image sensor at the frame rate of about the video rate and it is shown in Fig 5.5. The unit exposure time (T_0) is 6.4 ms and 4.8 ms for Ground glass plate and Intralipose, respectively. The speckle variance (K^2) was calculated in the fixed ROI of 7 × 7 pixels over 20 frames. The K^2 of 20 frames are averaged out. The calculated K^2 is fitted with the following speckle model which is the same model used for simulation of high-speed camera data.

$$K^2(T) = \frac{\langle (I - \langle I \rangle)^2 \rangle}{\langle I^2 \rangle} = \rho^2 \frac{e^{-2x} - 1 + 2x}{2x^2} + 4\rho(1-\rho)\frac{e^{-x} - 1 + x}{x^2} + v_n \qquad 5.3$$

Before fitting, the normalization of the measured K^2 was done with the K^2 of the static ground glass plate at the longest exposure time of 6.4 ms [3] [4]. Generally, normalization is performing with the shorter exposure time. But to alleviate the effect of sensor noise and photon shot noise, longest exposure time was used to choose K^2. The value of K^2 obtained by the static ground glass plate at the exposure time of 6.4 ms is 0.1709. Note that the speckle averaging parameter (β) is not used in the speckle model. From table 5.2, it is clear that the unit exposure time (T_0) for ground glass plate and Intralipose was optimized as 6.4 ms and 4.8 ms, respectively.

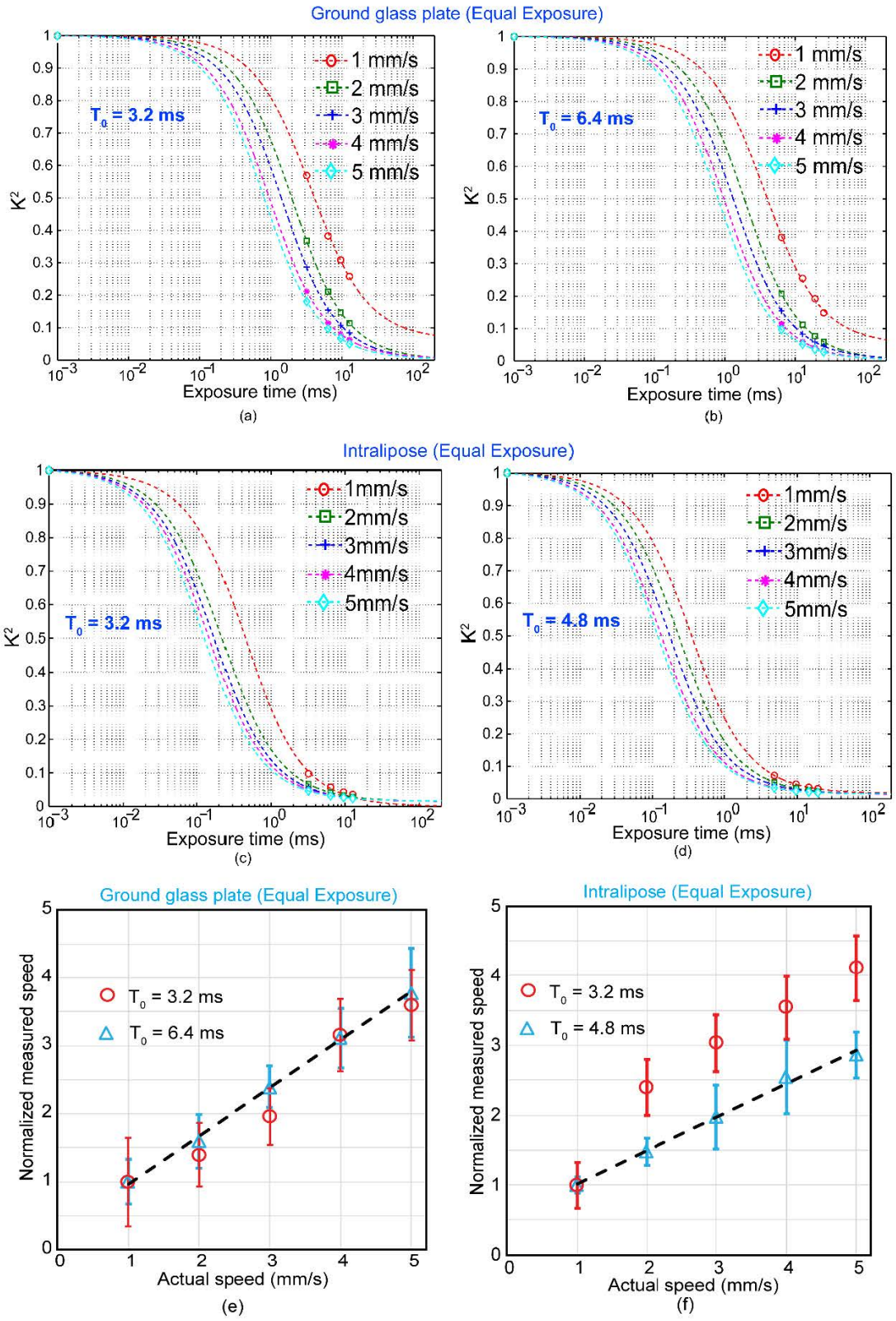

Fig. 5.6 K^2 curve and velocity profile of equal exposure pattern (a) (b) (e) Ground glass plate (c) (d) (f) Intralipose

Table 5.2 Comparison of flow speed-to-noise ratio

Velocity (mm/s)	Flow Speed to Noise Ratio (FNR)			
	Ground glass plate		Intralipose	
	T_0 = 3.2 ms	T_0 = 6.4 ms	T_0 = 3.2 ms	T_0 = 4.8 ms
1	1.002	**2.119**	2.377	**3.973**
2	2.258	**3.259**	5.404	**4.873**
3	3.875	**6.775**	6.935	**3.112**
4	5.285	**6.443**	7.271	**3.827**
5	6.209	**5.309**	8.366	**7.076**

5.3.2 Exponential Pattern Exposure Pattern

The measurement was carried out with exponential exposure pattern to compare the performance of exposure patterns in terms of FNR. The signals to each tap (G1-4) which are controlled programmatically by FPGA is shown in Fig. 5.5.

Fig. 5.7 FPGA controllable signals to 4-tap (Exponential exposure)

The ratio of shortest to longest exposure time is 1:8 and the unit exposure time (T_0) is increases exponential in manner between each taps. The raw speckle image captured by 4-tap sensor with exponential exposure case is shown in Fig. 5.8.

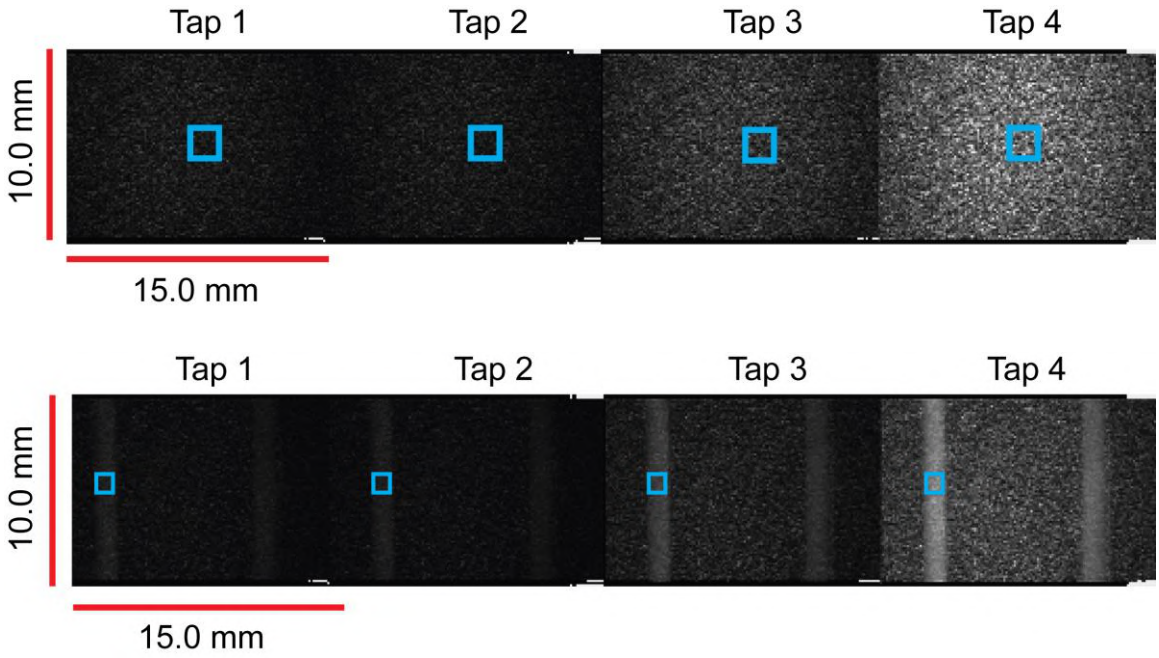

Fig. 5.8 Exponential exposure raw speckle images. (a) Ground glass plate (b) Intralipose

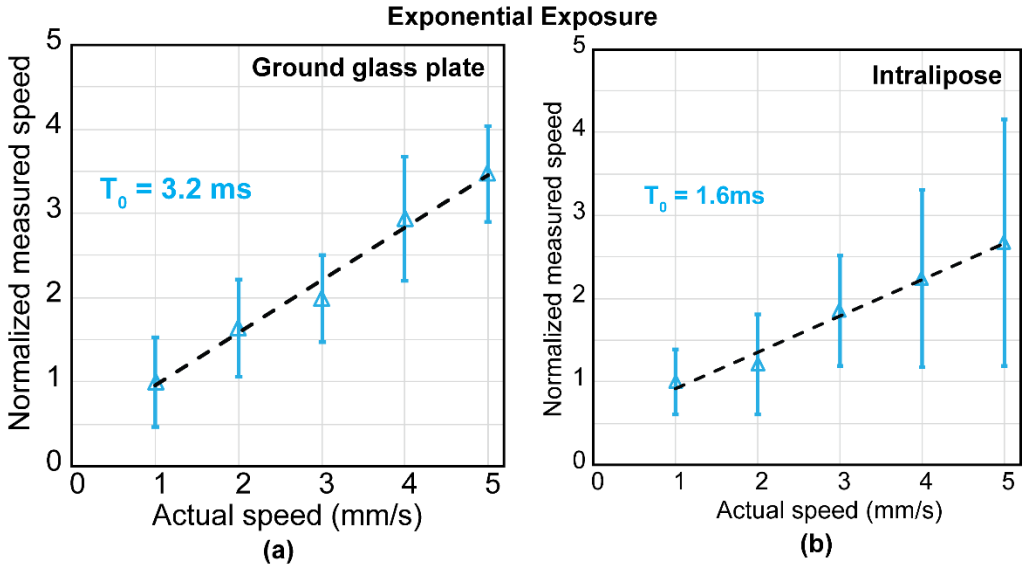

Fig. 5.9 Velocity profile of exponential exposure. (a) Ground glass plate (b) Intralipose

The unit exposure time (T_0) of expoenetial exposure case is optimized as 3.2 ms and 1.6 ms for Ground glass plate and Intralipose, respectively. From the comaprison of FNR, it is evident that equal exposure case is better suitable for monitoring the flow speed with less error rate. The exponetial exposure case may suitable for monitoring wide range of flow speed.

5.3.3 Generation of Flow Speed Map

The flow speed maps of Ground glass plate and Intralipose were mapped with equal exposure pattern case and it is shown in Fig 5.10. The equal exposure case has better FNR to map the flow speed. In Fig. 5.10 (b), the two tubes were placed. The upper tube was filled with Intralipose which was in flow condition (dynamic). And the tube in the lower side filled with Intraipose which was in static condition. However, brownian motion was found in the static intralipose fluid.

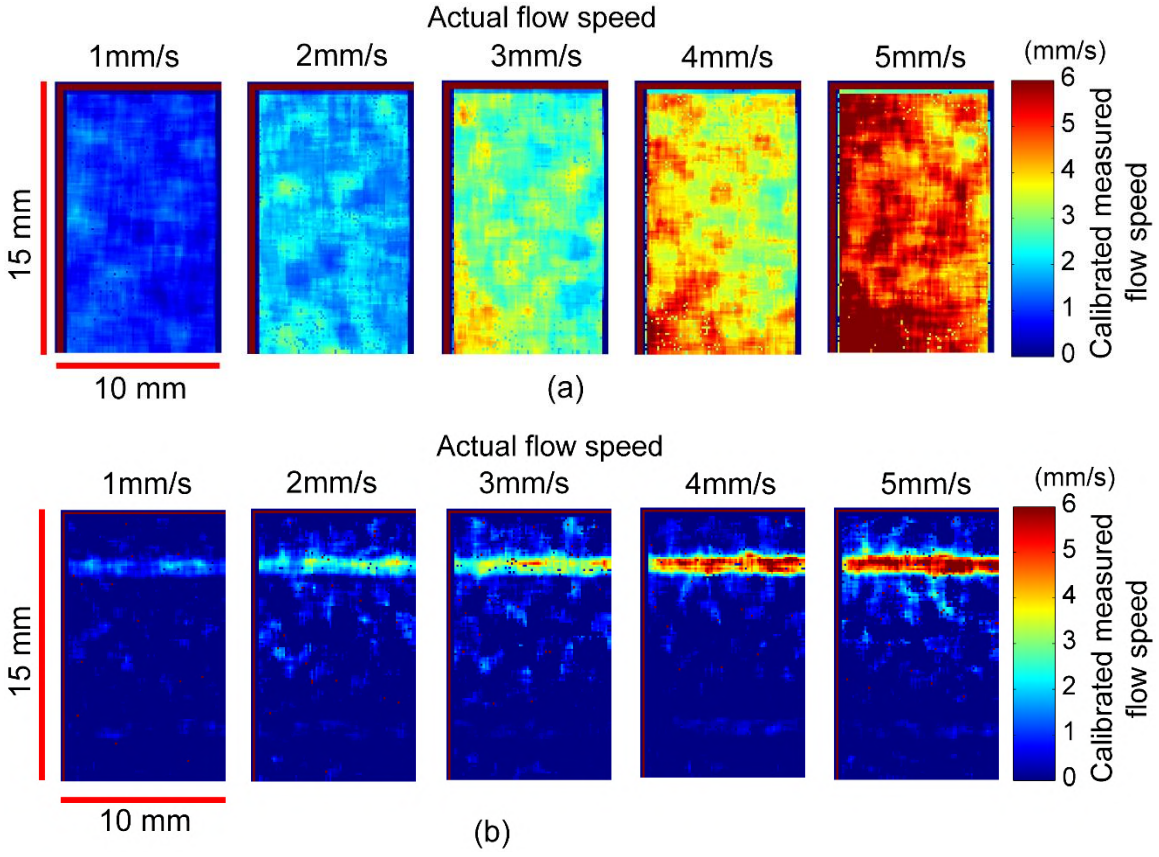

Fig. 5.10 Flow speed map of 4-tap CMOS image sensor (a) Ground glass plate (b) Intralipose

The flow speed map with absolute value was obtained by some calibration. The MELSCI system cannot quantify the absolute flow speed because of several limitations [5]. The calibration is based on a simple linear fitting and the equation is expressed as [6]:

$$V_{MELSCI} = \gamma \times \frac{1}{\tau_c} + \delta \qquad 5.4$$

where γ and δ are calibration factors (slope and y-intercept). Thus the calibrated measured flow speed is expressed as:

$$V_{CAL} = \frac{\lambda}{2\pi\tau_c}\,(V_{MELSCI} - \delta) \qquad 5.5$$

The calibration parameters (γ, δ) to calculate the calibrated measured flow speed for the ground glass and Intralipose are (0.04, 0.0143) and (0.2594 0.2898), respectively.

5.4 Movie Acquisition of Flow Speed with 4-tap Sensor

The measurement was done with Intralipose to demonstrate the potential of a multi-tap charge modulator to perform near-video-rate MELSCI. The two capillary tube with the diameter of 1mm was placed in the phantoms. The capillary tube at top and bottom side of the phantom shows the flowing and the static Intralipid fluid, respectively. From the quantitative comparison of exposure pattern, it is evident that the equal exposure case has better estimation of flow speed with lower error rate. Therefore, the equal exposure case with the optimized unit exposure time (T_0) of 4.8 ms was used to monitor the Intralipose flow speed changes. The Intralipose fluid pushed by the syringe pump at the rate of 0.017, 0.047, 0.077, 0.177 and 0.277 ml/min, which corresponds to 0.4, 1.0, 1.7, 3.8, 6.0 mm/s. The measurement was carried out for 60 seconds and the total of 2700 raw speckle images was captured with a frame rate of 45fps. The flow speed changes at every 12 seconds.

The data processing was done offline using MATLAB R2014b to estimate the calibrated measured flow speed and to generate the flow speed maps. During data processing, 40 frames were utilized for each flow speed and a total of 200 frames were utilized to make a movie. The generated video file enables the visualization of the flow speed changes and it demonstrated that the laboratory-developed multi-tap charge CMOS image sensor can monitor the flow speed changes at the frame rate of about the video-rate.

5.5 Summary

Multi-Exposure Laser Speckle Contrast Imaging (MELSCI) system was built with laboratory-developed multi-tap charge modulation CMOS image sensor which can monitor blood flow changes at about the video rate. The measurement was carried out with ground glass plate and Intralipose to demonstrate the potential of 4-tap to measure the flow speed changes. The flow speed was varied from 1-5 mm/s. The designed exposure patterns were implemented with 4-tap sensor and its performance was compared based on the Flow speed-to-Noise Ratio (FNR). The measurement results suggested that, the equal exposure can monitor the flow speed with lower error rate. The unit exposure time (T_0) of the multi tap sensor for ground glass and Intralipose measurements were optimized as 6.4 ms and 4.8 ms. Finally, to mimic the real-time blood flow changes, the demonstration was performed with 4-tap sensor at the video rate of 45 fps to acquire the flow speed maps of Intralipose flow changes to prepare a movie.

Bibliography

1. K. Kondo *et al.*, “A Built-in Drift-field PD Based 4-tap Lock-in Pixel for Time-of-Flight CMOS Range Image Sensors,” Int'l Conf. on Solid State Devices and Materials, J-7-03, pp. 5–6, 2018.

2. A. Fuentes-Garcia, J. C. Ramirez-San-Juan, N. Salazar-Hermenegildo, B. Choi, R. Ramos-Garcia, and E. Mendez-Aguilar, "Effects of speckle/pixel size ratio on temporal and spatial speckle-contrast analysis of dynamic scattering systems: Implications for measurements of blood-flow dynamics," Biomed. Opt. Express., vol. 4, no. 10, pp. 1883-1889 (2013).

3. L. M. Richards, S. S. Kazmi, K. E. Olin, J. S. Waldron, D. J. Fox, and A. K. Dunn, "Intraoperative multi-exposure speckle imaging of cerebral blood flow," J. Cereb. Blood Flow Metab., vol. 37, no. 9, pp. 3097–3109 (2017).

4. M. Chen, X. Chen, P. Li, D. Wen, Y. Wang, Q. Huang, and J. Lu, "Improving the estimation of flow speed for laser speckle imaging with single exposure time," Opt. Lett., vol. 42, no.1, pp. 57-60 (2016).

5. D. D. Duncan and S. J. Kirkpatrick, "Can laser speckle flowmetry be made a quantitative tool?," J. Opt. Soc. Am. A **25**(8), 2088 (2008).

6. S. Sun, B. R. Hayes-Gill, D. He, Y. Zhu, N. T. Huynh, and S. P. Morgan, "Comparison of laser Doppler and laser speckle contrast imaging using a concurrent processing system," Opt. Lasers Eng. vol. 83, pp. 1–9 (2016).

Chapter 6

Conclusion

The recent trends in the development in the high-speed CMOS image sensor paved the way for the development of multi-exposure laser speckle contrast imaging (MELSCI). The high-speed sensor can reproduce two-dimensional (2D) blood flow imaging with quantitative analysis in real-time. However, the high-speed camera need large internal memory to store and process the speckle images. It does not argue well in terms of power efficient and cost efficient. So high power consumption, need of large memory and high processing capability may lead to large and expensive hardware.

6.1 Main Findings

In this study, a power-efficient MELSCI system was implemented with laboratory-developed multi-tap charge modulation image sensor for blood flow speed imaging at near video rate (~ 30 fps). The multi-tap originally developed for time-of-flight (ToF) range imaging application. The multi-tap CMOS image sensor operates in the global shutter mode and every pixel is implemented with multi-storage nodes (FD1-4). The problem of inter-frame delay was alleviated because there is no idle time in exposure. The exposure time for each tap are programmable and can be implement with FPGA. The different exposure patterns (coded, equal, exponential) were designed to implement with multi-tap sensor. In order to evaluate the effectiveness of the proposed method and to finds the suitable exposure pattern and optimum camera exposure time, the simulation was

performed with high-speed camera data. A ground on a motorized stage and Intralipose flowing in a tube which controlled by syringe pump were measured. The measurement was carried out for 1 second. The total of 40000 raw speckle images was captured by high-speed camera data with a sampling frequency of 40 kHz and with a temporal resolution of 25 μs. The acquired raw speckle images were constructed into 9 datasets to perform data processing. Each dataset consists of 4096 raw speckle images with a total exposure time of 102.4 ms. The longer exposure time were obtained by synthesizing the shortest exposure time of 25 μs. For example, summing of 2 images give the exposure of 50 μs, 4 images into 1 ms and a total of 4096 images will give an exposure time of 102.4 ms. The K^2 value for synthesized 13 exposure times were calculated from the measured data using binary tree averaging algorithm. The ROI of 7 × 7 pixels were used for calculation. The dense K^2 curve with and without averaging algorithm were compared. It was clear that, the averaging helps to improve the calculation of K^2, especially at lower exposure time. Because at lower exposure time, the signal level is less and it affect by noise.

The simulation of multi-tap sensor was performed with reference high-speed camera data. The exposure pattern of coded, equal and exponential were used for simulation. During simulation, several unit exposure time (T_0) were used under the constraint that the longest exposure time is less than 33 ms (less than one frame period for the video rate). The calculated K^2 value by simulation was compared with measured K^2 value. Both K^2 value matched each other. At first, the fitting was done with the speckle model which does not consider the effect of static scatterers. In fitting the high speed camera data, three parameters (β, v_n, τ_c) were estimated. But in 4-tap case, the fitting was done by assuming β as K^2 value measured by static ground glass at shorter exposure time of 25 μs. The assumption was required, because estimating 3 parameters from 4 data points was difficult. The parameters of v_n and τ_c were estimated. From correlation time (τ_c), the flow speed was estimated. The measured or estimated flow speed is not absolute flow speed value. Because of several hindrances, the calibration is essential in LSCI to find the absolute flow speed. Although, the flow speed was extracted with the current speckle model, the assumption of static scatterers (ρ) in the speckle model is essential to avoid the underestimation of flow speed value. The fitting was carried out by considering the effect

of static scatterers, In the fitting, one additional data points was considered with an assumption that the normalized K^2 becomes unity for a sufficiently short exposure time

(1 μs was considered in this study). This is because only four data points were not satisfactory for fitting. The comparison of multi-tap sensor with high-speed camera was done in terms of flow speed. The longer exposure time mostly resulted in higher sensitivity. The quality of estimated speed was evaluated by the flow-speed-to-noise ratio (FNR). FNR is defined as the ratio of the estimated speed to the standard deviation of estimated speed. The FNRs for the different T_0 was compared. The T_0 which give high FNR was considered as optimum exposure time. Overall, the equal exposure pattern gives higher FNR than the exponential exposure pattern. T_0 was optimized as 6.4 ms and 3.2 ms for ground glass plate and Intralipose, respectively.

After the verification of multi-tap sensor by simulation, the implementation of multi-exposure laser speckle contrast imaging system with multi-tap charge modulation CMOS image sensor was carried out. The basic characterization was done with Ground glass plate and Intralipose. The flow speed of 1mm/s to 5 mm/s with an incremental step size of 1mm/s was used. The experiments with a four-tap CMOS image sensor demonstrated that a flow speed map was obtained at a moderate frame rate of 35 fps and 45 fps for ground glass plate and Intralipose, respectively. The movie acquisition of Intralipose flow speed change was demonstrated with 4-tap sensor at a video rate.

Appendix

Investigation of Optimal Taps

In this study, MELSCI was performed with video rate acquisition using 4 -tap CMOS image sensor. The arbitrary exposure is implemented by programming the GX (X = 1-4) signals. However, to taking advantage of the programmable exposure, four taps may not be optimal. Investigation on the number of optimal taps per pixel and exposure patterns is necessary in future work.

In designing a multi-tap CMOS image sensor, we have a tradeoff between the number of taps per pixel and the pixel size. The charge transfer gate, charge storage diode, and readout circuit are essential for each tap. We have confirmed that approximately $10 \times 10\mu m^2$ pixel is possible in a 0.18μm CMOS image sensor process and $22.4 \times 22.4\mu m^2$ pixel with 8 taps has been developed in 0.11μm CMOS image sensor process [1]. Basically, pixels with many taps are useful to measure the whole shape of the K^2 curve. An increase in the number of taps can contribute to two advantages: the increase of the estimated signal to noise ratio due to the averaging effect and complete estimation of all the parameters, ρ, β, τ_c, and v_o when illumination intensity is sufficiently strong.

To understand the effectiveness of averaging effect with 6-taps and 8-taps, the simulation was carried out with the reference high-speed camera data. The simulation of 6-taps and 8-taps with high-speed camera data were done in MATLAB R2017b. The simulation results will help to investigate the optimal number of taps and its potency to

measure flow speed. In future the simulation results will help to build up the MELSCI system with increased number of taps.

The equal exposure pattern and exponential exposure pattern using 6-taps and 8-taps were designed. The exponential exposure patterns with different total number of taps assigned with same unit exposure time of T_0 taps (N = 2, 4, 6) were designed. N is the total number of taps assigned for the same unit exposure time of T_0. For example, the ratio of exposure time for 8-taps with exponential exposure pattern (N = 4) is given as: [T_0 T_0 T_0 T_0 $2T_0$ $4T_0$ $8T_0$ $16T_0$].

Simulation of 6-taps with High-Speed Camera Data

The equal exposure pattern with 6-taps are shown in Fig A. 1 The ratios of the shortest to the longest exposure times are 1:6. Because of increase in the total number of taps, the averaging of signals can be performed in a better manner. Therefore, the standard deviation of the calculated contrast value is expected to improve. For example, to synthesize images for an effective exposure time of $T_1 = T_0$, 6 combinations are possible in comparison to the 4 with 4-taps. For $T_2 = 2T_0$, combination of 5 can be done in comparison to 3 in case of 4-taps. For exponential exposure pattern with 6-taps, N = 2 and 4 combinations were designed and shown in Fig A. 3 and Fig A. 5.

The equal exposure pattern with 6 taps was simulated with the high-speed camera data (Ground glass plate). The comparison plot of fitted K^2 curve for various unit exposure time (T_0) of 0.1 ms, 0.4 ms, 1.6 ms, 3.2 ms were shown in Fig A. 2. In case of exponential exposure pattern (N = 2), the various T_0 of 0.1 ms, 0.4 ms, 0.8 ms, 1.6 ms were simulated and plotted in Fig A. 4. The longer T_0 is expected to produce a good fit of K^2 values and provides a largest mean FNR. The mean FNR of various unit exposure times (T_0) was estimated. The mean FNR plot for various exposure patterns of 6-taps were compared with equal exposure pattern of 4-taps.

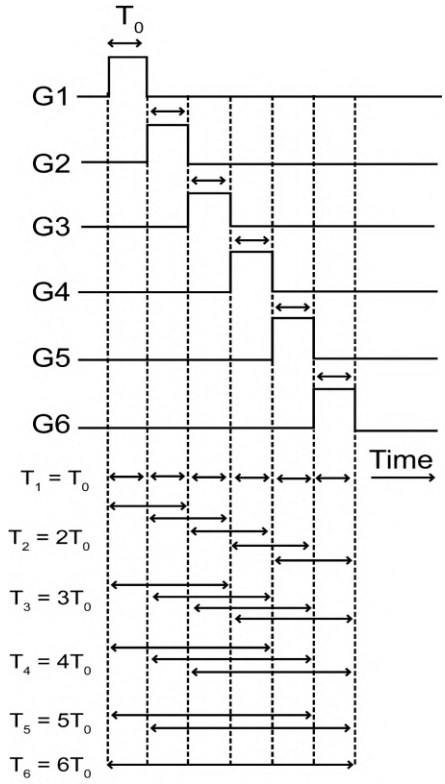

Fig A. 1 Equal exposure pattern (6-tap)

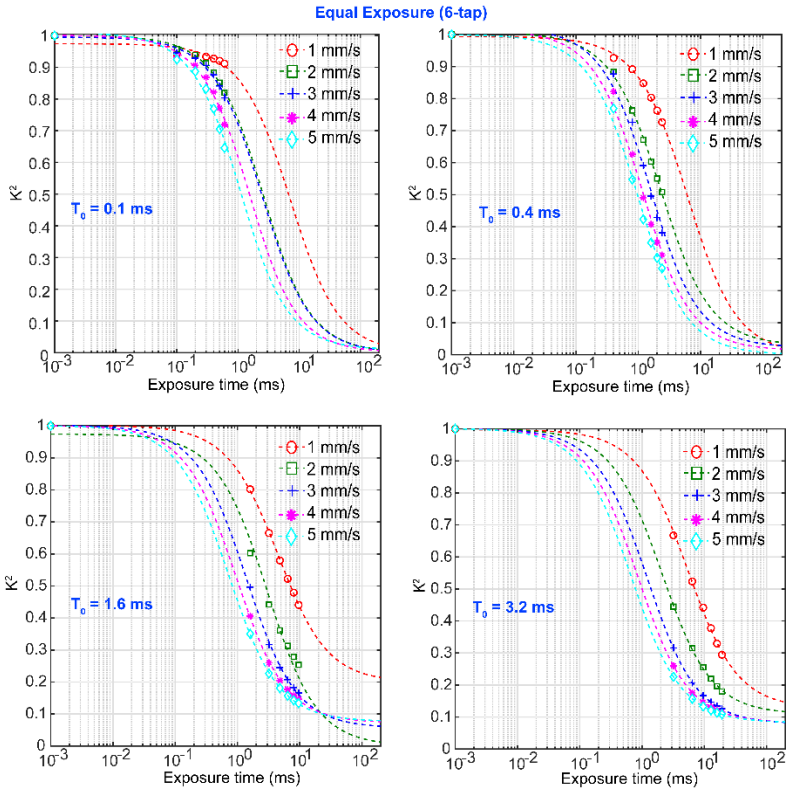

Fig A. 2 Fitted K^2 curve of 6-tap sensor (Equal exposure)

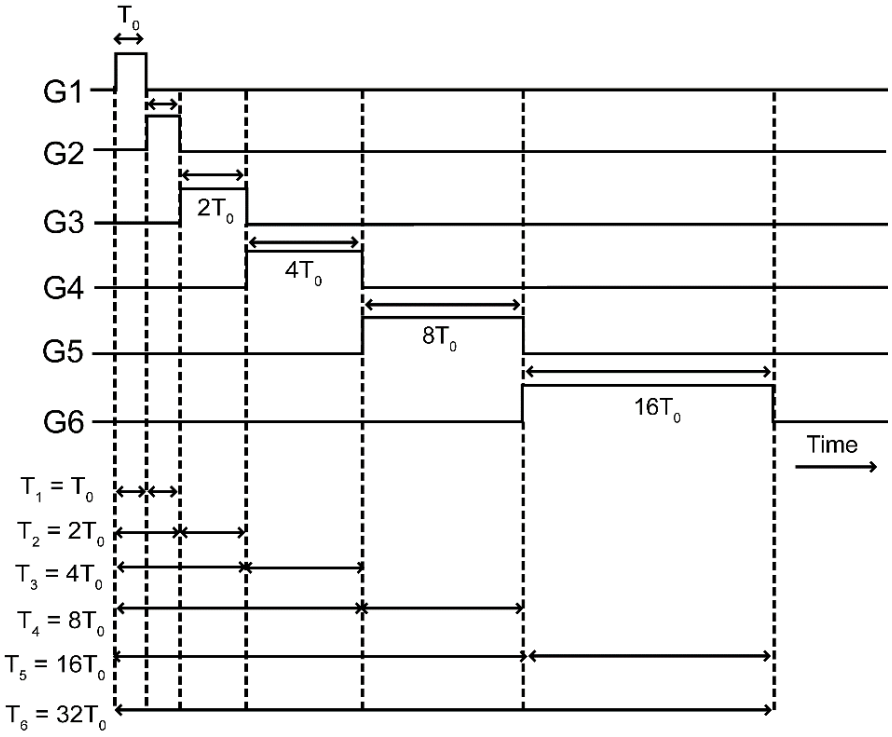

Fig A. 3 Exponential exposure pattern (6-tap, N = 2)

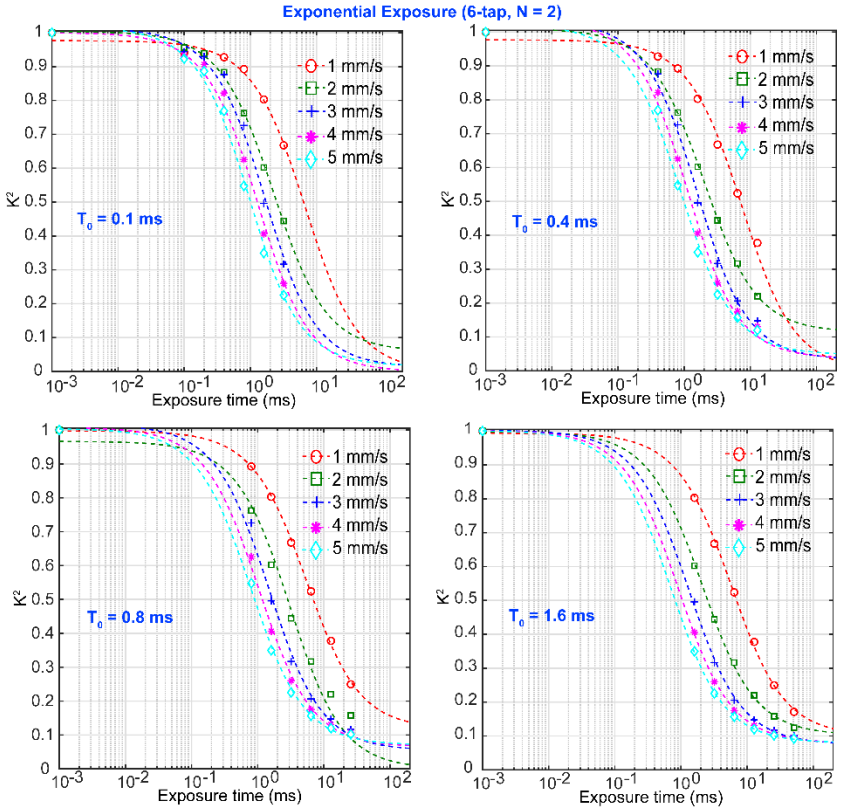

Fig A. 4 Fitted K^2 curve of 6-tap sensor (Exponential exposure, N = 2)

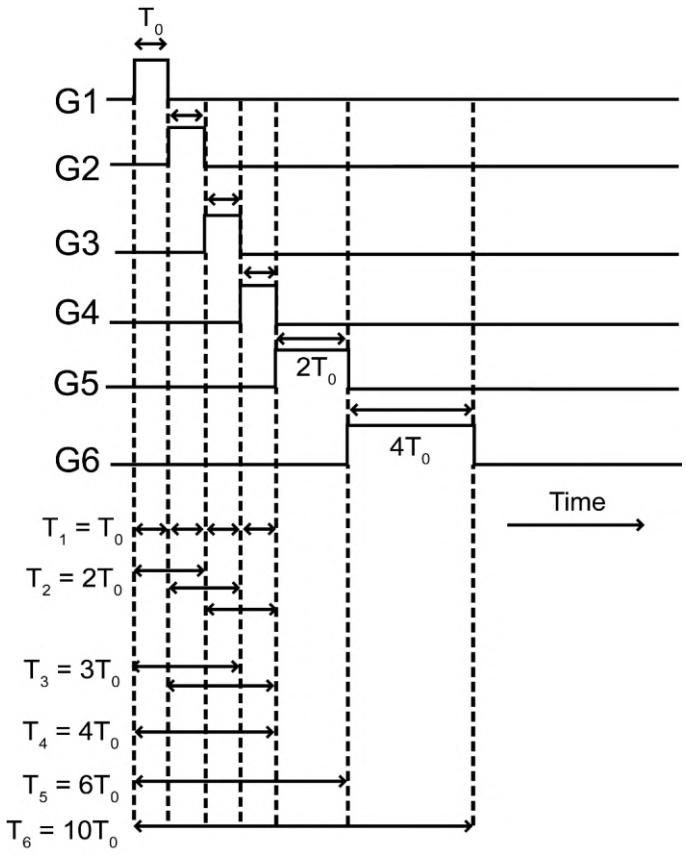

Fig A. 5 Exponential exposure pattern (6-tap, N = 4)

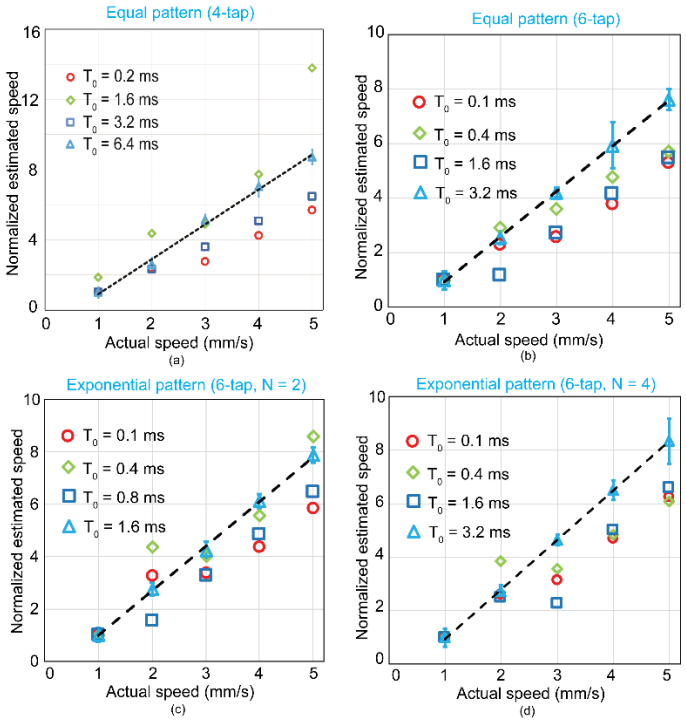

Fig A. 6 Normalized estimated flow speed vs. actual flow speed

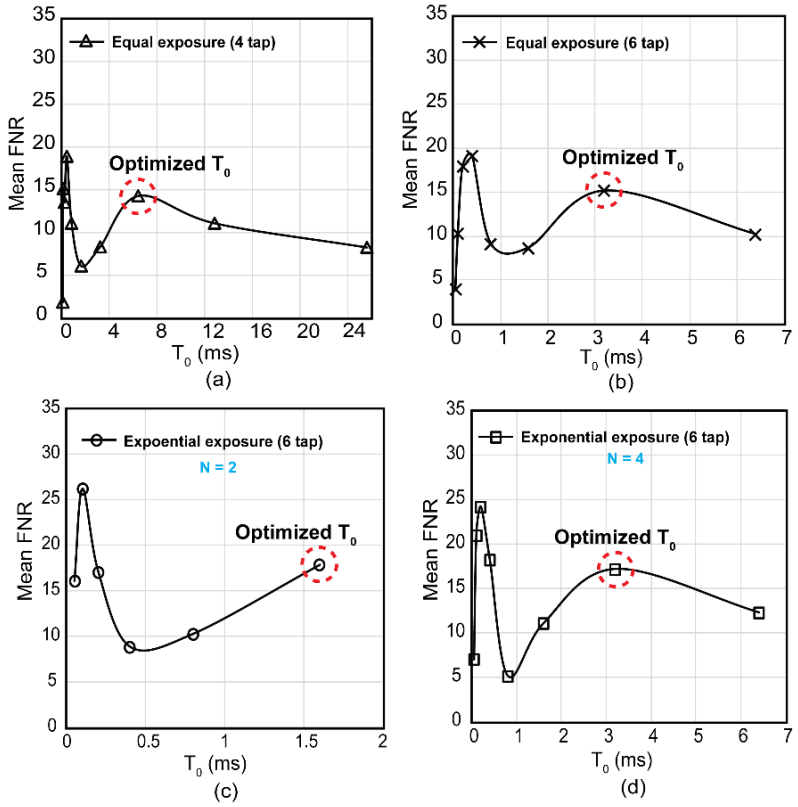

Fig A. 7 Mean FNR vs. T_0

The comparison of mean FNR with various exposure patterns were shown in Fig A. 7. The equal exposure with 6-taps gives inappreciable increase in mean FNR in comparison with equal exposure of 4-taps. But, the optimal exposure time (T_0) of 3.2 ms is sufficient to monitor the flow speed with 6-taps (equal exposure). In case of 4-taps T_0 was 6.4 ms. The mean FNR plot of exponential exposure pattern (N = 2 and 4) were compared and shown in Fig. 7.7 (c) and (d), respectively. From the comparison, it is understood that the exponential patterns provide better mean FNR than equal exposure pattern of 4-taps and 6-taps. The one reason is that the exponential exposure pattern covers a wide of range of exposure time from T_0 to $10T_0$. In case of equal exposure, it covers from T_0 to $6T_0$. The exponential exposure of N = 2 and 4 provided the mean FNR of 17.85 and 17.21, respectively. There is no significant difference in the mean FNR value. So in conclusion, the exponential exposure pattern with 6-taps (N = 2) provides the better performance in the measure of flow speed in comparison to the equal exposure pattern of 4-taps and 6-taps. The flow speed shown in Fig A. 6 also confirms that the exponential exposure pattern (6-taps, N = 2) can measure flow speed with improved SNR.

Simulation of 8-taps with High-Speed Camera Data

The equal exposure pattern with 8-taps is shown in Fig A. 8. The averaging of signals can be performed in the efficient way because of increase in the number of taps. The mean FNR of 8-tap is expect to be higher than the mean FNR of 4-tap and 6-tap equal exposure pattern.

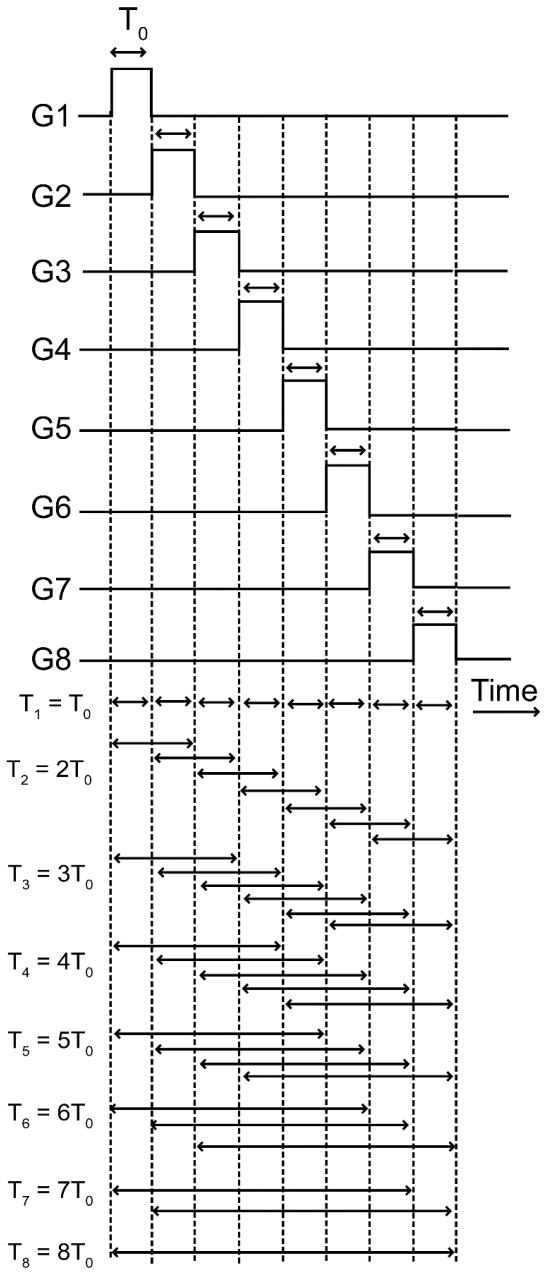

Fig A. 8 Equal exposure pattern (8-tap)

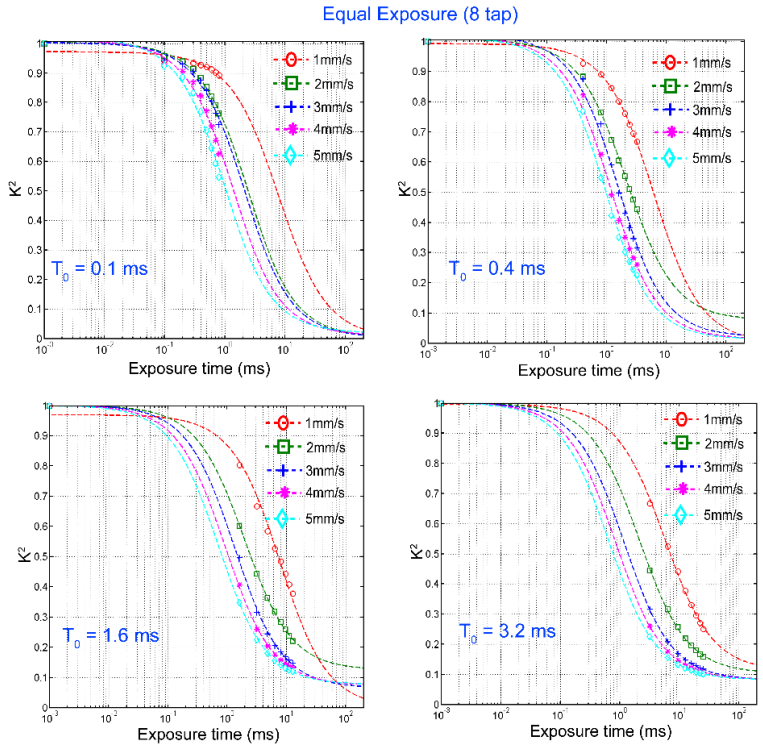

Fig A. 9 K^2 curve of equal exposure pattern (8-tap)

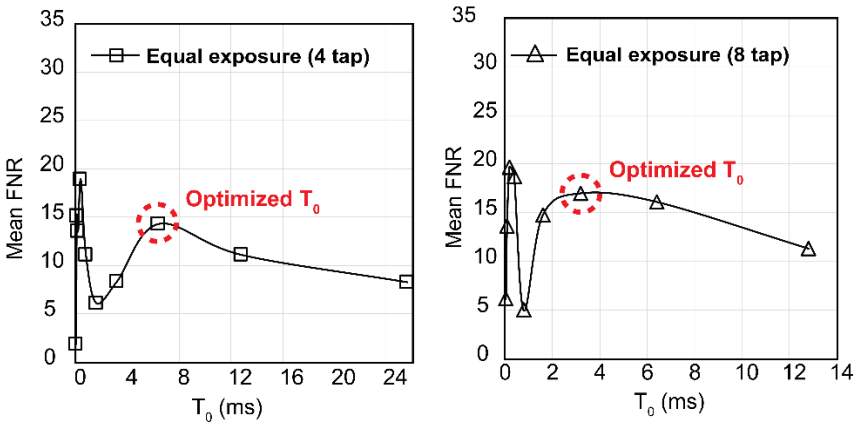

Fig A. 10 Mean FNR comparison of equal exposure pattern (4-tap and 8-tap)

The mean FNR of equal exposure at optimized T_0 were quantitatively estimated as 14.29 (4-tap), 15.14 (6-tap) and 16.97 (8-tap). The signal to noise ratio of 8-tap due to the better averaging effect shows the slighter improvement as expected as shown in Fig A. 10. But still the improvement is not so significant in comparison with 4-tap. Therefore, the utilization of exponential exposure pattern with 8-tap may be an effective way to improve the signal to noise ratio.

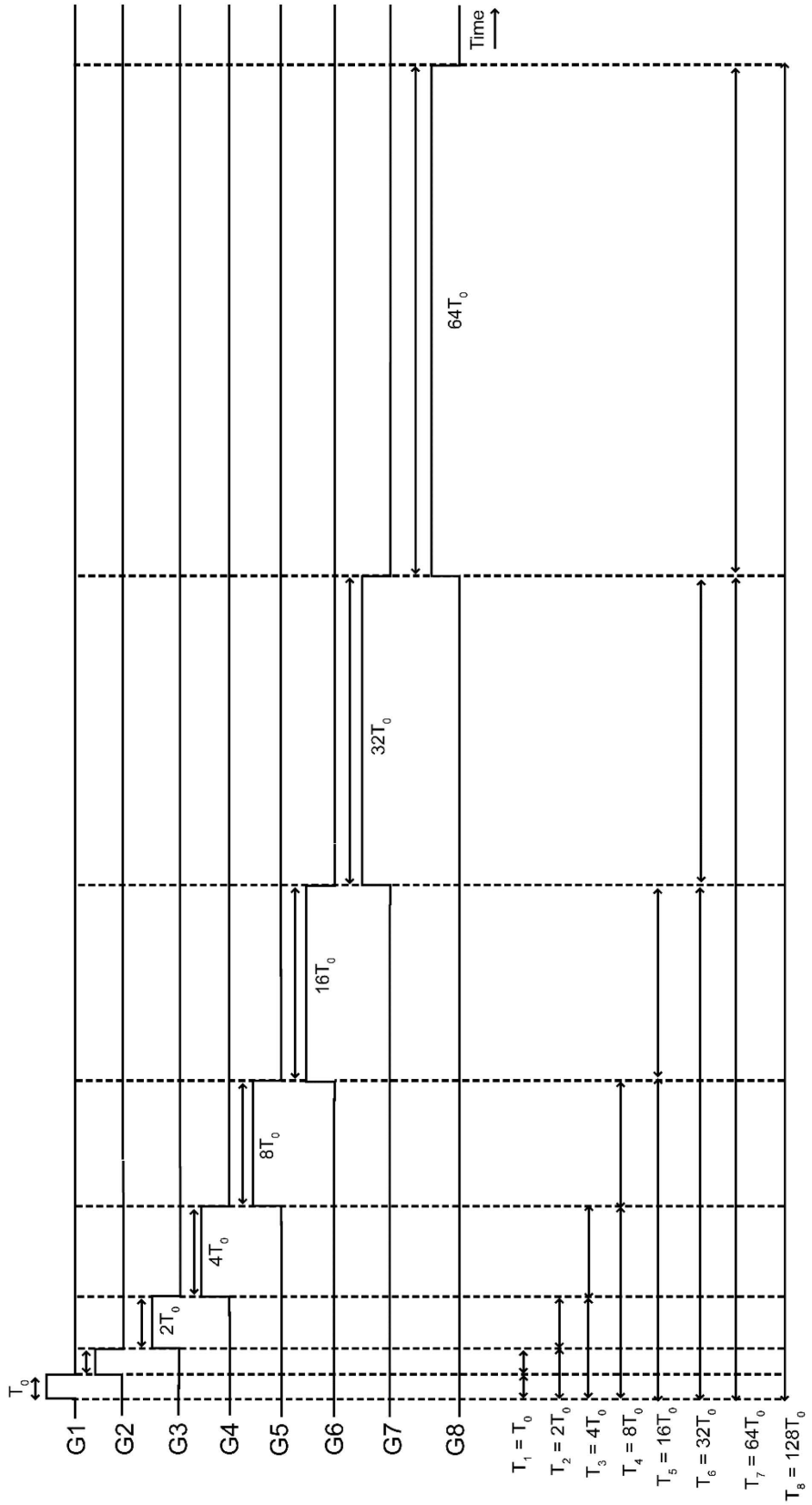

Fig A. 11 Exponential exposure pattern (8-tap, $N = 2$)

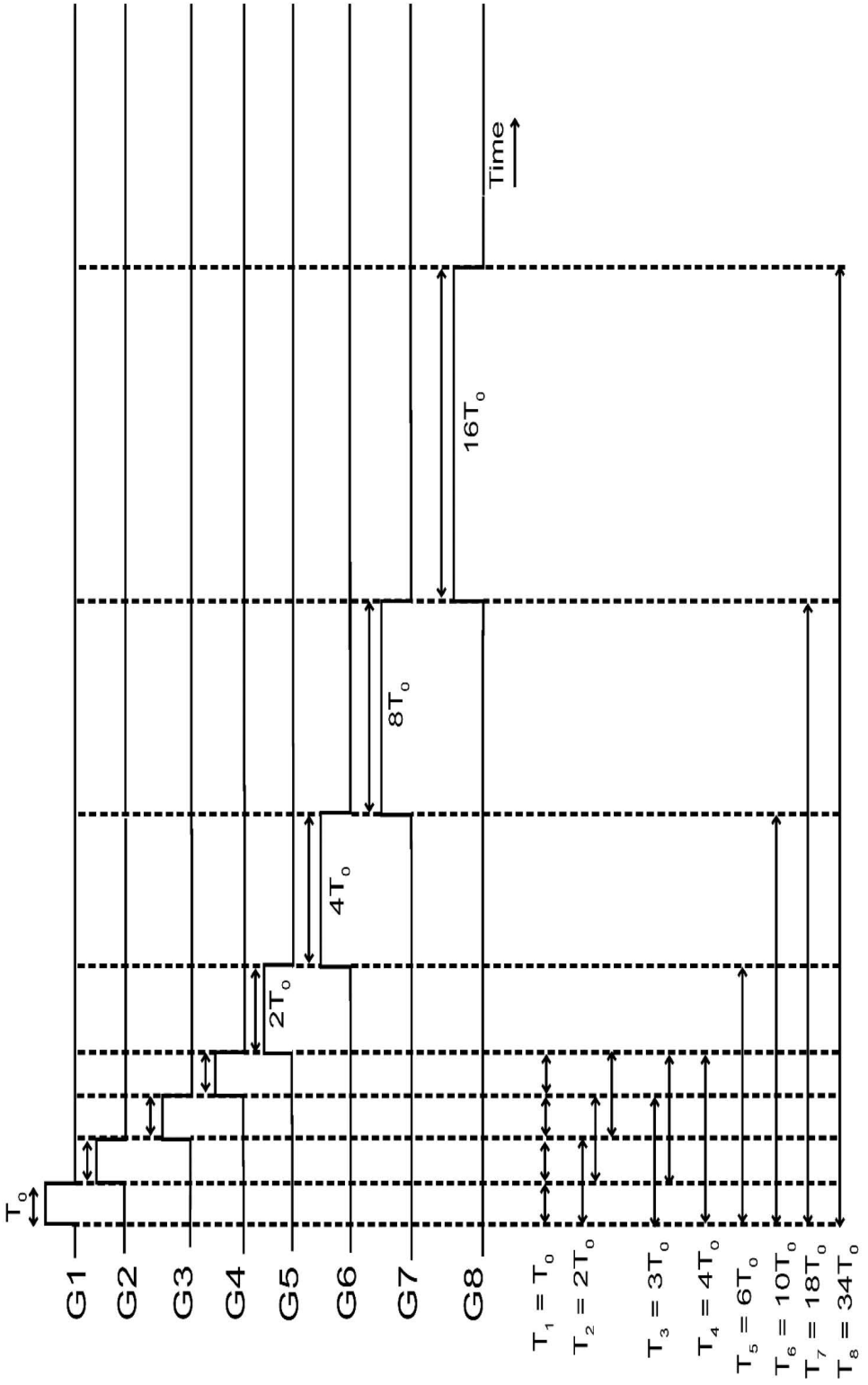

Fig A. 12 Exponential exposure pattern (8-tap, $N = 4$)

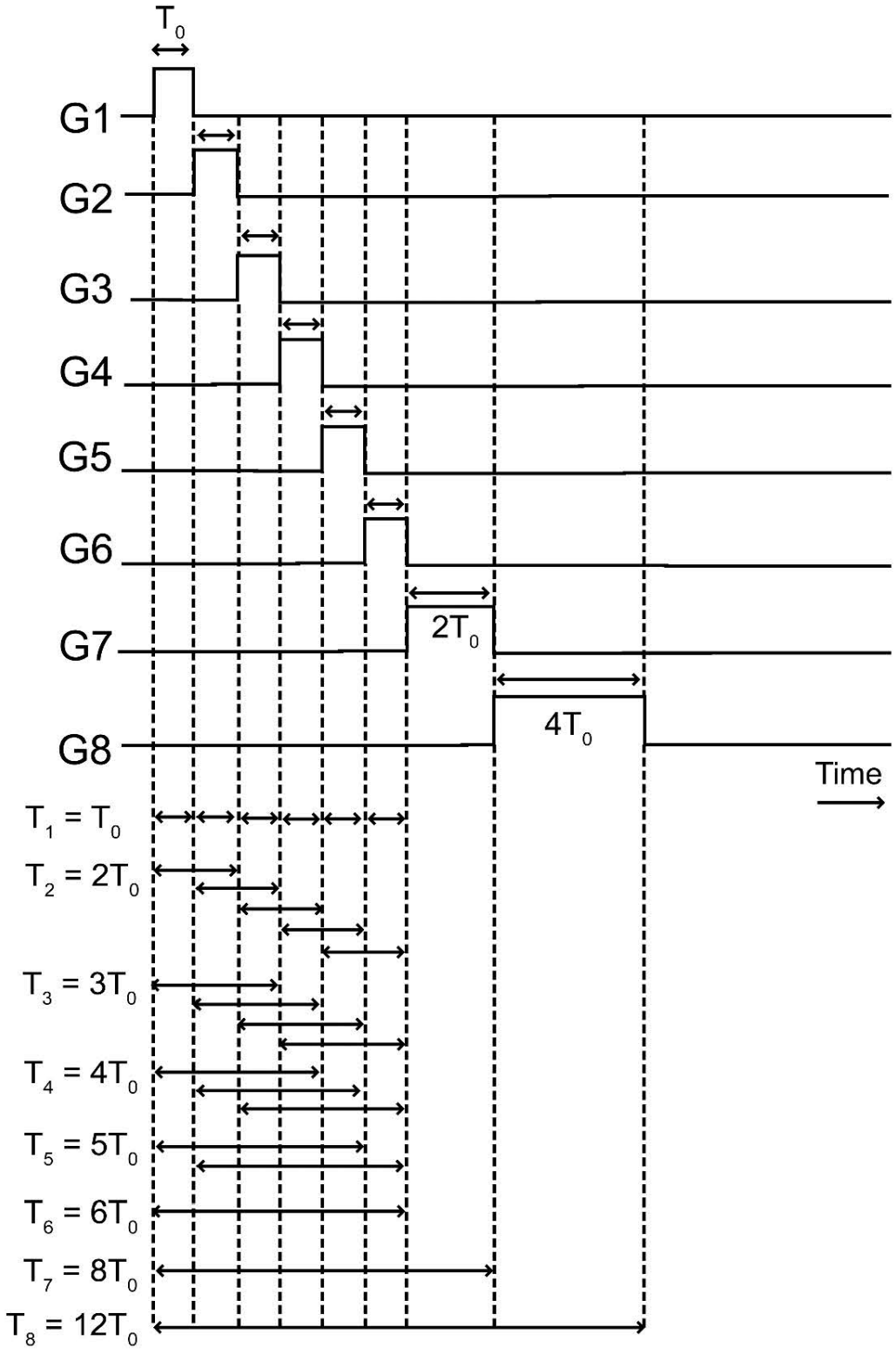

Fig A. 13 Exponential exposure pattern (8-tap, $N = 6$)

The mean FNR plot of exponential exposure pattern (8-tap) for various N's were compared with equal exposure pattern (8-tap) and it is shown in Fig A. 14.

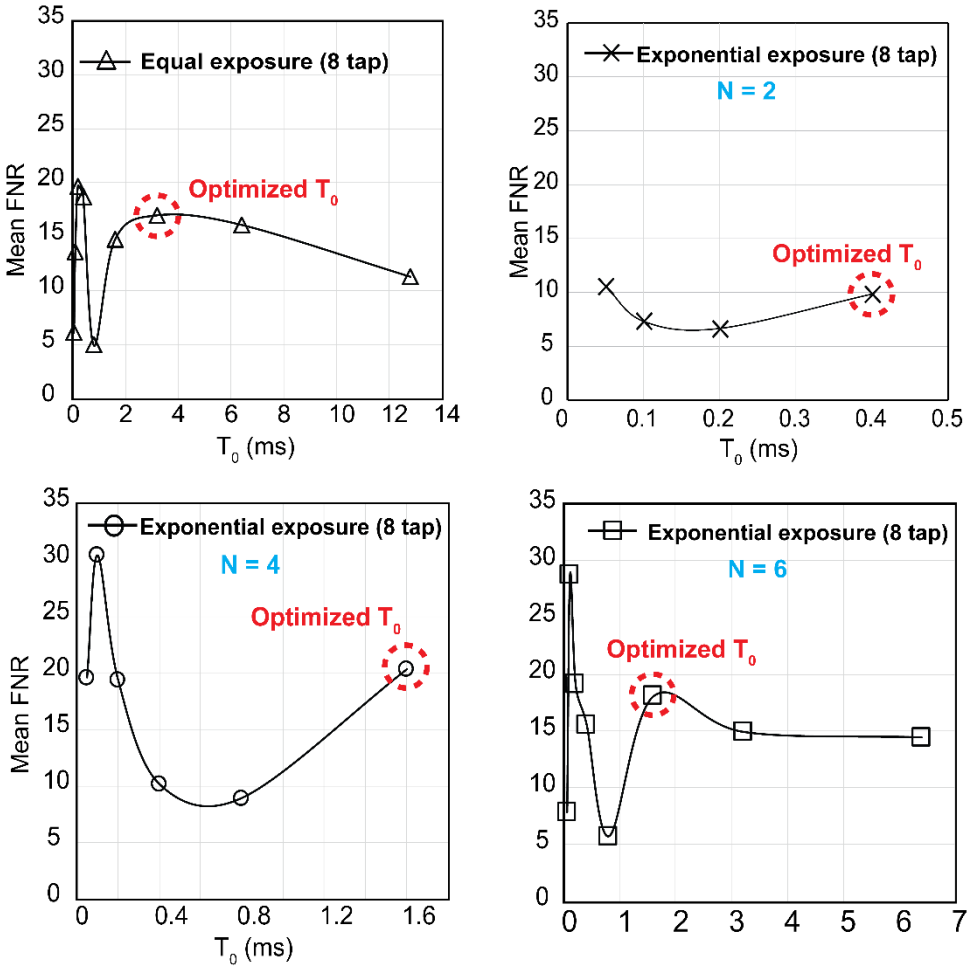

Fig A. 14 Mean FNR comparison of equal exposure (8-tap) and exponential exposure pattern (8-tap, N = 2, 4, 6)

From the comparison of mean FNR, it is evident that the exponential exposure pattern can provide the better FNR in comparison to equal exposure case (8-tap). But choosing the optimal *N* (count of same T_0) is very essential. As expected, the N of 4 and 6 provide the better signal to noise ratio. N of 2 does not provide the efficient averaging effect because of the ineffective utilization of 8-taps. N of 4 and 6 effectively utilized the 8-taps to perform the averaging. Mean FNR of N = 4 and 6 is quantitatively estimated as 20.32 and 18.08, respectively. The significant difference in the mean FNR is not observed. Therefore, the optimal N was chosen based on the longest exposure time (T_8).

N = 4 and 6 gives the total longest exposure time of $34T_0$ and $12T_0$, respectively. The unit exposure time is 1.6 ms (N = 4 and 6). The longest exposure time (T_8) for N = 4 and 6 is 54.4 ms and 19.2 ms, respectively. Therefore, the exponential exposure pattern (8-tap, N = 4) provides the highest signal to noise ratio with a total acquisition time of 54.4 ms. At the same time, the longest exposure times will help to monitor a wide range of flow speeds. Because the ratio of longest to shortest exposure time is higher. From simulation, it is evident that the utilization of 8-tap with an optimal exponential exposure pattern can improve the accuracy in the estimation of flow speed.

The important thing to notice is that the mean FNR of high-speed camera is 14.78. But the mean FNR obtained by the 6-taps exponential exposure pattern 8-taps exponential exposure pattern is higher than the reference high-speed camera. The one possible reason might be, the shorter exposure times of 1 μs is assigned in simulating 6-taps and 8-taps and short exposure times (0.05 ms to 1 ms) are not presence in the K^2 curve. To investigate the mean FNR of high-speed camera, the high-speed camera data were processed by assigning the shorter exposure time of 1 μs and excluding short exposure time of 25 μs, 50 μs, 0.1 ms, 0.2 ms, 0.4 ms, 0.8 ms. The K^2 curve with and without short exposure times were compared in Fig A. 15.

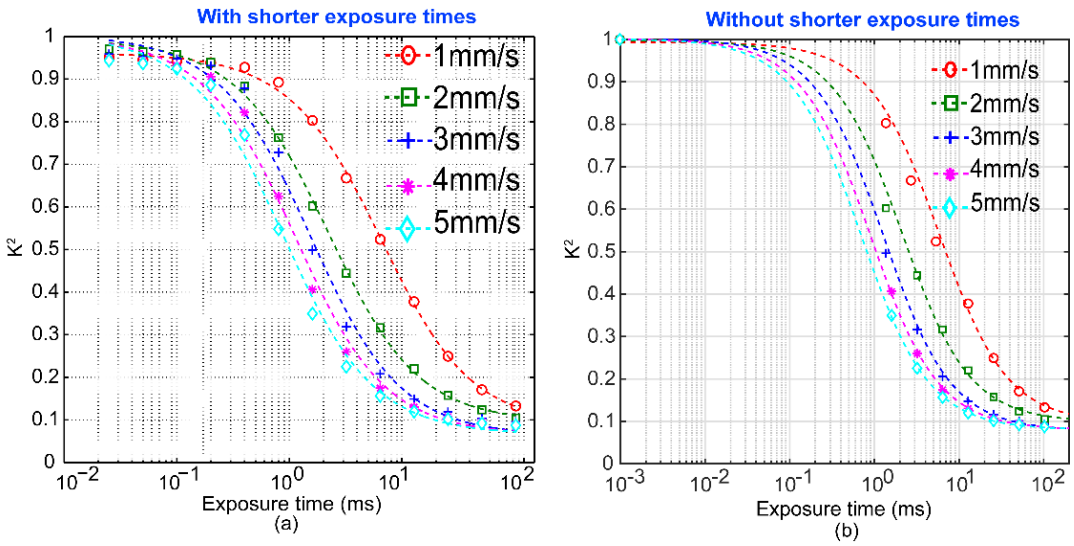

Fig A. 15 K^2 curve of high-speed camera (a) with short exposure times (b) without short exposure times

The high-speed camera without shorter exposure times provides the increased mean FNR of 18.41. The possible reasons are: (1) Because of convergence of all K^2 curve at the same point (2) The K^2 value measured at shorter exposure doesn't provide the better SNR and therefore eliminating these data points increased the SNR. The best case in each tap were compared. The summary of mean FNR obtained by various taps and patterns are given as a summary in Table A. 1.

Table A. 1 Comparison of mean FNR of high-speed camera, 4-tap, 6-tap and 8-tap

Actual speed (mm/s)	High-speed camera	High-speed camera (w/o short exposure time)	Equal pattern (4-tap) T_0 = 6.4 ms	Exponential pattern (6-tap, N = 2) T_0 = 3.2 ms	Exponential pattern (8-tap, N = 4) T_0 = 3.2 ms
1	10.77	7.52	6.43	6.56	6.28
2	18.93	15.17	8.83	14.02	13.23
3	11.48	27.02	19.21	14.84	20.87
4	13.02	25.71	14.66	24.87	24.98
5	19.71	16.65	22.33	28.95	36.25
Mean FNR	**14.78**	**18.41**	**14.29**	**17.85**	**20.32**

The simulation of 6-taps and 8-taps with reference high-speed camera data were performed. The various patterns were designed. The comparison of mean FNR were done to choose the optimal number of taps and best pattern. As a summary, 8-tap was found as an optimal number of tap in the investigation and exponential exposure pattern is best suitable for 8-taps. The summarized table gives a suggestion that the 8-taps with exponential exposure pattern (N = 4) will provide the better SNR to measure the wide range of flow speed. This simulation studies will help to implement the MELSCI system with increase number of taps in future.

Bibliography

1. S. Kawahito, K. Yasutomi, M.-W. Seo, K. Kagawa, Y. Shirakawa, and N. Teranishi, “Design of an 8-tap CMOS lock-in pixel with lateral electric field charge modulator for highly time-resolved imaging,” Proc. SPIE 10108(1), 101080N (2017).

List of Publications

Journal

1) Panneer Selvam Sivakumar, Keiichiro Kagawa, Christian Crouzet, Bernard Choi, Keita Yasutomi, Shoji Kawahito, "Multi-exposure laser speckle contrast imaging using a video-rate multi-tap charge modulation image sensor," Optics EXPRESS, Vol. 27, No. 18, pp. 26175-26191 (2019).

International and National Symposia and Workshops

1) P-S. Sivakumar, K. Kagawa, C. Crouzet, B. Choi, K. Yasutomi, S. Kawahito, "Simulation of Multi-Exposure Laser Speckle Contrast Blood Flow Imaging based on Multi-Tap Charge Modulator CMOS Image Sensor," Information Photonics, Apr. 2019.

2) P-S. Sivakumar, K. Kagawa, K. Yasutomi, S. Kawahito, "Simulation of Multi-Exposure Laser Speckle Contrast Blood Flow Imaging with Multi-Tap Charge Modulation Pixels," The 20th Takayanagi Kenjiro Memorial Symposium and The 4th ICNERE Joint Symposium, Nov. 2018.

3) P-S. Sivakumar, K. Kagawa, T. Takasawa, K. Yasutomi, S. Kawahito, "A Simulation of Multi-Exposure Laser Speckle Contrast Imaging using Multi-Tap Charge Modulation Pixels," 東北大学ー静岡大学合同サマーセミナー, Jul. 2018.

4) P-S. Sivakumar, K. Kagawa, B. Zhang, T. Takasawa, K. Yasutomi, S. Kawahito, "Multi-Tap Charge Modulation CMOS image sensor for Scanning-less Laser Doppler Flowmetry Imaging," The 2nd International Symposium on Biomedical Engineering, Nov. 2017.

5) P-S. Sivakumar, K. Kagawa, M-W. Seo, B. Zhang, T. Takasawa, K. Yasutomi, and S. Kawahito, “Measurement of 3-Tap 1MS/s CMOS Image Sensor for Multi-Point Fluorescence Correlation Spectroscopy,” International Symposium toward the Future of Advanced Researches in Shizuoka University, PS-3, pp.43, Jan. 2015.

6) P-S. Sivakumar, K. Kagawa, M-W. Seo, B. Zhang, T, Takasawa, K. Yasutomi, S. Kawahito, “Dark current and random noise measurement of 10x10-pixel multi-point fluorescence correlation spectroscopy CMOS image sensor,” IST, 2nd Asian Image Sensors and Imaging Systems Symposium, vol.38, no.47, IST2014-68, Dec. 2014.

7) 香川景一郎, P-S. Sivakumar, 高澤大志, 張博, 徐珉雄, 山本条太郎, 金城政孝 安富啓太, 川人祥二, “多点蛍光相関分光 CMOS イメージ センサの特性評価,” Optics and Photonics Japan 2014, 5D1, Nov. 2014.

8) 香川景一郎，徐珉雄，山本条太郎， 西岡優起，高澤大志， 張博， P-S. Sivakumar, 安富啓太，金城政孝，川人祥二， “多点多機能共焦点顕微鏡に向けた CMOS イメージンサの開発,” 2014 年第 39 回工学シ ンポジウム，『工学システム・光学素子の 計製作，評価を中心として』講演予稿集，pp.5-6, Jun, 2014.

Acknowledgement

At the outset, I bow The Almighty who given me a pleasant atmosphere, and institution to carry out my research work. I would like to place on record my deep sense of gratitude and heartfelt thanks to my supervisor Prof. Keiichiro Kagawa for providing me an opportunity to work in the field of CMOS image sensor. His inspiring guidance, timely suggestions and the constant encouragement throughout the course of this work made me to uplift my enthusiasm towards the productive research. He always made himself available to answer any questions and offered guidance whenever it was needed. Apart from the academic, Prof. Keiichiro Kagawa as a kind humane and well-wisher he paid at most care towards me which made be felt secured and to lead a pleasant life in Japan.

I express my profound gratitude to Prof. Bernard Choi, University of California, Irvine for his valuable instructive advice and useful suggestions on my research work. I would also like to thank Dr. Christian Crouzet for his support and guidance to carry out my research successfully. I would like to thank Prof. Shoji Kawahito and Prof. Keita Yasutomi who continuously provided me with guidance and supports. I would also like to thank my graduate committee members, Prof. Shoji Kawahito, Prof. Enoch Y. Park, and Prof. Egami Chikara for expending their invaluable time in examining my thesis and providing a lot of productive suggestions for improvement.

Next, I would like to thank Dr. Zhang Bo for his helps and advices in earlier part of the research. He is always helpful and patience in the discussions we had. Those discussions helped me a lot to achieve the greatness in the research. I wish to extend my sincere thanks to Dr. Lioe De Xing and Dr. Sumeet Shrestha for their supports and inspiration. I would like to thank to Dr. Seo Min-woong and Dr. Kamel Mars for their motivation towards the research. I would also like to thank Prof. Nobukazu Teranishi, Mr. Masashi Hakamata, Mr. Taishi Takasawa, Mr. Michio Fukuda, Ms. Rumi Fujihara, Ms. Seiko Nakamura, Ms. Satoko Tsuchiya, Ms. Eriko Ishizaki, Dr. Miao Lianghua, Dr. Hiroki Kamehama, Dr. Chen Cao, Dr. Lee Minho, Mr. Sanggwon Lee, Mr. Juyeong Kim, Mr. Shukri and all members of the Imaging Devices Laboratory for all the assistances given, and making the time in laboratory enjoyable and unforgettable.

I owe my deepest gratitude to Dr. M. Arivanandhan, Associate Professor, Anna University, India, and Dr. T. Murugu Thiruvalluvan for their support and guidance to purse the doctoral course at Shizuoka University. Their assistance offered me invaluable direction in my research endeavors. I would like to thank my cousin brother Dr. Subramanian Ramanathan, Nissei Electric, Japan for providing support and being there with me in my hard times. In addition, I would like to thank many other friends and fellow Indians at Shizuoka University. I thank you all for the fun and good memories we had together.

Finally yet importantly, I would like to thank the support and blessings received from my beloved parents P. Panneer Selvam and P. Vijayalakshmi and brother P. Venkatesh Kumar to carry out the doctoral study abroad. I would like to thank my father and mother-in-law C. Thiagarajan and K. Kaveri to understand my circumstances and help me to continue the research.

I present the thanks to my understanding and supporting wife Dr. T. Kiruthikadevi for her unlimited sacrifice to carry out my research pleasantly and in the best positive frame of mind. Without her I can’t imagine achieving my goal in the doctoral course. She endlessly supported me in each and every step in my doctoral course and I can’t express in mere words. Last but not the least, I thank all my family members for their everlasting love and support over the years.